Ultra-Low Voltage Electrowetting

A thesis submitted for the degree of
Doctor of Philosophy

Nico E. A. Cousens

Supervisor: Anthony R. J. Kucernak

Department of Chemistry
Imperial College London

Abstract

Electrowetting, the manipulation of surface wettability with an electric field, is an emerging technology used in next generation displays and cameras. This has been made possible by the development of 'electrowetting-on-dielectric' by Berge in 1993. However, such a system operates on large voltages poorly suited to portable devices.

In recent years, theoretical and experimental results have suggested that electrowetting using the interface between two immiscible electrolyte solutions (ITIES) may provide a solution to this problem. By applying less than 1 V to such a system, it is possible to induce substantial changes in the wettability—and hence the shape—of liquid droplets. However, there is a large degree of hysteresis in such a system meaning that there is a poor correlation between droplet shape and applied potential. Furthermore, the stability of the ITIES over long periods is of concern.

This thesis attempts to address the current problems with ITIES electrowetting highlighted above. By moving to smoother and more lubricated surfaces, a substantial reduction in hysteresis was seen. These surfaces were produced by template stripping. In addition, several other surfaces were prepared as potential electrowetting substrates. These involved surface functionalisation by plasma treatment or the reduction of diazonium compounds; preparation of ultra smooth glassy carbon and preparation of a hydrophobic conducting polymer. The potential range over which an ITIES is stable was also improved with the use of a novel mixed organic solvent phase.

By optimising the electrode and electrolyte compositions, an electrowetting system operating on less than 1 V with a contact angle range of 53° and a gap of only 100 mV between forward and reverse scans was possible. Other electrowetting systems with no hysteresis were also developed, although these did not operate within the potential limits defined by the onset of Faradaic processes.

Acknowledgements

First and foremost, I would like to thank my supervisor Professor Anthony Kucernak for all of his invaluable help, advice and inspiration.

Furthermore, I would also like to thank the following without whom, in all sincerity, this thesis would not have been possible: Prof. Alexei Kornyshev, Dr. Monica Marinescu, Vlad Turek, Dr. Daren Caruana, Steve Atkins, Prof. Alexander Bismark, Dr. Siti Shamsuddin, Andy Dolan, Dr. Tim Albrecht, Simon Dowland, George Barnes, David James, Graham Smith, Dr. Denis Kramer, Dr. Chris Zalitis and Dr. Venkat Narayanan.

This thesis is my own work in accordance with university guidelines.

Signed: Nico Cousens Date: 8th December 2012

Contents

List of Abbreviations

AFM	Atomic force microscopy
BTPPA	Bis(triphenylphosphoranylidene)ammonium
CH	Cyclohexane
CP	3-Chloro-1-propanol
CV	Cyclic voltammogram
DCE	1,2-Dichloroethane
DBH	1,6-Dibromohexane
EDOT-F	Pentadecafluoro-octanoic acid 2,3-dihydro-thieno(3,4-*b*)(1,4)dioxin-2-ylmethylester
EWOD	Electrowetting on dielectric
GC	Gouy-Chapman
HOPG	Highly oriented pyrolytic graphite
ITIES	Interface between two immiscible electrolytes
MWT	Mott and Watts–Tobin
PC	Propylene carbonate
PEDOT	Poly-(3,4-ethylenedioxythiophene)
PEDOT-F	Fluorinated PEDOT derivative
PTFE	Polytetrafluoroethylene
PZC	Point of zero charge
RHE	Reversible hydrogen electrode
RMS	Root mean square

TBAP	Tetrabutylammonium perchlorate
TBA	Tetrabutylammonium
TFPB	Tetrakis[3,5-bis(trifluoromethyl)phenyl]borate
TMA	Tetramethylammonium
TPB	Tetraphenylborate

List of Symbols

Latin

a_i^o	Activity of ion *i* in the oil phase
a_i^w	Activity of ion *i* in the aqueous phase
A_{de}	Droplet|electrode area
A_{dw}	Droplet|aqueous phase area
$c_{A^-}^w$	Anion concentration in aqueous phase
$c_{C^+}^w$	Cation concentration in aqueous phase
C	Capacitance
E	Energy
$E_{1/2}$	Half-wave potential
$E_i^{\theta'}$	Formal transfer potential of an ion *i*
f_1	Fraction of surface 1 with contact angle α_1
f_2	Fraction of surface 2 with contact angle α_2
F	Faraday constant
I	Current
K_{sp}^w	Aqueous solubility product
m_i^a	Mass transfer coefficient of ion *i* in phase *a*
m_i^b	Mass transfer coefficient of ion *i* in phase *b*
n	Number of moles of electrons transferred
r	Roughness factor
R	Ideal gas constant

s	Conductivity probe spacing
t	Thickness
T	Temperature
U	Potential
U_b	Bias potential
U_p	Pulse potential
U_{PZC}	Potential of PZC
V_d	Droplet volume
z_i	Charge on ion i

Greek

α	Contact angle
α_1	Contact angle on surface 1
α_2	Contact angle on surface 2
α_{flat}	Contact angle on flat surface
α_{PZC}	Contact angle at PZC
α_{rough}	Contact angle on rough surface
α_Y	Young contact angle
γ	Surface energy
γ_{da}	Droplet|air surface energy
γ_{de}	Droplet|electrode surface energy

γ_{ds}	Droplet|solid surface energy
γ_{dw}	Droplet|aqueous phase
γ_{sa}	Solid|air surface energy
γ_{we}	Aqueous phase|electrode surface energy
γ_{we}^{PZC}	Aqueous phase|electrode surface energy at PZC
ΔG	Gibbs energy
$\Delta G_{tr,i}^{\ominus,w\to o}$	Standard Gibbs energy of transfer of ion *i* from aqueous phase to oil
Δp	Laplace pressure
$\Delta_{IL}^{w}\phi_{A^-}^{\ominus}$	Standard anion transfer potential from aqueous phase to IL
$\Delta_{IL}^{w}\phi_{C^+}^{\ominus}$	Standard cation transfer potential from aqueous phase to IL
$\Delta_{o}^{w}\phi$	Galvani potential difference between aqueous and oil phases
$\Delta_{o}^{w}\phi_{tr.i}^{\ominus}$	Standard Galvani potential difference of ion transfer between aqueous and oil phases of ion *i*
$\bar{\varepsilon}_{de}$	Capacitive energy of droplet|electrode interface
$\bar{\varepsilon}_{dw}$	Capacitive energy of droplet|aqueous phase interface
$\bar{\varepsilon}_{we}$	Capacitive energy of aqueous phase|electrode interface
$\mu_i^{\ominus,o}$	Chemical potential of ion *i* in the oil phase under reference conditions
$\mu_i^{\ominus,w}$	Chemical potential of ion *i* in the aqueous phase under reference conditions
ρ	Resistivity
ϕ^o	Galvani potential in oil phase
ϕ^w	Galvani potential in aqueous phase

List of Figures

List of Tables

Chapter 1: Introduction

The structure of this thesis is such that Chapter 1 will introduce electrowetting. It begins with a description of simple wetting phenomena before moving on to how electric charge can affect the wetting of a surface. The rest of the chapter will cover the history of electrowetting from its inception in 1875 by Gabriel Lippmann right through to cutting edge applications in microfluidics and display technologies. It will also look at the theory and first experimental demonstrations of electrowetting with two electrolytes which were the direct inspiration for this thesis. Chapters 2, 3 and 4 will then describe efforts directed at solving many of the issues associated with electrowetting at low voltages. These issues include stabilisation of the liquid|liquid interface and the preparation of very smooth, fluorinated surfaces to create a 'lubricated' electrode. Finally, Chapter 5 will bring all of these foundations together to provide a systematic study of electrowetting at exceptionally low voltages.

1.1 Wetting

Wetting is the phenomenon by which a liquid spreads across a surface. While some liquids may completely wet a solid, others repel the surface and form droplets. The extent of wetting or surface coverage is characterised by the contact angle a droplet makes at the three-phase line (designated by alpha in Figure 1). This line is the point at which the solid surface, liquid droplet and surrounding medium meet.

1.1.1 The Young equation

The contact angle of a liquid droplet on a solid surface surrounded by air is related to the surface energies of its three interfaces by the Young equation:[1]

$$\cos \alpha_Y = \frac{\gamma_{sa} - \gamma_{ds}}{\gamma_{da}} \qquad \text{(Equation 1)}$$

where α_Y is the Young contact angle as shown in Figure 1. These interfaces, measured in units of energy per unit area[i], are γ_{ds} the droplet|solid surface energy, γ_{da} the droplet|air surface energy and γ_{sa} the solid|air surface energy. The *vertical bar* symbol is used throughout this thesis to designate an interface between two phases. If the droplet|solid surface energy is smaller than the solid|air surface energy the contact angle will be less than 90°, as is the case for metals, such as gold. For water droplets such materials are termed hydrophilic. If, on the other hand, the situation is reversed and the droplet|solid surface energy is larger than the solid|air surface energy, the contact angle will be greater than 90°. Such materials are termed hydrophobic and are often made from organic polymers with fluorinated chains, such as the polymer polytetrafluoroethylene (PTFE) which is the most hydrophobic. This phenomenon is illustrated in Figure 1. The Young equation is of course applicable to any three phase system and the following chapters will be predominantly concerned with aqueous droplets surrounded by an immiscible organic liquid phase.

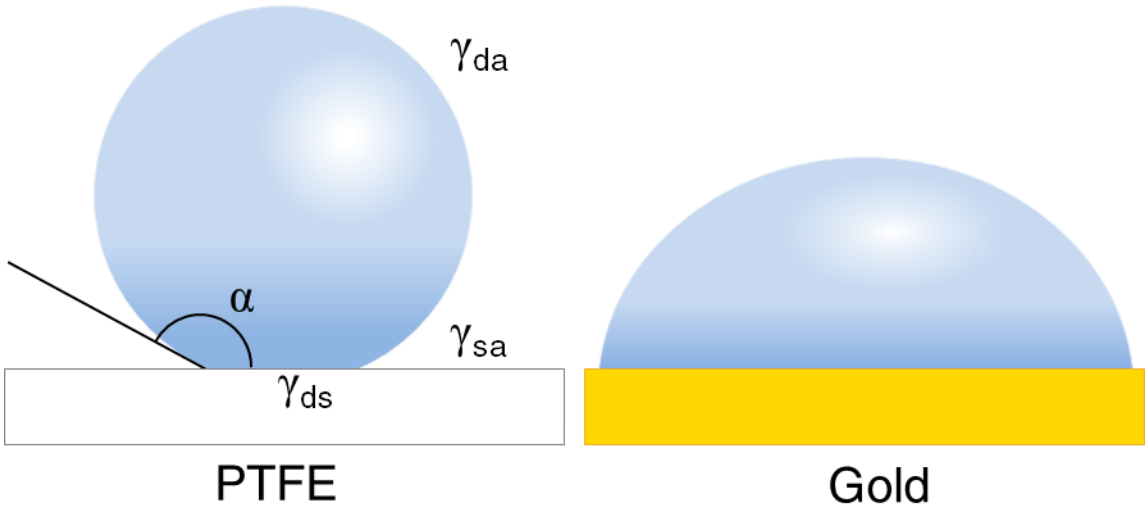

Figure 1|The Young equation relates the contact angle, α, to the surface energies of the droplet|solid (γ_{ds}), droplet|air (γ_{da}) and solid|air (γ_{sa}) interfaces. Pictured are a water droplet on a very hydrophobic PTFE surface and on a hydrophilic gold surface. The three-phase line, in this case, is the point at which solid, droplet and air all meet.

[i] Units of force per unit length are equivalent and are commonly used for surface tension, which refers exclusively to the liquid|air surface energy. Surface energy is a generic term covering all interfaces such as solid|liquid or liquid|liquid interfaces as well as liquid|air.

1.1.2 Heterogeneous surfaces

Beyond simple homogeneous surfaces, the patterning or nano-structure of a surface will also affect its wettability.

Wetting on surfaces composed of two different materials is described by the Cassie equation:[1]

$$\cos\alpha = f_1 \cos\alpha_1 + f_2 \cos\alpha_2 \qquad \text{(Equation 2)}$$

where f_1 and f_2 are the fractions of surfaces with contact angles a_1 and a_2 respectively.

A special application of the Cassie equation occurs for nano-structured surfaces with a very large roughness or real surface area.[2] In such a situation, rather than wet the entire surface it becomes favourable to trap air pockets under the droplet as illustrated in Figure 2. This trapping of air results is an unusual application of (Equation 2, where α_1 is the droplet|solid contact angle and α_2 the droplet|air contact angle.

1.1.3 Surface roughness

As mentioned above, surface roughness also has an effect on the macroscopic contact angle. Surface roughness exaggerates the contact angle of the perfectly flat surface according to the following relation:[1]

$$\cos\alpha_{rough} = r\cos\alpha_{flat} \qquad \text{(Equation 3)}$$

where α_{rough} is the contact angle of the rough surface, α_{flat} is the contact angle of the perfectly flat surface and r is the roughness factor which is the ratio of the real surface area to the projected surface area. Hence hydrophobic surfaces appear more hydrophobic and hydrophilic surfaces appear more hydrophilic as they get rougher.

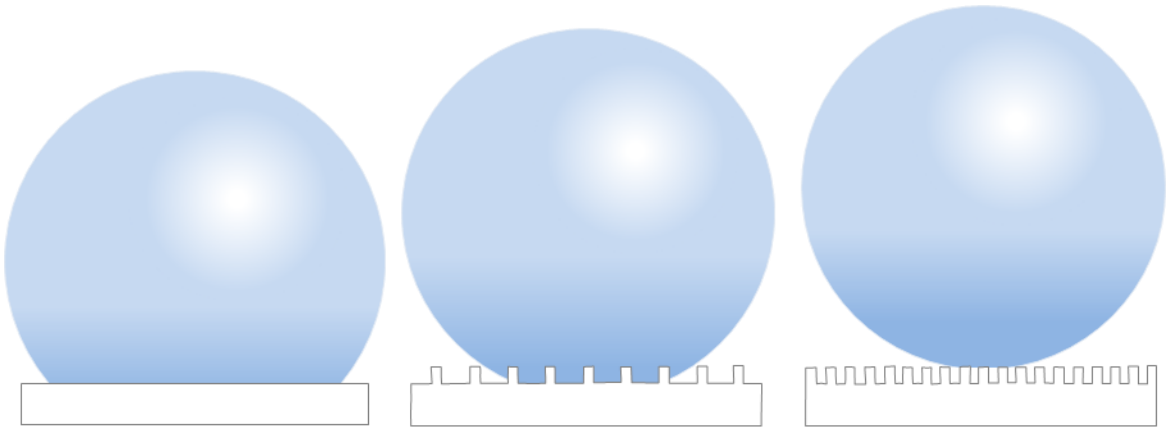

Figure 2|(Left) A water droplet on a flat hydrophobic polymer surface exhibits the natural equilibrium contact angle. (Middle) A rougher surface exaggerates the macroscopic contact angle. (Right) When the surface is very rough air pockets are trapped under the droplet, as this is a lower energy configuration. This is known as the Cassie-Baxter state.

1.2 Contact angle hysteresis

A concept essential to this thesis is that of contact angle hysteresis, which is also closely related to pinning of the three-phase line.

Contact angle hysteresis is generally considered to result from a combination of surface roughness; surface heterogeneity; rearrangement of the surface under the droplet; or surface adsorption of solutes or impurities in the droplet.[1] Surface roughness or heterogeneity results in pinning when the droplet becomes trapped in a local energy minimum, from which it cannot easily escape. This trapping of the droplet means that as it spreads or contracts across a surface it will not reach the contact angle predicted by the Cassie or Young equations, which corresponds to its true minimum energy state (Figure 3). It has been shown that this type of pinning can be overcome by agitating the droplet with an external force such as a lateral vibration.[3] The agitation gives the droplet an energy 'kick', helping it break free of its trapped state.

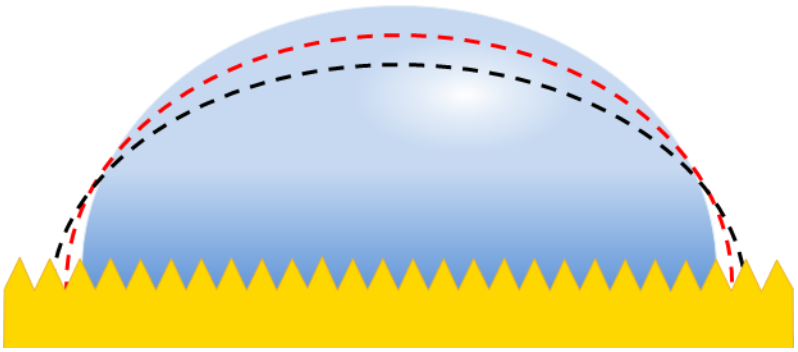

Figure 3|This droplet is pinned on a rough surface. It exhibits a larger contact angle than the predicted Young contact angle (black outline) because the intermediate contact angle (red outline) through which the droplet must pass is higher in energy.

If the surface is able to reorganise itself, perhaps due to the presence of mobile adsorbates, a much more complicated situation arises. If a reproducible contact angle is desired this scenario must be avoided. In essence, the pinning in this situation is due to the spontaneous formation of an inhomogeneous surface. An extreme example of this is known as 'autophobicity'. When a surfactant containing water droplet spreads across a clean hydrophilic surface, the surfactants adsorb onto the surface with the hydrophobic half of the molecule left pointing into the droplet. The surfactants then turn the surface into a hydrophobic one and the water droplet subsequently contracts irreversibly.[4,5]

Similarly, if the droplet contains a high salt concentration, the salt may be deposited onto the underlying surface, particularly at the three-phase line if the droplet slowly evaporates. This process will pin the droplet.

Therefore, because the aim is to reduce hysteresis in an electrowetting system, these sources of pinning should be removed as far as is possible.

1.3 Electrowetting

When an electrolyte solution comes into contact with a charged surface, ions in the solution migrate to the interface, screening the charge. These interfacial charges, separated by a small

distance, behave as a capacitor and store electrostatic potential energy. The separated charges are known as an electrochemical double layer capacitor. It is localised at the interface and therefore contributes to the total surface energy, still measured in energy per unit area. If the surface charge can be varied, it becomes possible to vary the total surface energy. This process can result in a change in the shape of a droplet, as dictated by the Young equation. It is this change in shape, resulting from an electrically induced change in surface wettability, which is known as electrowetting.

1.3.1 Early electrowetting studies

Electrowetting was first described by Gabriel Lippmann in 1875 when he noticed that the addition of electrostatic charge could modify capillary forces at an interface.[6] Then in the 1930s Frumkin et al. used the same principle to study oil droplets on mercury surrounded by an aqueous electrolyte.[7] The experimental geometry used by Frumkin is described in Figure 4. As a potential is applied to the mercury electrode, an electrochemical double layer forms at the interface between the electrode and the aqueous phase. The migration of charge to the interface is spontaneous and therefore must lead to a reduction in the surface energy. Consequently, the electrode|aqueous phase interface grows at the expense of the electrode|droplet interface.

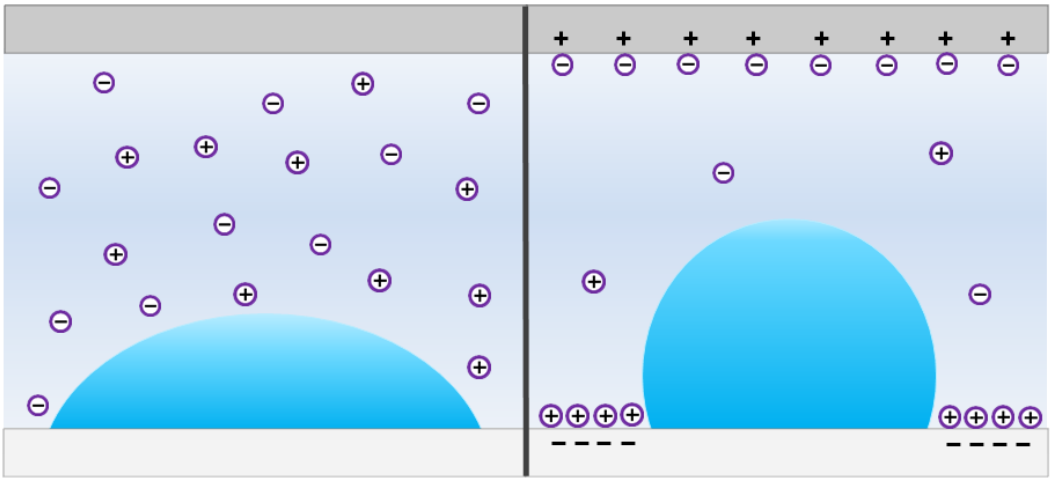

Figure 4|Geometry of the early electrowetting experiments performed by Frumkin. A toluene droplet sits on a mercury electrode surrounded by an ionic solution. When a potential is applied an electrochemical double layer forms at the electrode|aqueous phase interface. This lowers the surface energy and the contact angle changes in accordance with the Young equation.

The contact angle shows a parabolic dependence on the applied potential with a minimum at the point of zero charge (PZC), where the PZC is the potential at which the electrical surface charge density is zero and therefore the point at which there is no electrostatic contribution to surface energy. The parabolic dependence stems from the relationship between the applied potential and the energy stored in the double layer capacitor:

$$E = \frac{1}{2}C(U - U_{PZC})^2 \qquad \text{(Equation 4)}$$

where E is the energy stored in the capacitor, C is the double layer capacitance, U is the applied potential and U_{PZC} is the potential at the point of zero charge.

Thus, the electrode|aqueous phase surface energy in the presence of an external potential can be divided into two separate components:

$$\gamma_{we} = \gamma_{we}^{PZC} - \frac{1}{2}C(U - U_{PZC})^2 \qquad \text{(Equation 5)}$$

where γ_{we} is the total aqueous phase|electrode surface energy and γ_{we}^{PZC} is the aqueous phase|electrode surface energy at the PZC. γ_{we}^{PZC} can be thought of as the surface energy arising from potential independent intermolecular interactions such as Van der Waals forces and dipole interactions. This simple model assumes that the double layer capacitance is independent of potential. While this is not the case, this added complication does not alter the outcome of this line of argument.

If we insert this new term for the aqueous phase|electrode surface energy into the Young equation, the dependence of the contact angle on potential is revealed:[8]

$$\cos\alpha = \cos\alpha_{PZC} - \frac{C(U - U_{PZC})^2}{2\gamma_{dw}} \qquad \text{(Equation 6)}$$

where α_{PZC} is the contact angle at the PZC and γ_{dw} is the droplet|aqueous phase surface energy. If physically reasonable values for these parameters are used (let α_{PZC}=30°, C=20 μF cm^{-2}, γ_{da}=10 mJ m^{-2}), the decrease in cos α is five times the square of the applied potential (measured in Volts). These values would mean the contact angle would have increased to 56° at 0.25 V versus PZC and would have attained a maximum 180° at 0.93 V. Therefore, as Frumkin found experimentally, small potentials induce substantial changes in the contact angle.

There are two main limitations to this approach to electrowetting. Firstly, the range of accessible contact angles is largely determined by the range of accessible potentials. In turn, this is limited by the onset of Faradaic processes which are irreversible electrochemical reactions at the electrode. Secondly, a reproducible variation in contact angle has only been seen on mercury. Mercury is unique in that it is atomically smooth and homogeneous and thereby unsusceptible to pinning. However, as mercury is a liquid, there is little possibility to use this method for the portable applications of electrowetting discussed later.

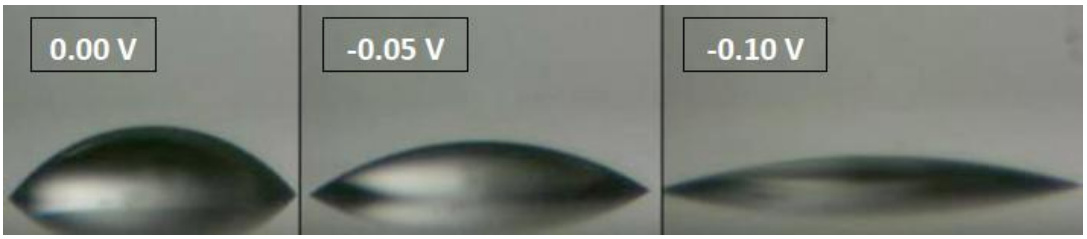

Figure 5|[Taken from Cousens[9]] A recreation of Frumkin's experiment from 1932. A 1,2-dichloroethane droplet sits on a mercury electrode surround by 0.1 mol dm^{-3} LiCl solution. Potentials are versus an Ag/AgCl reference electrode.

1.3.2 Further developments in electrowetting

After Frumkin, it appears that very little work was done on electrowetting for the next four decades. Eventually, however, interest slowly began to return. In 1981, Beni and Hackwood devised an electrowetting display and optical switch based on the flow of liquids driven by changes in surface wettability.[10-12] Their first device designs used gold or indium tin oxide electrodes although later devices used mercury. Not very much is known about the limitations or successes of this system and there is no analysis of the electrowetting response. In 1992, Sondag-Huethorst and Fokkink demonstrated electrowetting on gold coated with an insulating alkane-thiol layer.[13,14] The thiols were terminated with a ferrocene group which could be reversibly oxidised. On doing so, there was a change in the wettability of the surface with a maximum contact angle variation of about 25°. However, this showed a very large hysteresis owing to reorganisation of the thiol layer as discussed in Section 1.2. The largest reproducible change in contact angle was only 10°. Whitesides et al. also used a thiol modified gold surface to design an electrowetting system.[15] By electrochemically adsorbing/desorbing an alkane terminated thiol, the contact angle of an oil droplet on the electrode was varied.

These methods of electrowetting are fundamentally different to those presented thus far because the surface energy is changed by altering the chemical nature of the surface rather than an increase in electrostatic potential energy. Nonetheless, the Whitesides method enables a change in contact angle of 91° at a rate of approximately 2 Hz, the disadvantage being that only two different contact angles are accessible while conventional electrowetting can access any contact angle (in principle).

1.3.3 Electrowetting on dielectric

The biggest leap forward for electrowetting came with the development of *electrowetting on dielectric*, commonly known as EWOD. This technology, pioneered by Berge in the 1990s, is currently used in many electrowetting devices.[16,17] However, despite its maturity and wide application, EWOD has several limitations, opening the door for new types of electrowetting.

The basic geometry for EWOD is shown in Figure 6. It shows an immiscible oil droplet surrounded by water containing a simple salt, much as before. Crucially however, the oil and water are separated from the electrode by a thin layer of dielectric material which prevents Faradaic processes occurring. When a potential is applied, ions migrate to the dielectric|aqueous phase interface storing energy in a capacitor. This process lowers the surface energy resulting in electrowetting. Again the energy stored in the capacitor is described by (Equation 4) shown earlier. When (Equation 4) is combined with the Young equation, the result is the Lippmann-Young equation relating applied potential to contact angle for EWOD systems:[17]

$$\cos\alpha = \cos\alpha_Y + \frac{CU^2}{2\gamma_{dw}} \qquad \text{(Equation 7)}$$

where α_Y is the Young contact angle and γ_{dw} is the surface energy of the droplet|aqueous phase. This is very similar to (Equation 6 except that the PZC is usually neglected in this instance as the required voltages are much larger than the PZC.

The capacitance of the interface is now much smaller because of the larger separation of the charges either side of the dielectric layer. While the Lippmann-Young equation states that this reduces the magnitude of the electrowetting response, this is compensated for by the large potentials which can be applied. Furthermore, because the energy stored increases with the square of the potential, a large change in contact angle can still be achieved.

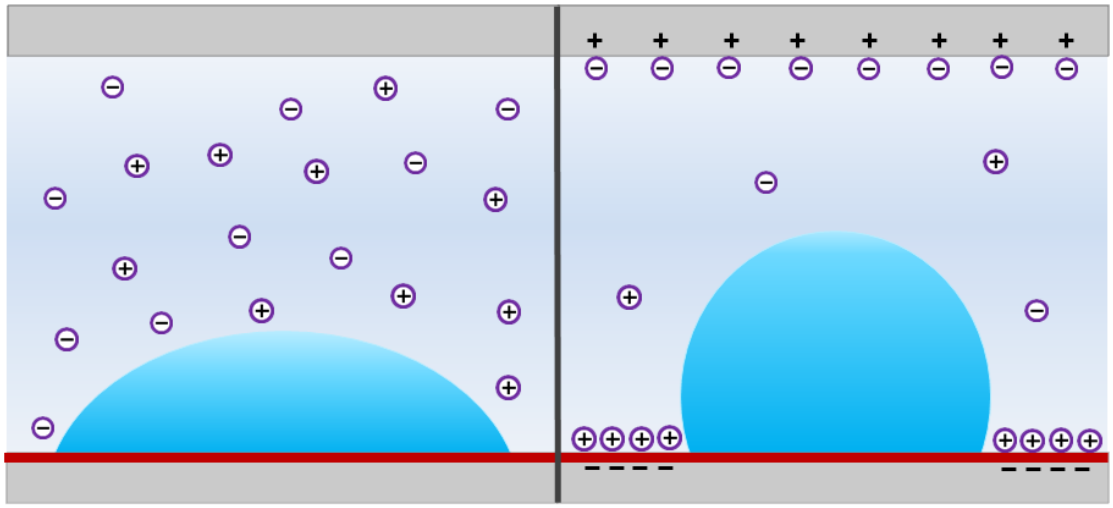

Figure 6|EWOD is similar to conventional electrowetting with the addition of a dielectric layer on top of the electrode, where the electrode is now solid rather than liquid mercury. The dielectric layer prevents Faradaic processes at the electrode, allowing large potentials to be applied.

The nature and thickness of the dielectric layer are very important. At very large potential gradients the dielectric material will breakdown. This problem means that while thin layers increase the capacitance of the interface they are also less robust. Usually, the dielectric layer is a combination of an oxide coated with a hydrophobic polymer. The oxide is robust with a larger relative permittivity while the polymer can be used to tailor the wetting properties of the interface. Wetting properties are essential for two reasons. Firstly, as can be seen from the Lippmann-Young equation, the minimum attainable contact angle is the Young angle, or the angle in the absence of an applied bias. Thus, a small Young angle increases the range of attainable contact angles. Secondly, Berge et al. have shown that a small Young angle and low surface polarity reduce contact angle hysteresis, an important result inspiring much of the work in Chapter 4 of this thesis.[18]

As well as being limited by breakdown of the dielectric layer, a phenomenon known as 'contact angle saturation' limits the contact angles accessible to EWOD. While the Lippmann-Young equation suggests that a contact angle of 180° is attainable (this corresponds to de-wetting of the droplet from the surface), instead the contact angle becomes constant at large potentials. The reason behind this is still the subject of debate but probably results from the

large electric fields in the vicinity of the three phase line which can ionise the surroundings and inject charge carriers into the dielectric layer.[8]

Similar to EWOD is dielectrophoresis. This phenomenon is identical to EWOD except that an AC potential is needed and there are no electrolytes present in either phase. Despite being a fundamentally different phenomenon, dielectrophoresis has almost identical capabilities and limitations to EWOD and therefore has similar potential applications.[8]

The one obvious set back of EWOD is the large operating potential. While Berry has reported a 100° contact angle change with only a 3 V bias, portable devices using electrowetting continue to operate at 15-120 V.[19-21] Given that lithium-ion batteries used in the majority of today's portable technologies have a nominal cell potential of only 3.6 V, an electrowetting system operating below 3.6 V might greatly reduce the energy consumption, size and complexity of these devices. The 'two electrolyte' electrowetting system discussed in the next section is a possible way to achieve this.

1.4 Electrowetting with two electrolytes

Electrowetting with two electrolytes was first proposed by Monroe, Daikhin, Urbakh and Kornyshev in 2006.[22] By putting an electrolyte in the droplet as well as the surrounding phase they devised a model of electrowetting which predicted a change in contact angle at very low potentials.

Firstly, this section will describe the nature of the interface between two immiscible electrolyte solutions—commonly referred to by the acronym ITIES—which is of importance to the model. Then it will give a brief description of this model before finally looking at the first experimental results of electrowetting with two electrolytes.

1.4.1 The interface between two immiscible electrolytes

An ITIES consists of two immiscible liquids—one liquid is usually water; the other an oil such as 1,2-dichloroethane (DCE) or nitrobenzene.[23] The water or aqueous phase of an ITIES contains an inorganic electrolyte such as LiCl, which consists of small ions with a high charge density. The organic phase contains a bulky organic electrolyte of opposite nature like tetrabutylammonium tetraphenylborate (TBATPB). Crucially, the electrolytes are selected such that they are soluble in only one of the phases. Therefore, not only are the two solvents immiscible, the electrolytes dissolved in them are restricted to their respective halves of the interface.

The main consequence of an ITIES is that when a potential is applied across the liquid|liquid interface, a back-to-back ionic double layer forms. This double layer means that the liquid|liquid interface now behaves as a capacitor where before it didn't. This concept is shown in more detail in Figure 7. Also shown is the potential distribution. The potential drop is distributed exclusively across the four double layers where the local electric fields can be as high as 10^7 V cm^{-1}.[24] This is not the case for EWOD or conventional electrowetting because not all liquids in contact with the electrode contain an electrolyte. As a result the electric field distribution for EWOD is much more complicated. This is partly why EWOD modelling is so difficult and contact angle saturation phenomena are currently poorly understood.

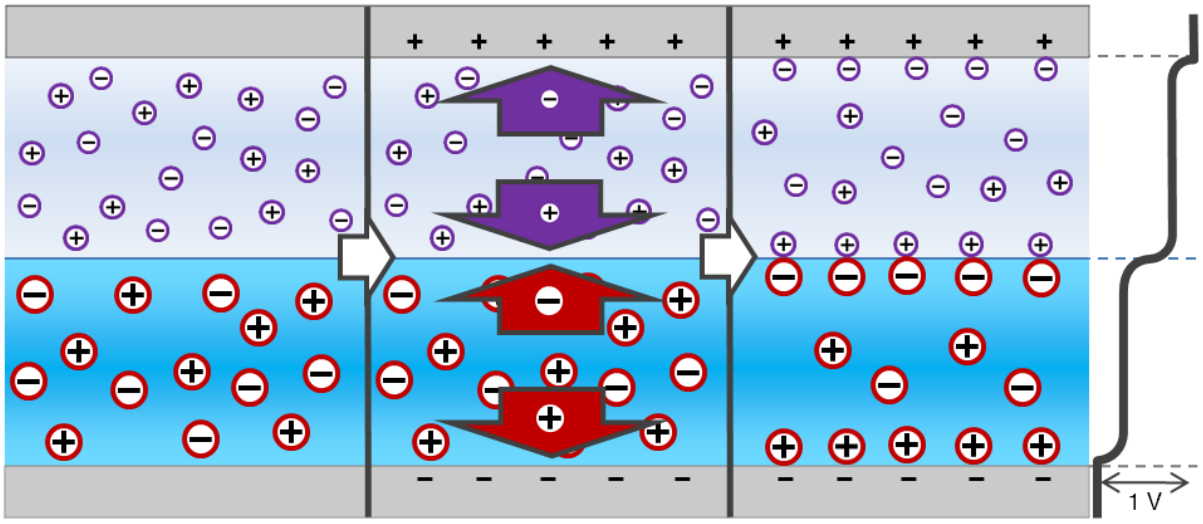

Figure 7 | Illustration of the formation of a back-to-back electrical double layer when an ITIES is polarised. The top half contains an inorganic salt dissolved in water while the bottom half contains a bulky organic salt in an organic solvent. When a bias is applied (1 V) the ions migrate to the electrodes. The ions are restricted to their respective phases resulting in the formation of a back-to-back electrochemical double layer. (Far right) The electric field distribution shows how the potential decays in the double layers and not in the bulk.

An ITIES is possible because the Gibbs energy of transfer of ions from one phase to the other is prohibitively high. However, as the potential across the droplet increases, the potential drop, or Galvani potential difference, across the ITIES also increases. Eventually it becomes energetically favourable for the ion to cross the interface and the ITIES begins to break down. The potential at which this occurs is defined by the Gibbs energy of transfer of the ion.[25]

When working with an ITIES it is essential to know beyond which potentials ion transfer will occur and cyclic voltammetry of the liquid|liquid interface is the best tool for determining this. It is useful to see at which potentials significant currents, resulting from ion transfer, arise. About the PZC there is no ion transfer across the interface and only a small current is seen as a result of the double layer charging. As seen in Figure 8, when the potential moves away from the PZC, eventually there is a sharp rise in current. Whether this current is a result of inorganic ions moving into the organic phase or organic ions moving to the aqueous phase depends on which process is more energetically costly. Of course, if both ion transfers are of similar energy, both will contribute to the current simultaneously.

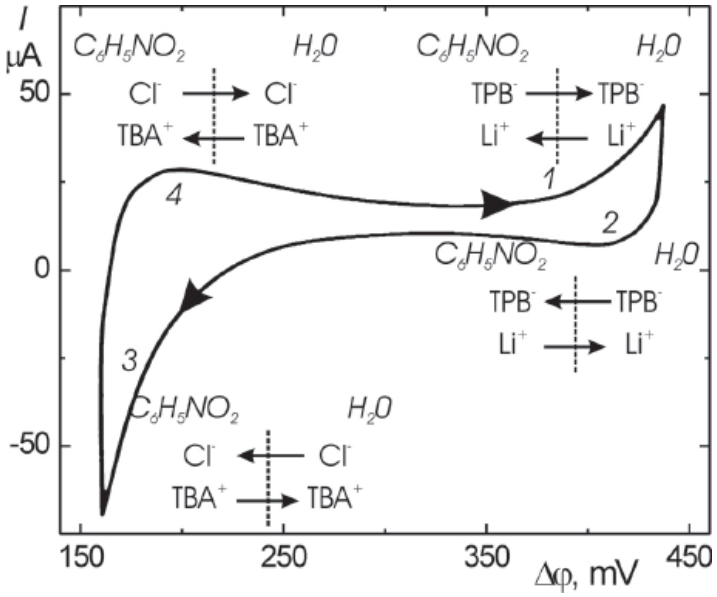

Figure 8|[Taken from Vanýsek[26]] Cyclic voltammogram of the ITIES formed from LiCl in water and TBATPB in nitrobenzene. About the PZC (at approximately 300 mV) there is a small double layer charging current. At each end of the voltammogram ion transfer currents arise.

1.4.2 Electrowetting with ITIES

The geometry for electrowetting with an ITIES is essentially the same as for conventional electrowetting but with the addition of electrolyte to the droplet. In conventional electrowetting or EWOD only the electrode|aqueous phase surface energy changes. However, when there is electrolyte in the droplet, ions migrate to all three interfaces (Figure 9) and all three surface energies become potential dependant. The next section will cover how the consequences of this have been modelled in detail by Monroe et al., however, a quick inspection of the Young equation gives an idea of what might happen. The difference between the electrode|aqueous phase and electrode|droplet surface energies is divided by the droplet|aqueous phase surface energy. Therefore, the contact angle becomes very sensitive to changes in the droplet|aqueous phase surface energy. It was hoped that as a result, there would be a larger driving force for shape change. This would make low voltage shape change on non-ideal surfaces possible. An added consequence of electrowetting with ITIES is a

smothering of the tendency of electric fields to diverge at the three-phase boundary. In EWOD this distorts the truncated spherical shape of the droplet but this effect is negligible with ITIES.[8] This means that if the densities of both liquids are similar, or if the droplet is small—negating buoyancy effects—the droplet will be a perfect truncated sphere. This makes it an ideal lens, as discussed further in Section 1.5.

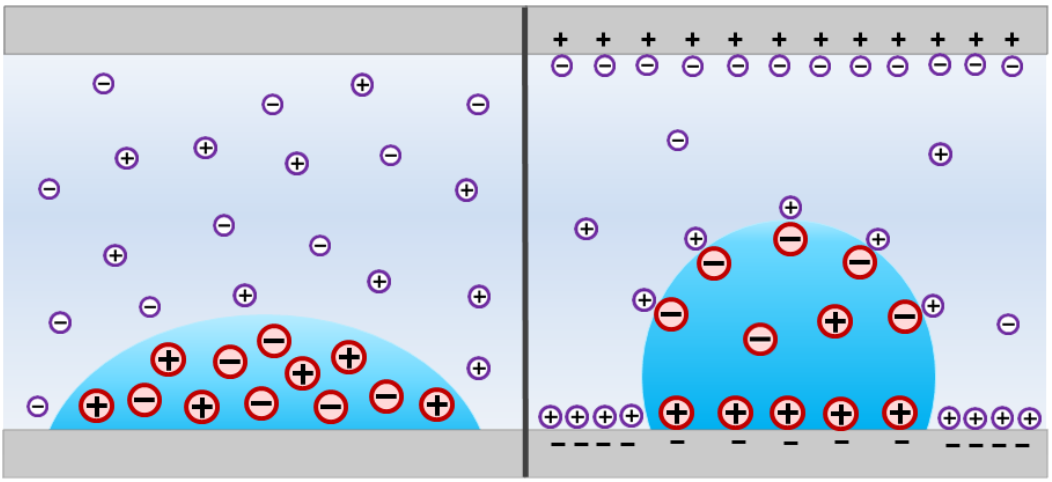

Figure 9|Electrowetting with ITIES. The addition of electrolyte to the droplet means that all three droplet surface energies are now potential dependant, where previously only the aqueous phase|electrode surface energy was affected. The Young equation shows that the contact angle is particularly sensitive to the liquid|liquid energy. Therefore, changing this surface energy may result in a significant contact angle change.

1.4.3 Theoretical model

The model devised by Monroe, Daikhin, Urbakh and Kornyshev calculates the droplet geometry which minimises the Gibbs energy of the droplet at a given potential. The full equation is given below[27-30]:

$$\Delta G = [\gamma_{de} - \gamma_{we} + \bar{\varepsilon}_{de} - \bar{\varepsilon}_{we}]A_{de} + [\gamma_{dw} + \bar{\varepsilon}_{dw}]A_{dw} + V_d\Delta_p \qquad \text{(Equation 8)}$$

where d, e and w are the droplet, electrode and aqueous phase respectively, γ is the surface energy due to intermolecular interactions, $\bar{\varepsilon}$ is the capacitive energy (based on the potential

dependant capacitance and potential drop), A is the area, V_d is the droplet volume and Δ_p the Laplace pressure. The surface energy terms are assumed to be independent of potential. The capacitances of the double layers are estimated using standard electrochemical double layer theory. The best description of the double layers are Verway-Niessen theory and Gouy-Chapman (GC) diffuse-layer theory combined with the elementary Mott and Watts–Tobin (MWT) approximation for the inner-layer part.[31] These models have been justified by experiment: the structure of the ITIES has been probed by surface energy measurements, cyclic voltammetry, electrochemical impedance spectroscopy and optical second harmonic generation (SHG).[32-36] SHG actually provides direct optical measurement of the accumulation of electrolyte in the interfacial region. Due to the screening of the electric field at each interface the potential distribution can be calculated analytically. Obviously, the electric field distribution is needed to calculate the potential drop across the double layers and thus calculate the energy stored therein. This essential element is why the model cannot be applied to EWOD: the complex electric field distribution is unknown.

Using experimental data for surface energies and capacitances, the resulting curves of potential against contact angle predict that low potentials induce large changes in droplet shape, with the contact angle eventually reaching 180°. They also predict that increasing the electrolyte concentration, whilst keeping the electrolyte concentrations inside and outside of the droplet equal, should increase the electrowetting response.

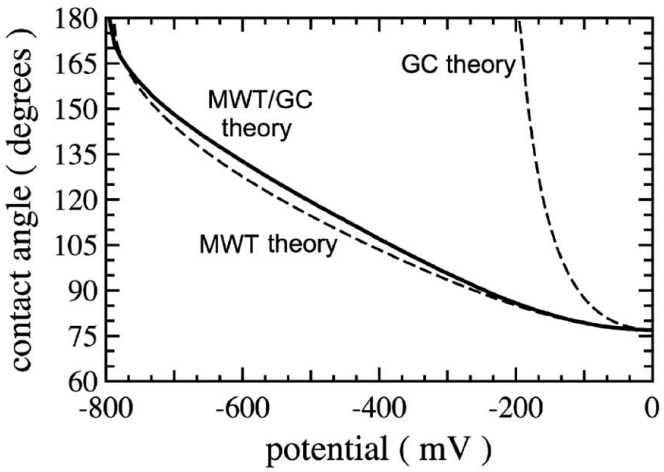

Figure 10 | [Taken from Monroe[30]] Theoretically derived graphs of the electrowetting response of a droplet with a Young contact angle of 77°. The different lines correspond to different models of the double layer capacitance.

1.4.4 Experimental results

1.4.4.1 First experimental results

The first experimental tests of ITIES electrowetting were performed by Kucernak and Sleightholme.[37] Using a droplet of nitrobenzene containing TBATPB, surrounded by aqueous LiCl on a sputtered gold electrode, they were able to achieve a reversible change in contact angle from approximately 100° to 130° for less than 1 V. However, while this is a very promising result, there is a very large hysteresis between the forward and reverse scans. That is to say that the relationship between the contact angle and potential is dependent on the contact angle prior to a change in potential. Furthermore, the change in angle, 30°, is relatively small.

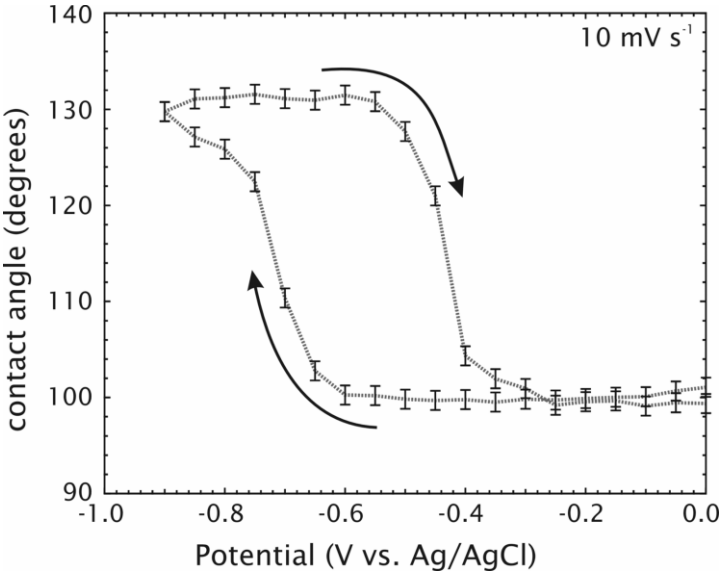

Figure 11|[Taken from Kornyshev et al.[37]] Low voltage driven contact angle variation for a 0.1 μL nitrobenzene droplet containing 0.01 mol dm^{-3} TBATPB surrounded by 0.5 mol dm^{-3} aqueous LiCl on a sputtered gold electrode. A large hysteresis can be seen between forward and reverse scans.

So critically, electrowetting with ITIES solves the issue of a high operating voltage but several other issues, essential to the performance of an electrowetting device, need to be resolved. For example, this technology would not be suitable for electro-variable lenses where the desired contact angle must be achieved quickly and precisely to obtain sharply focused images.

Like the Lippmann-Young equation for EWOD, the theory also predicts a maximum contact angle of 180° at large potentials. For unknown reasons this was not been seen experimentally. Instead, contact angle saturation is seen and the largest contact angles achieved were less than 140°. In this instance however, breakdown of the dielectric layer (used in EWOD) cannot be invoked to explain the phenomenon. Also the model predicts a symmetric electrowetting response about the PZC. However, ITIES electrowetting was only seen at potentials negative of the PZC, with no response seen at positive potentials.

1.4.4.2 Pulsing

In order to reduce hysteresis in the system described above, Kornyshev et al. applied a sequence of short (50 μs), high voltage (2-3 V) pulses on top of the applied bias potential.[37] As mentioned earlier, small vibrations can be used to 'de-pin' droplets by giving them a small kick of energy to escape their trapped state. This pulsing method uses the same principle but is much more convenient for an electrowetting system. The pulses last only 50 μs to ensure that no Faradaic processes have time to occur. As seen in Figure 12, the pulses seem to drive the droplet towards an equilibrium contact angle.

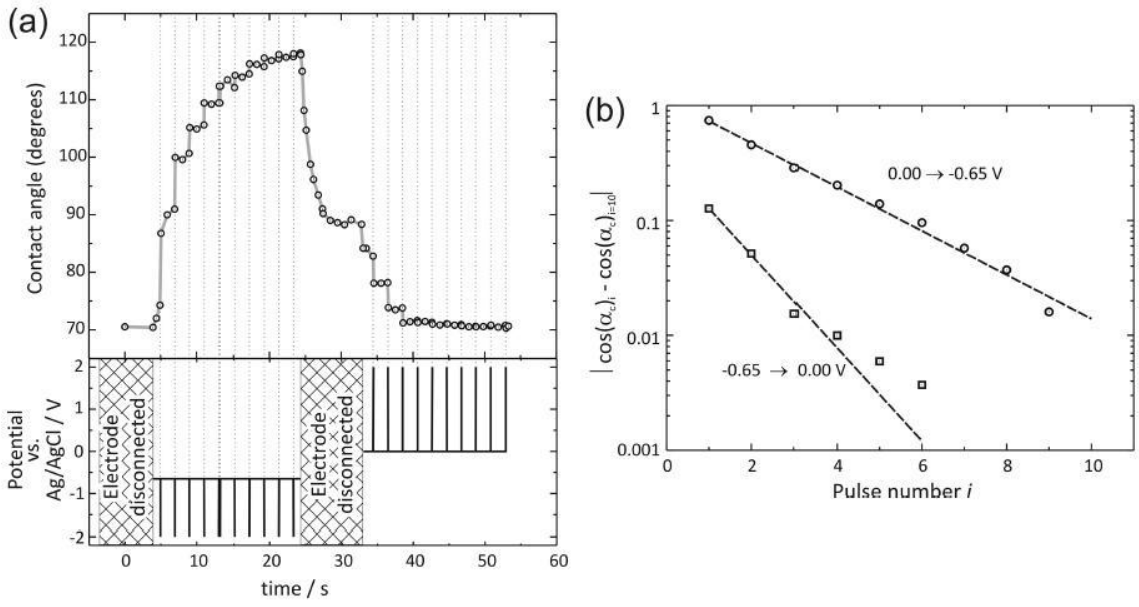

Figure 12|[Taken from Kornyshev et al.[37]] Illustration of how contact angle pinning is reduced by a pulsed-potential control technique. (a) Electrowetting dynamics for a 0.1 μL droplet of 0.1 mol dm^{-3} TBATPB in nitrobenzene surrounded by aqueous 0.5 mol dm^{-3} LiCl on a sputtered-gold substrate. Pinning is reduced by potential pulses of ±2.0 V over the constant bias of –0.65 or 0.00 V versus Ag/AgCl. The lower part of the diagram shows the applied potential profile. During the periods 0-4.5 s and 24-32 s, the electrode was disconnected and so the potential is uncontrolled. (b) Absolute difference between the cosine of the angle in the *i*th pinned state and the 'final' value of this cosine, which is essentially established after the tenth pulse. It can be seen that the droplet approaches an equilibrium shape.

This pulsing method has been dealt with theoretically by Marinescu et al.[38,39] There are two forces assumed to be acting on the droplet when a potential is applied. A driving force, which tends to bring the droplet to its equilibrium shape for the applied potential, and a friction force opposing this motion. As the displacement of the three-phase contact line after each pulse is much larger than the characteristic dimension of the roughness of the studied gold surface, the resistance to the motion of the contact line can be described in a first approximation by a position independent mean friction force. A good fit with experimental data is achieved (Figure 13).

Figure 13 also illustrates how a small percentage change in the frictional force can have a large effect on the observed contact angle. The frictional force can be seen to affect both the maximum and minimum contact angles, where large frictional forces limit the contact angle range. There is also a dramatic difference in the contact angle change after the first pulse: with a frictional force of 1.80×10^{-5} N the angle changes by only 13° while for a frictional force of 1.50×10^{-5} N the angle changes by 25°.

Such a model is useful because it can provide valuable insight into the importance of particular parameters such as surface friction and PZC. This in turn allows better informed decisions to be made on how to improve an electrowetting system.

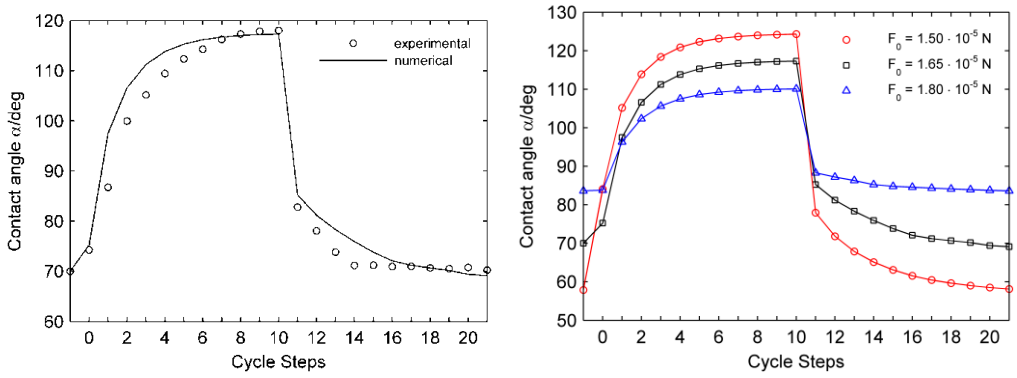

Figure 13 | [Taken from M. Marinescu[39]] (Left) Model of electrowetting dynamics facilitated by pulsing. Experimental results presented in Figure 12 with modelled fit. Cycle Steps: (**–1**) position after U_p = 1 V on U_b = 0, (**0**) U_b = –0.65 V, (**1**-**10**) U_p = –1 V, (**11**) U_b = 0, (**12**-**21**) U_p = 1 V. (Right) Predicted effect of friction force F_0 on final contact angle. Experimental parameters: –0.65/0 V biases, –1/1 V pulses, TBATPB conc. = 0.1 mol dm^{-3}, LiCl conc. = 0.5 mol dm^{-3}. Other parameters: droplet mass = 1.2×10^{-10} kg, water/nitrobenzene viscosity difference = 0.3×10^{-5} kg s^{-1}, Young's angle = 1°, U_{pzc} = 0.3 V,

friction force = 1.65×10^{-5} N. U_p, U_b and U_{pzc} are the pulse potential, bias potential and point of zero charge respectively.

1.4.4.3 Challenges

Clearly, there are still several hurdles to overcome before two electrolyte electrowetting can realistically compete with EWOD. Pulsing reduces pinning but does not eliminate the problem while also complicating the system. It also has a much slower response time than EWOD. Therefore, an electrode/electrolyte combination which is unyielding to the effects of pinning would be a better solution. Furthermore, owing to its cost, gold is not an ideal electrode material.

The quality of fit of the theoretical model for two electrolyte electrowetting is also yet to be confirmed. This would need to be done on an electrode which exhibited no or very little pinning.

1.5 Applications of electrowetting

Based on EWOD, various electrovariable optical devices have been designed. These designs should work equally well with EWOD and ITIES electrowetting. Electrowetting has also found use in microfluidic devices.

1.5.1 Lenses

Electrovariable lenses, pioneered by Varioptic, are already on the market and can be used in mobile phones, webcams and barcode readers to name but a few applications.[40,41] If, as is usually the case, the oil and water phases of an electrowetting system have different refractive indices, light entering the droplet will be refracted. Furthermore, if the densities of the two phases are similar and if the droplet is kept small, the droplet naturally takes on the shape of a spherical cap, which is the shape of a lens. The key difference in an electrovariable system is that rather than moving the lens mechanically to bring objects into focus, the shape of the droplet is controlled by the applied potential to vary its focal length. This reduces both

susceptibility to mechanical failure and the volume the lens occupies. Of course, opaque electrodes such as the ones described above cannot be used without a design modification. Instead, the droplet sits inside an open annulus made from two different electrodes. The concept is shown in Figure 14.

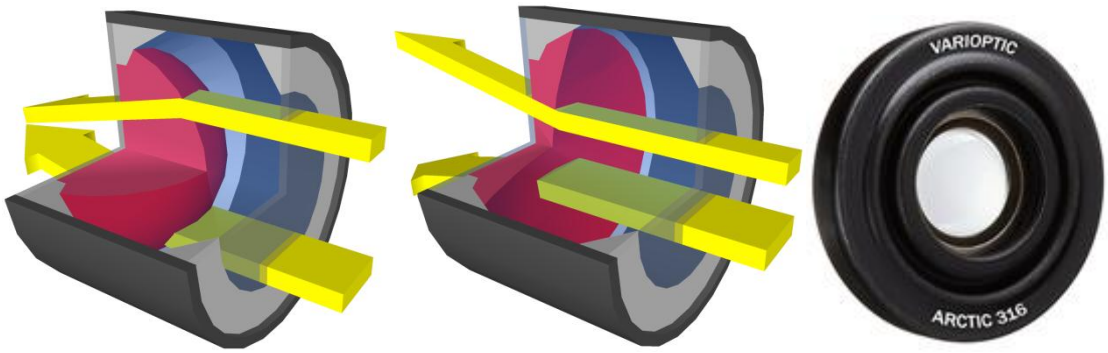

Figure 14 | (Left and middle) Cross section of an electrowetting lens. The droplet (shown in red) rests on the sides of an annular electrode. It acts as a lens as it has a different refractive index to the surrounding aqueous phase. Its curvature can be varied incrementally from convex to concave by changing the potential applied. (Right) [Taken from www.varioptic.com, May 2012] Electrowetting variable focus liquid lens made by Varioptic. The metal case diameter is 7.75 mm. Suitable for 30 fps video. Operating temperature range of –20 to 60 °C. The lens contains no mechanical components.

One potential limitation is the distortion of the lens by gravity. The extent of the distortion is determined by the difference in densities of the two fluids and the surface energy between them. Using water and oil the limit of the lens diameter is about 10 mm. Large lenses are possible if the density of the surrounding medium is equal to that of the droplet and this can be achieved using water and specially engineered silicone oils.

1.5.2 Displays

Another promising application of electrowetting is for display technologies. If the droplet contains a dissolved dye, electrowetting can be used to cause the droplet to fill or vacate a small cell, thus altering the cell's colour. Using this principle displays which are similar in

appearance to liquid crystal displays can be made. Crucially however, these displays are much more energy efficient (with energy savings in the range of 50-80 per cent compared to liquid crystal displays).[42] The high energy efficiency arises from the fact that no energy is consumed while the picture is static. This approach is also a competitor for use in electronic paper. For a review of EWOD pixel design see Andelman et al.[40]

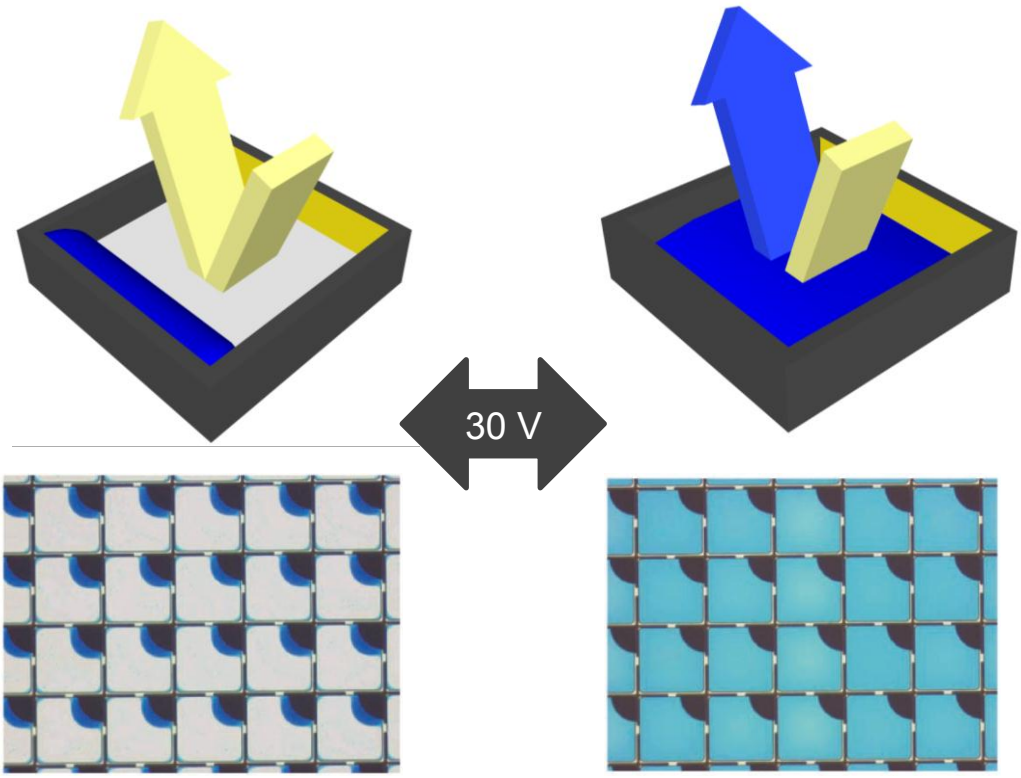

Figure 15 | [Photograph taken from Feenstra[43]] Cartoon and photograph of an electrowetting pixel. When a potential is applied the droplet covers the bottom of the cell. The droplet contains a dye to colour the pixel. When the potential is turned off the cell returns to its original configuration.

1.5.3 Digital microfluidics

The fastest growing application of electrowetting is in the field of microfluidics. Using EWOD, discrete droplets can be moved onto individually addressable electrodes, so called 'digital microfluidics'. A series of electrodes are designed so that by turning one electrode off and its neighbour on, a droplet will hop between them. It is possible to create, cut, transport

and merge droplets in this way (Figure 16).Uses include all current applications of lab-on-a-chip based microfluidics such as the polymerase chain reaction and other bioassays.[44,45]

Droplets can also be moved by dielectrophoresis, the manipulation of a pure electrolyte free liquid using an AC field, and this is often preferred as whatever is contained within the droplets (perhaps chemical reactants or biological material) is not contaminated by the presence of an electrolyte.

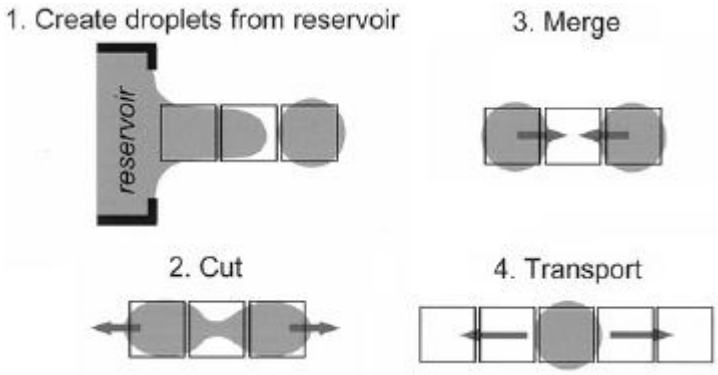

Figure 16|[Taken from Kim[46]] Illustration of the four fundamental droplet operations needed in microfluidics. The operations are controlled by the switching on or off of the discrete electrodes.

1.5.4 Other applications

Unusual uses of electrowetting include: the use of high frequency AC electrowetting of an air bubble as a means of underwater propulsion;[47,48] an electrowetting beam deflector which, through the use of multiple electrodes, can control the angle of a flat meniscus;[49] miniaturized ultrasound scanners;[50] and liquid-state field-effect transistors which work by electrowetting between competitive insulating and conducting fluids to control the on/off current.[51]

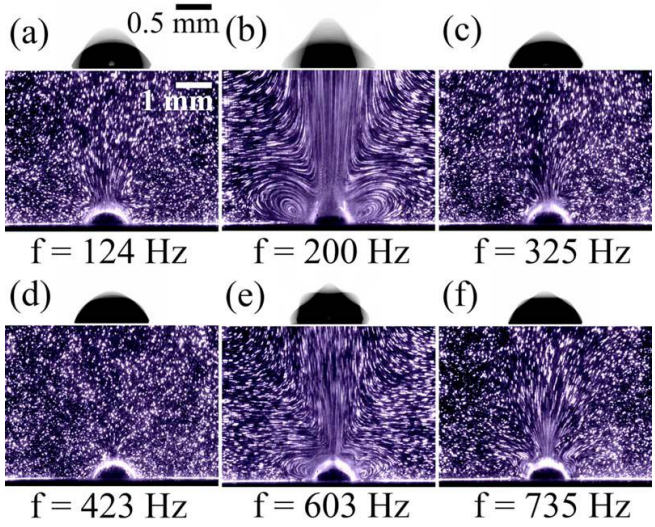

Figure 17 | [Taken from Kang[24]] Streamlines and oscillation patterns for oscillating bubbles at different frequencies. Bubble volume = 1 μL and V_{RMS} = 80 V.

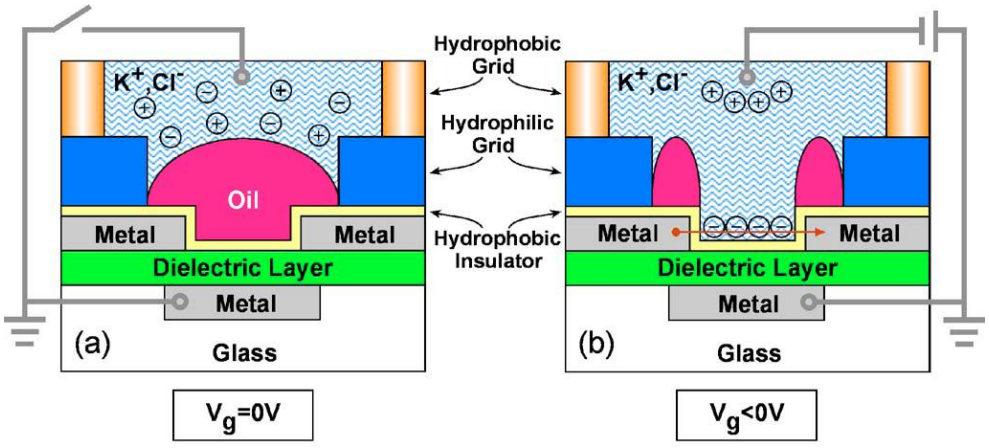

Figure 18 | [Taken from Kim[51]] Illustration of the principle behind a liquid-state field-effect transistor, or LiquiFET. It operates with a 2.5-3 V drain voltage with on/off current ratios greater than 10000:1.

1.6 Conclusions

While electrowetting has a long history starting with Lippmann in 1875, it is only fairly recently that it has made the transition from being a phenomenon of purely fundamental interest to becoming a practical technology. This is done by companies such as Liquavista who

now produce electrowetting displays. These displays, along with other current applications, are based on EWOD, which enables the fast and reliable manipulation of liquid droplets. Nonetheless, EWOD requires a large voltage to work, increasing the power consumption of these devices.

Recently, electrowetting with ITIES has been shown to enable droplet manipulation on solid surfaces using much lower voltages. However, this is not without issue as the droplets are 'pinned', limiting the control over droplet shape. Despite efforts to alleviate this issue using a 'voltage pulsing' technique; fast, reproducible droplet shapes are still not possible.

The hope of this thesis is that the ITIES electrowetting phenomenon might be better understood both at a practical and fundamental level. The primary obstacle to IITES electrowetting is pinning, and the following chapters describe methods to try to reduce this. These methods range from producing ultra-flat surfaces, to creating fluorinated, yet conductive, electrodes. Furthermore, as ITIES electrowetting is still a relatively unstudied phenomenon, the effect of the aqueous phase electrolyte and droplet composition is also studied, with some unexpected results. Another issue, the stability of the liquid|liquid interface, is also resolved. All of these effects are finally brought together to create an optimised low voltage electrowetting system.

1.7 References

1 Adamson, A. W. & Gast, A. P. *Physical Chemistry of Surfaces*. 6th edn, (John Wiley & Sons, Inc., 1997).

2 Cassie, A. B. D. & Baxter, S. Wettability of Porous Surfaces. *Transactions of the Faraday Society* **40**, 546-551 (1944).

3 Daniel, S., Chaudhury, M. K. & de Gennes, P. G. Vibration-actuated Drop Motion on Surfaces for Batch Microfluidic Processes. *Langmuir : the ACS journal of surfaces and colloids* **21**, 4240-4248 (2005).

4 Adamson, A. W. *Physical Chemistry of Surfaces*. 5th edn, (John Wiley & Sons, Inc., 1990).

5 de Gennes, P. G. The Dynamics of Reactive Wetting on Solid Surfaces. *Physica A: Statistical Mechanics and its Applications* **249**, 196-205, doi:10.1016/s0378-4371(97)00466-4 (1998).

6 Lippmann, G. Relation entre les Phénomènes Électriques et Capillaires. *Ann. Chim. Phys.* **5**, 494-549 (1875).

7 Frumkin, A. N., Kabanow, B. & Nekrasow, M. Kapillarelektrische Erscheinungen und Benetzung von Metallen durch Elektrolytlösungen. *I. Phys. Z. Sovijetunion* **1**, 255-284 (1932).

8 Mugele, F. & Baret, J.-C. Electrowetting: From Basics to Applications. *Journal of physics. Condensed matter* **17**, R705 (2005).

9 Cousens, N. E. A. *Shape Changing Liquid Droplets*, Imperial College London, (2009).

10 Beni, G. & Hackwood, S. Electro-wetting Displays. *Applied physics letters* **38**, 207-209 (1980).

11 Beni, G., Hackwood, S. & Jackel, J. L. Continuos Electro-wetting Effect. *Applied physics letters* **40**, 912-914 (1982).

12 Jackel, J. L., Hackwood, S. & Beni, G. Electro-wetting Optical Switch. *Applied physics letters* **40**, 4-6 (1982).

13 Sondag-Huethorst, J. A. M. & Fokkink, L. G. J. Potential-dependent Wetting of Octadecanethiol-modified Polycrystalline Gold Electrodes. *Langmuir* **8**, 2560-2566, doi:10.1021/la00046a033 (1992).

14 Sondag-Huethorst, J. A. M. & Fokkink, L. G. J. Potential-Dependent Wetting of Electroactive Ferrocene-Terminated Alkanethiolate Monolayers on Gold. *Langmuir* **10**, 4380-4387, doi:10.1021/la00023a074 (1994).

15 Gorman, C. B., Biebuyck, H. A. & Whitesides, G. M. Control of the Shape of Liquid Lenses on a Modified Gold Surface Using an Applied Electrical Potential across a Self-Assembled Monolayer. *Langmuir* **11**, 2242-2246, doi:10.1021/la00006a063 (1995).

16 Vallet, M., Berge, B. & Vovelle, L. Electrowetting of Water and Aqueous Solutions on Poly(ethyleneterephthalate) Insulating Films. *Polymer* **37**, 2465-2470 (1996).

17 Quilliet, C. & Berge, B. Electrowetting: A Recent Outbreak. *Current Opinion in Colloid & Interface Science* **6**, 34-39, doi:10.1016/s1359-0294(00)00085-6 (2001).

18 Maillard, M., Legrand, J. & Berge, B. Two Liquids Wetting and Low Hysteresis Electrowetting on Dielectric Applications. *Langmuir* **25**, 6162-6167, doi:10.1021/la804118y (2009).

19 Hayes, R. A. & Feenstra, B. J. Video-speed Electronic Paper Based on Electrowetting. *Nature* **425**, 383-385 (2003).

20 Kuiper, S. & Hendriks, B. H. W. Variable-focus Liquid Lens for Miniature Cameras. *Applied physics letters* **85**, 1128-1130 (2004).

21 Berry, S., Kedzierski, J. & Abedian, B. Low Voltage Electrowetting Using Thin Fluoroploymer Films. *Journal of colloid and interface science* **303**, 517-524 (2006).

22 Monroe, C. W., Daikhin, L. I., Urbakh, M. & Kornyshev, A. A. Principles of Electrowetting with Two Immiscible Electrolytic Solutions. *Journal of physics. Condensed matter* **18**, 2837-2869 (2006).

23 Markin, V., Volkov, A. & Volkova-Gugeshashvili, M. Structure of Nonpolarizable Water/nitrobenzene Interface: Potential Distribution, Ion Adsorption, and Interfacial Tension. *The journal of physical chemistry. B* **109**, 16444-16454 (2005).

24 Flatté, M., Kornyshev, A. & Urbakh, M. Nanoparticles at Electrified Liquid-liquid Interfaces: New Options for Electro-optics. *Faraday discussions* **143**, 109-115 (2009).

25 Reymond, F., Fermin, D., Lee, H. & Girault, H. Electrochemistry at Liquid|Liquid Interfaces: Methodology and Potential Applications. *Electrochimica Acta* **45**, 2647-2662 (2000).

26 Vanysek, P. & Ramirez, L. Interface between Two Immiscible Liquid Electrolytes: A Review. *Journal of the Chilean Chemical Society* **53**, 1455-1463 (2008).

27 Monroe, C., Daikhin, L., Urbakh, M. & Kornyshev, A. Principles of Electrowetting with Two Immiscible Electrolytic Solutions. *Journal of physics. Condensed matter* **18**, 2837-2869 (2006).

28 Monroe, C. W., Daikhin, L. I., Urbakh, M. & Kornyshev, A. A. Electrowetting with Electrolytes. *Physical Review Letters* **97**, 136102 (2006).

29 Monroe, C., Urbakh, M. & Kornyshev, A. The Distinctive Electrowetting Properties of ITIES. *Journal of physics. Condensed matter* **19**, 375113 (2007).

30 Monroe, C., Urbakh, M. & Kornyshev, A. Double-Layer Effects in Electrowetting with Two Conductive Liquids. *Journal of the Electrochemical Society* **156**, P21-P28 (2009).

31 Monroe, C. W., Urbakh, M. & Kornyshev, A. A. Double-Layer Effects in Electrowetting with Two Conductive Liquids. *Journal of the Electrochemical Society* **156**, P21-P28, doi:10.1149/1.2971190 (2009).

32 Conboy, J. & Richmond, G. Examination of the Electrochemical Interface between Two Immiscible Electrolyte Solutions by Second Harmonic Generation. *The journal of physical chemistry. B* **101**, 983-990 (1997).

33 Koczorowski, Z., Paleska, I. & Kotowski, J. Streaming Method Study of Interfaces between Immiscible Electrolyte-Solutions. *Journal of electroanalytical chemistry and interfacial electrochemistry* **235**, 287-298 (1987).

34 Girault, H. & Schiffrin, D. The Measurement of the Potential of Zero Charge at the Interface Between Immiscible Electrolyte-Solutions. *Journal of electroanalytical chemistry and interfacial electrochemistry* **161**, 415-417 (1984).

35 Trojánek, A. n., Lhotský, A., Mareček, V. r. & Samec, Z. Limited Agreement between the Interfacial Tension and Differential Capacity Data for the Polarised Water|1,2-dichloroethane Interface. *Journal of Electroanalytical Chemistry* **565**, 243-250, doi:10.1016/j.jelechem.2003.10.018 (2004).

36 Samec, Z., Lhotský, A., Jänchenová, H. & Mareček, V. r. Interfacial Tension and Impedance Measurements of Interfaces between Two Immiscible Electrolyte

Solutions. *Journal of Electroanalytical Chemistry* **483**, 47-56, doi:10.1016/s0022-0728(00)00051-6 (2000).

37 Kornyshev, A. A. *et al.* Ultra-low-voltage Electrowetting. *The Journal of Physical Chemistry C* **114**, 14885-14890, doi:10.1021/jp101051e (2010).

38 Marinescu, M., Urbakh, M., Barnea, T., Kucernak, A. R. & Kornyshev, A. A. Electrowetting Dynamics Facilitated by Pulsing. *The Journal of Physical Chemistry C* **114**, 22558-22565, doi:10.1021/jp1052634 (2010).

39 Marinescu, M. *Electrovariable Liquid Interfaces for Optical Applications: Structure and Dynamics*, Imperial College London, (2012).

40 Shamai, R., Andelman, D., Berge, B. & Hayes, R. Water, Electricity, and Between ... On Electrowetting and Its Applications. *Soft matter* **4**, 38-45 (2008).

41 Kuiper, S. & Hendriks, B. in *IEEE Spectrum* (2004).

42 Ehrlich, D. *Liquavista Launches Low Power Displays*, <http://www.cleantech.com/news/3716/liquavista-launches-low-power-displays> (2008).

43 Feenstra, J. in *Information Display* Vol. 22 2-5 (2006).

44 Berthier, J. *et al.* Some Examples of Micro-devices for Biotechnology Developed at the Department of Technologies for Life Sciences and Healthcare of the LETI. *International Journal of Nanotechnology* **7**, 802-818 (2010).

45 Jensen, E. C., Bhat, B. P. & Mathies, R. A. A Digital Microfluidic Platform for the Automation of Quantitative Biomolecular Assays. *Lab on a chip* **10**, 685-691 (2010).

46 Cho, S., Moon, H. & Kim, C. Creating, Transporting, Cutting, and Merging Liquid Droplets by Electrowetting-based Actuation for Digital Microfluidic Circuits. *Journal of microelectromechanical systems* **12**, 70-80 (2003).

47 Chung, S. Electrowetting Propulsion of Water-floating Objects. *Applied physics letters* **95**, 014107 (2009).

48 Ryu, K., Zueger, J., Chung, S. & Cho, S. Underwater Propulsion Using AC-Electrowetting-Actuated Oscillating Bubbles for Swimming Robots. *Mems 2010: 23rd Ieee International Conference On Micro Electro Mechanical Systems, Technical Digest*, 160-163 (2010).

49 de Boer, B. Control of an Electrowetting-based Beam Deflector. *Journal of applied physics* **107**, 063101 (2010).

50 Deladi, S. Miniaturized Ultrasound Scanner by Electrowetting. *Applied physics letters* **97**, 064102 (2010).

51 Kim, D. Y. Liquid-state Field-effect Transistors using Electrowetting. *Applied physics letters* **90**, 43507 (2007).

Chapter 2: Liquid|Liquid Interfaces

At the end of Chapter 1 the first experimental results of electrowetting with an interface between two immiscible electrolytes (ITIES) were discussed. In Chapter 2, a major practical concern with this system is addressed: the stability of the ITIES over the range of potentials used for electrowetting. In order to nullify this potential complication, the ITIES electrolytes and solvents were optimised, resulting in a polarisation window in excess of 1.2 V. This ITIES polarisation window optimisation leads into the development of a new type of ITIES, the interface between an ionic liquid and an organic solvent.

2.1 Extending the ITIES polarisation window

2.1.1 Motives

As will be discussed in more detail below, at large potentials an ITIES breaks down as ions begin to cross from one phase to the other. However, for ITIES electrowetting, the value of the potential applied across the liquid|liquid interface is not known. This is because the potential applied to the whole system is shared between the liquid|liquid and solid|liquid interfaces. The Galvani potential difference across the ITIES will be less than the total applied bias, but this may still be a substantial potential. For example, when 1 V is applied to the entire system versus PZC, even if only 10 per cent of this potential is dropped across the liquid|liquid interface, 100 mV can be enough to drive ions across the interface (this can be seen from Figure 8, page 39).

The stability of the ITIES is a concern for at least three reasons. Firstly, the long term stability of the system is paramount: there is no value in an electrowetting system that will cease to function after several hours. Secondly, the transfer of ions between two phases creates a pseudo-capacitance which may cause electrowetting, but not for the putative reasons given in Chapter 1.[1] It is also assumed in the theoretical model of Monroe et al. that the ITIES behaves ideally at all potentials. Finally, transferring ions can precipitate in the opposite phase; this leads to 'hazing' of the interface which interferes with the surface's optical properties.

The potential drop can be estimated theoretically, which, based on the model of Monroe et al., has been done by Marinescu.[2] As illustrated in Figure 19, the potential drop over the ITIES is indeed only a small percentage of the total potential drop between the electrodes. It predicts that by using 0.001 mol dm^{-3} electrolyte in the droplet and 0.5 mol dm^{-3} electrolyte in the aqueous phase, there is a maximum potential drop across the interface of approximately ±150 mV. Therefore, assuming that there are no detrimental effects to the electrowetting response, as large a polarisation window as possible would seemingly be important.

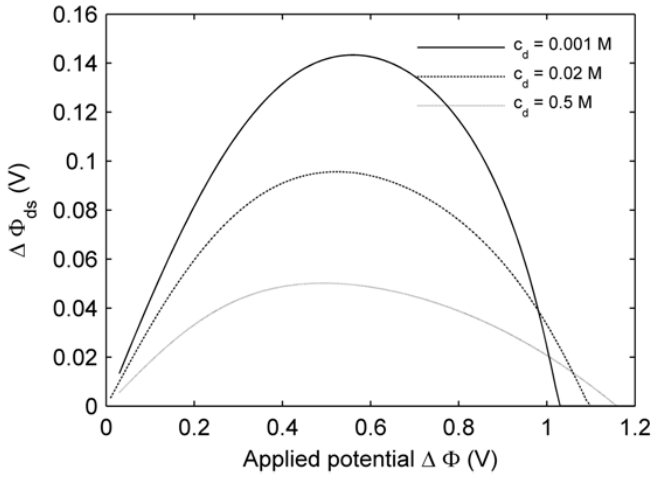

Figure 19|[Taken from Marinescu[2]] Potential across a nonspecific ITIES with monovalent ions as a function of applied system potential where $\Delta\ \Phi_{ds}$ is the potential drop between the droplet and surrounding, c_d is the concentration in the droplet and the concentration in the surrounding phase is 0.5 mol dm^{-3}. It can be seen that the potential across the liquid|liquid interface decreases with increasing droplet electrolyte concentration.

2.1.2 Ion transfer

When a potential is applied across the liquid|liquid interface a back-to-back ionic double layer forms. This is possible because the Gibbs energy of transfer of ions from one phase to the other is prohibitively high. However, as the potential across the interface increases, the Galvani potential difference across the ITIES increases.[3] This potential is defined as:

$$\Delta_o^w \phi = \phi^w - \phi^o \qquad \text{(Equation 9)}$$

where the superscripts *w* and *o* indicate the water and oil phases, respectively, and ϕ is the Galvani potential. With increasing potential difference, it becomes energetically favourable for ions to cross the interface, and the ITIES begins to break down. The Gibbs energy of transfer, $\Delta G_{tr,i}^{\ominus,w\to o}$, of the ions defines the potential at which ion transfer occurs because equilibrium across the interface requires that:

$$\Delta_o^w \phi = \Delta_o^w \phi_{tr,i}^{\ominus} + \frac{RT}{z_i F} ln\left(\frac{a_i^o}{a_i^w}\right) \qquad \text{(Equation 10)}$$

$$\Delta_o^w \phi_{tr,i}^{\ominus} = \frac{\Delta G_{tr,i}^{\ominus,w\to o}}{z_i F} = \frac{\mu_i^{\ominus,o} - \mu_i^{\ominus,w}}{z_i F} \qquad \text{(Equation 11)}$$

here $\mu^{\ominus}_i$ is the chemical potential of ion *i* in the respective phase under reference conditions.[4] Consequently, the Gibbs energy of transfer is an essential parameter to consider when choosing electrolytes. The term $\mu_i^{\ominus,o} - \mu_i^{\ominus,w}$ is roughly equal to the difference in solvation energies of species *i* between the oil and water phases.

Cyclic voltammetry of the liquid|liquid interface is commonly used for determining the size of a polarisation window as it can efficiently detect ion transfer currents arising as a consequence of the applied potential. Close to the PZC, there is no net ion transfer across the interface and only a small current is seen as a result of the charging of the double layers. As the potential moves away from the PZC, eventually a sharp rise in current is seen. This current is a result of inorganic ions moving into the organic phase or organic ions moving into the aqueous phase depending on which is more energetically favourable. Figure 20 below shows a typical cell for this type of work.

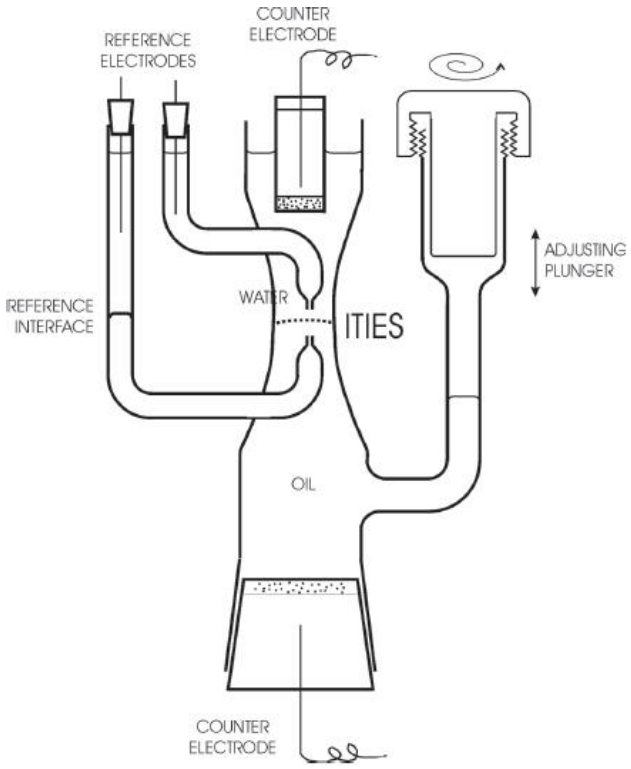

Figure 20|[Taken from Vanýsek[5]] Diagram of a four electrode cell used to study the cyclic voltammetry of an ITIES. The adjusting plunger is used to position the interface between the two reference electrodes. The diameter of the cell where the interface is positioned is kept small (approximately 5 mm) to reduce the total ionic current and minimise resistive losses.[6,7]

The ion transfer currents are governed by the same principles as conventional redox processes at the electrode|solution interface. Usually this is in the mass transport limited domain where electron transfer is fast and the current limiting step is diffusion. The half-wave potential, $E_{1/2}$, of a transferring ion, as measured by cyclic voltammetry, is therefore related to the formal transfer potential of an ion *i*, $E_i^{\theta'}$, by the mass transfer coefficients, m_i, of ion *i* in each phase:

$$E_{1/2} = E_i^{\theta'} - \frac{RT}{z_i F} \ln \frac{m_i^a}{m_i^b} \qquad \text{(Equation 12)}$$

It is usually taken that $\frac{m_i^a}{m_i^b}$ is equal to the reciprocal of the ratio of the viscosities of the respective solvents because these values are difficult and time consuming to measure.[8,9] This way the standard Gibbs energy of transfer of an ion, *i*, can be calculated:[8]

$$\Delta G_{tr,i}^{\ominus,w\to o} = -nFE^{\ominus\prime} \qquad \text{(Equation 13)}$$

This method is convenient when the concentration of the ion of interest is low and hence the peak currents are also low. This is generally the case only when the ion of interest is not the supporting electrolyte, which is required to be more concentrated in order to instil the conductivity of the electrolyte solutions and also prevent migration of ions of the species of interest. The potentials at which the supporting electrolyte transfers are described as the limits of the ITIES polarisation window. Due to the precipitation of ion pairs at the interface when large ion transfer currents are seen, along with the large resulting resistive losses, it is difficult to accurately measure the half-wave potential of supporting electrolyte ions. A non-trivial solution to this, relating the forward and return peak currents to the half-wave potential, has been formulated by Shao et al.[9]

As seen in (Equation 11, the Gibbs energy of transfer depends upon the relative chemical potential of an ion in the aqueous phase and oil phase. The chemical potential is closely related to the solvation energy of the ion as solvation of the ion by other molecules is the primary component of its Gibbs energy. Solvation energies are a net result of a complex interplay between solute and solvent. Nonetheless, three fundamental aspects provide a structured approach to alter the Gibbs energy of solvation and, thus, the polarisation window: the interaction between the ions and water, namely hydrophobicity of the ions in the organic phase and hydrophilicity of the ions in the aqueous phase; interaction between the ions and the organic solvent (that is, the solvation strength of the organic solvent); and many-body interactions such as the salting out effect.[7]

2.1.3 Electrolyte effects

The properties of the electrolytes used in the ITIES are essential in expanding the potential range over which the ITIES is stable. This section discusses what electrolyte properties result in a large window.

The more hydrophobic an ion is, the more it will want to reside in the oil phase and the larger its Gibbs energy of transfer between water and oil will be. Without needing to know what the

actual energy of transfer is, ions that are hydrophobic by intuition can be chosen to try to find an electrolyte with a large polarisation window. Hydrophobicity of organic ions should increase with the ion size and with the inclusion of hydrophobic atoms such as fluorine.[10] This can be seen in a study by Lhotský et al. where the ITIES polarisation window increases as the length of the alkyl chains of a quaternary ammonium ion are increased.[11] Similarly Kontturi et al. have demonstrated this effect using the *p*-[4-chlorotetrakis]tetraphenylborate anion rather than the more common yet related tetraphenylborate anion. The former salt simply substitutes a hydrogen atom on the phenyl ring for a chlorine atom, yet this small change results in a 200 mV or 50 per cent increase in the size of the polarisation window.[12]

The aqueous phase is as important as the organic phase in determining the polarisation window. Aqueous ions should have a very high charge density and solvation energy in water. These include ions such as Li^+, Mg^{2+}, F^- and SO_4^{2-}.

The salting out effect can also be used to increase the polarisation window. This can be understood as the competition for water molecules in the aqueous phase resulting in the exclusion of other ions. For example, in a concentrated solution (2 mol dm^{-3}) of $MgSO_4$ in water there is strong demand for water molecules to solvate and stabilise the highly charged ions. If another ion is introduced, this must be solvated at the expense of $MgSO_4$ ions raising the phase's internal energy. This higher internal energy increases the Gibbs energy of transfer into the aqueous phase, as shown by Schiffrin et al.[7,13] This effect does not show a linear increase in Gibbs energy of transfer with concentration, but begins to have a dramatic effect at a critical concentration. As with traditional salting out phenomena, the effect is more prolific with electrolytes higher in the Hofmeister series.[7,13]

Based on the above criteria, the organic electrolyte studied was bis(triphenylphosphoranylidene) ammonium tetrakis[3,5-bis(trifluoromethyl)phenyl]borate. This electrolyte, shown in Figure 21, is similar to the electrolyte bis(triphenylphosphoranylidene) ammonium tetrakis(pentafluorophenyl) borate commonly used by the group of Girault which has been shown to give large polarisation windows.[14,15] This was compared to tetrabutylammonium tetraphenylborate (TBATPB), the electrolyte which was used for the first electrowetting experiments by Kornyshev et al.[16] A broad range of electrolytes in the aqueous phase were also studied.

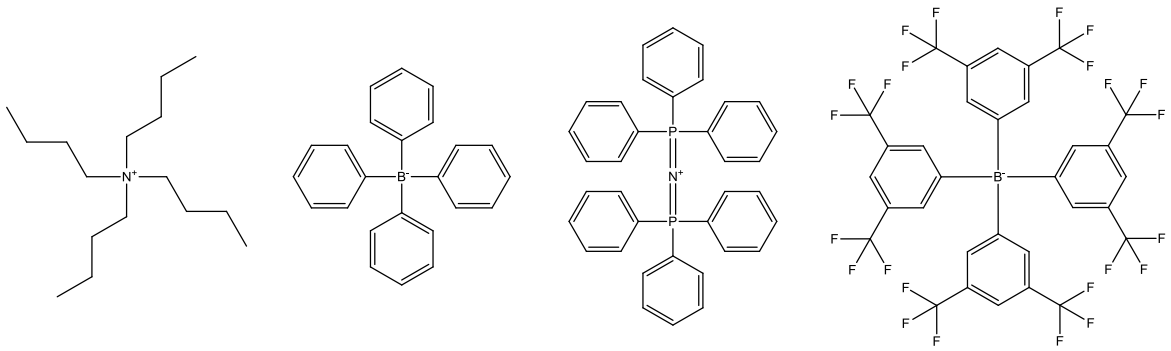

Figure 21|(Left to right) Chemical structure of tetrabutylammonium, tetraphenylborate, bis(triphenylphosphoranylidene)ammonium and tetrakis[3,5-bis(trifluoromethyl)phenyl]borate ions. The two ions on the left, used for the first electrowetting experiments, are clearly smaller than the ions on the right, suggesting they would be less soluble in water and therefore less likely to cross the ITIES.[16]

2.1.4 Solvent effects

It has also been suggested that changing the solvent could be an effective way of increasing the polarisation window.[17] The effect of solvent derives from the fact that ions have different solvation energies in different solvents. For instance, the standard Gibbs energy of transfer of Mg^{2+} from water to nitrobenzene is 64 kJ mol^{-1}, while its transfer from water to 1,2-dichloroethane (DCE) is 114 kJ mol^{-1}.[18] This is why DCE has superseded nitrobenzene (relative permittivities of 10.7 and 34.8 respectively) as the most common ITIES solvent.[19] When choosing an organic solvent there are two constraints: the solvent must be almost totally immiscible with water and must also be able to dissolve organic salts. The solvent 1,6-dibromohexane (DBH) was found to satisfy these criteria while also being very non polar (relative permittivity of only 5.0), potentially restricting transfer of ions from the aqueous phase.[19] Furthermore, cyclohexane (CH) was mixed with DCE to create a 'tailored' solvent. Specifically, pure CH is unsuitable as it will not dissolve organic salts. However, it was found that when it is combined with a better solvent such as DCE, this mixture is able dissolve the desired salt while remaining relatively non-polar, creating a solvent with an ideal blend of properties.

2.1.5 Experimental

The organic electrolyte BTPPATFPB was precipitated from two solutions of BTPPACl (≥98%, Fluka) and NaTFPB (kindly supplied by Prof. T. Kakiuchi, Kyoto University) dissolved in a 1:2 mixture of methanol and water and then recrystallised from hot acetone. TBATPB (≥99%, Sigma), NaCl (≥99.8%, Sigma-Aldrich), LiCl (99.0%, Aldrich), $MgCl_2$ (99.0%, Aldrich), KCl (≥99.5%, Sigma-Aldrich), 37% HCl (reagent grade, Sigma-Aldrich), LiF (≥99.995%, Aldrich), NaF (99.5%, Sigma-Aldrich), $MgSO_4.7H_2O$ (analytical grade, VWR), TMACl (≥99.0%, Fluka), DCE (≥99.0%, Sigma-Aldrich), DBH (98% Acros Organics) and CH (≥99%, Sigma-Aldrich) were used as supplied. Aqueous solutions were prepared with ultrapure water (resistivity 18.2 MΩ cm) from a Millipore Elix 5 water purification system. The temperature of all experiments was 20±2 °C.

The electrochemical cell was a four electrode cell similar in principle to that used by Samec et al. and illustrated in Figure 22.[6] The surface area of the interface was 0.28 cm^2. An oil/water junction (5 mmol dm^{-3} aqueous BTPPACl) with Ag/AgCl wire was used as the reference electrode for the organic phase and an Ag/AgCl wire was used for the aqueous phase. The aqueous phase was doped with tetramethylammonium chloride (TMACl) as a reference for the potential scale of the Galvani potential difference ($\Delta^o_w \varphi$ [TMA^+] = 160 mV).[20]

A Gamry Reference 600 potentiostat was used to study the cyclic voltammetry of the liquid|liquid interface. The scan rate was 10 mV s^{-1}. The positive and negative potential limits of the scans were determined by the potential at which a current of 1 μA cm^{-2} was measured. The cyclic voltammograms (CVs) reported here are the tenth scan. Following initial variations in current, after about five scans the CVs would remain constant.

The relative permittivity of the mixed solvent was measured using a homemade capacitance cell and a Solartron 1260 Impedance Analyser. The cell consisted of two parallel glass slides (75mm×25 mm) sputtered with gold, separated by two glass coverslips (approximately 340 μm). A range of solvents with relative permittivities similar to that of the mixed solvent were used to calibrate the cell.

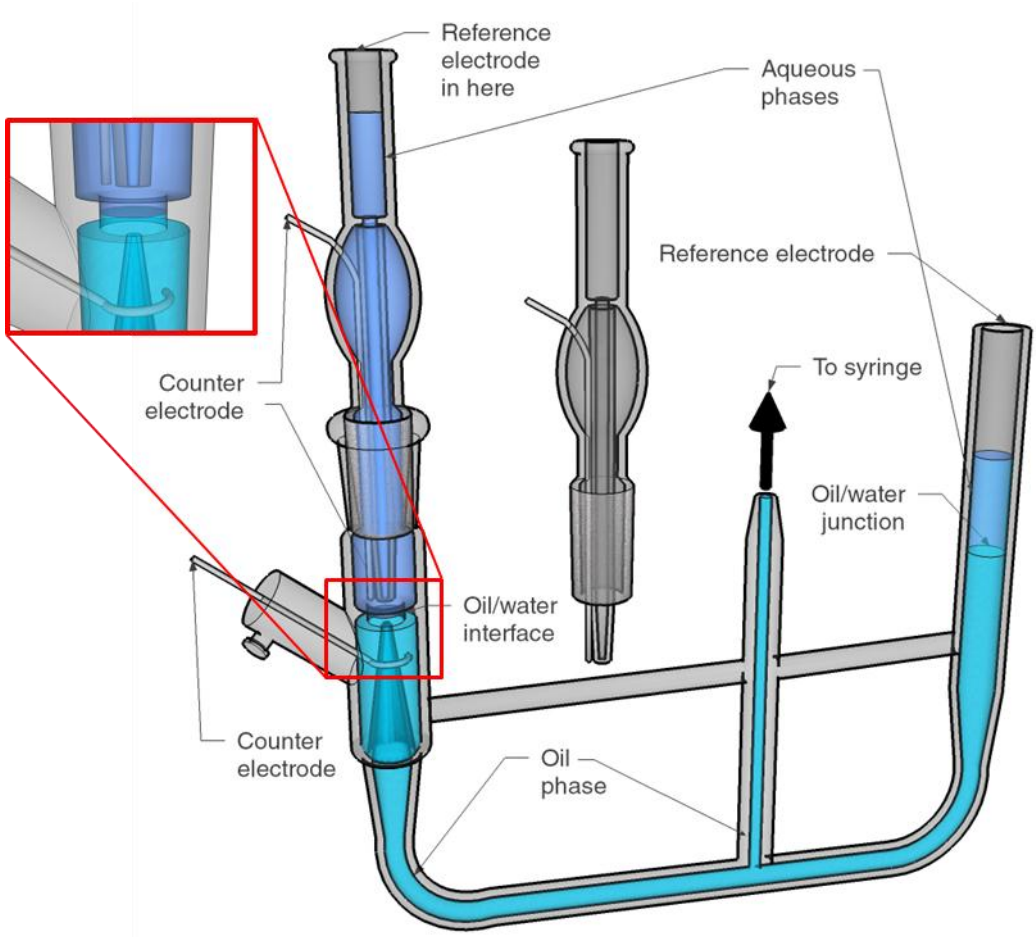

Figure 22 | Experimental cell for characterising the electrochemical window of an ITIES.

2.1.6 Results and discussion

2.1.6.1 Hydrophobicity of the organic ions

First the effectiveness of BTPPATFPB compared to TBATPB was established. The use of this very bulky organic electrolyte had the desired effect in that the polarisation window was increased from about 200 mV to 700 mV (Figure 23). The potential limits throughout were arbitrarily defined as the potential at which the current rises to ± 1 μA cm^{-2}. This suggests that the ITIES between TBATPB and NaCl is limited by the transfer of TBA^+ and TPB^- ions. This was confirmed when the salt in the aqueous phase (NaCl) was changed to a more hydrophilic salt (such as LiF) and there was no effect on the potential limits. Conversely,

varying the organic salt does vary the potential limits. As is seen in the next section, when BTPPATFPB is used, the window becomes dependant of the salt in the aqueous phase.

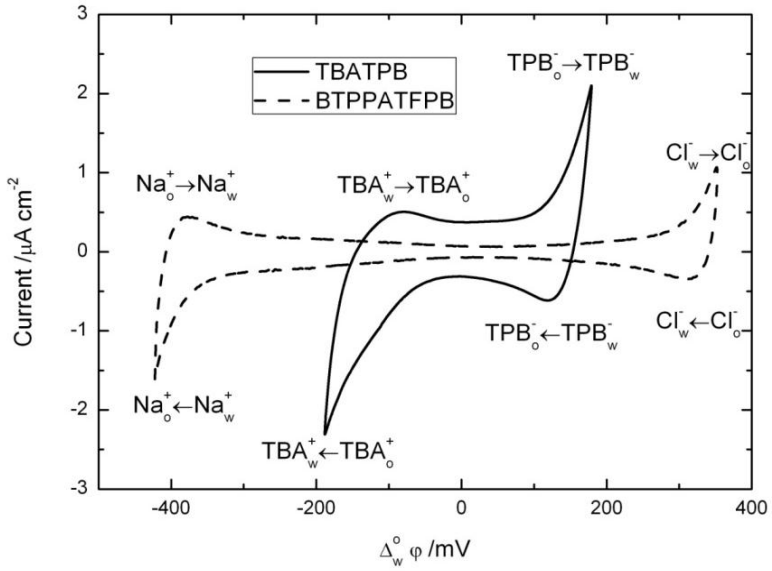

Figure 23|Illustration of the effect of using 1 mmol dm^{-3} BTPPATFPB in the DCE organic phase rather than TBATPB, also 1 mmol dm^{-3}, which contains much smaller ions. The electrolyte in the aqueous phase is 5 mmol dm^{-3} NaCl. Scan rate = 10 mV s^{-1}. The flat regions of the cyclic voltammograms indicate where the ITIES is stable.

2.1.6.2 Hydrophilicity of the aqueous ions

When the extremely hydrophobic BTPPATFPB is in the organic phase, it can be seen that the potential limits change as the aqueous electrolyte is varied (Figure 24, Table 1). This suggests that the potential limits are defined by the inorganic salt rather than the organic salt.[i] Figure 24 shows the windows for NaCl, LiF and $MgSO_4$. Unsurprisingly, at negative potentials Mg^{2+} transfers after Na^+ and Li^+ because it is bivalent and therefore has a higher charge density. At positive potentials, the monovalency of F^- seems to be balanced by its small radius while the bivalency of SO_4^{2-} is counteracted by its larger radius and both transfer at the same potential. It follows that the larger monovalent chloride ion transfers at a lower potential.

[i] It is still possible that the transfer of $MgSO_4$ ions ($MgSO_4$ shows the largest polarisation window) is limited by the organic electrolyte. However, as will be seen later, results from salting out using $MgSO_4$ seem to imply that this is not the case.

As well as illustrating the trend in hydrophilicity of these ions and showing that the aqueous electrolyte does indeed have a significant effect on the polarisation window, these particular salts are highlighted because they were found to give the largest windows for a chloride salt, a monovalent salt and a bivalent salt. The chloride salt, although it has the smallest window, is useful because it can be used with a small and convenient Ag/AgCl wire reference electrode. LiF provides the largest window for a monovalent electrolyte, for which the ITIES electrowetting model has been derived. Furthermore, fluoride is preferable to chloride because it does not specifically adsorb onto gold, a potential complication when using chloride (for electrowetting in particular). $MgSO_4$ provides the largest window although an ITIES electrowetting system with bivalent ions has not yet been modelled.

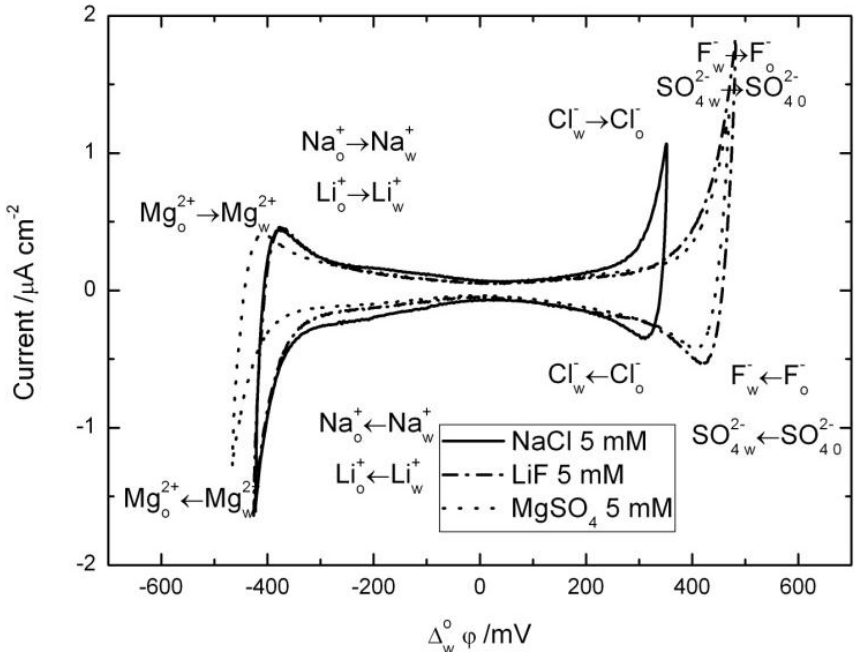

Figure 24|CVs of 5 mmol dm^{-3} NaCl, LiF or $MgSO_4$ in water with 1 mmol dm^{-3} BTPPATFPB in DCE. Scan rate = 10 mV s^{-1}. The Galvani potential differences ($\Delta^{o}_{w}\varphi$) have been calculated by using the standard transfer potential of the TMA^+ ion ($\Delta^{o}_{w}\varphi$=160 mV) as a reference.

If the window is limited by inorganic ions as seems to be the case, this puts a fundamental limit on the window size. This is because there are no suitable ions with a greater charge density than the likes of Li^+, Mg^{2+}, F^- and SO_4^{2-}. While ions such as Al^{3+} or Be^{2+} do have a

higher charge density, they strongly affect the solution pH (for example $AlCl_3$ forms HCl in water) meaning that H_3O^+ and OH^- ions start to limit the window instead. In the next section, to further increase the window, the organic solvent is changed to raise the energy of these ions in the phase they transfer to.

2.1.6.3 Organic solvent

In order to further extend the polarisation window beyond the limits seen above, rather than changing the ions, the organic phase was changed. As has already been noted, solvent has a very significant effect on the standard Gibbs energy of transfer of an ion. The two solvents chosen to replace DCE were DBH and a 1:1 mixture of DCE and CH. DBH has a relative permittivity of 8.5 and the relative permittivity of the mixture was measured to be 5.1 ±0.1.[21] These values are lower than the relative permittivity of DCE, yet crucially, they also dissolve BTPPATFPB (concentrations >10 mmol dm^{-3} at room temperature are possible in the mixed solvent).

Figure 25 shows the polarisation windows resulting from the mixed DCE:CH solvent. There is a substantial increase in the size of the windows for all electrolytes tested. Taking $MgSO_4$ as an example, compared to DCE the window increases from 911 mV to 1208 mV, an increase of over 30 per cent. Furthermore, this window is believed to be largest window reported in the published literature.[22]

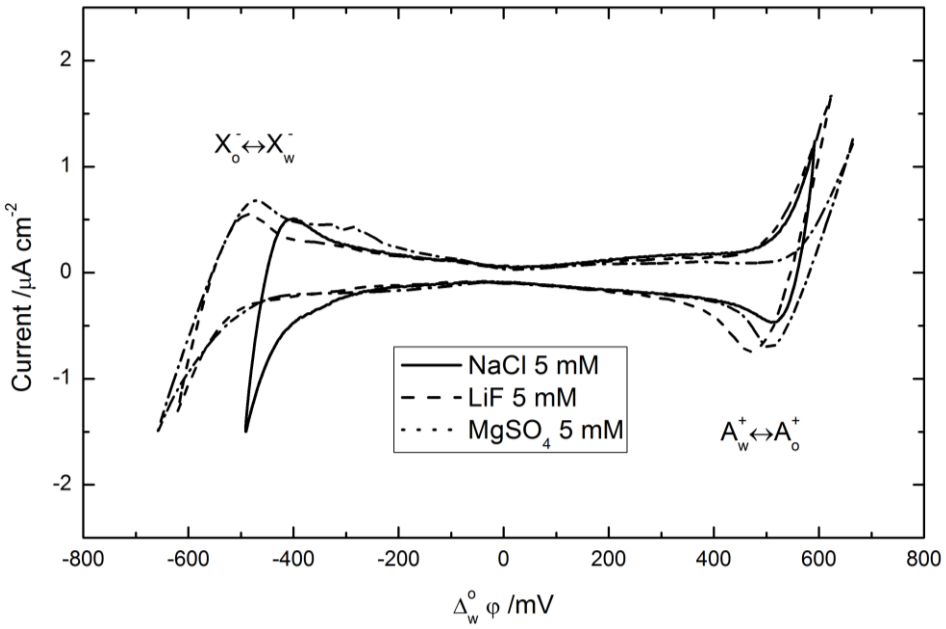

Figure 25 | CVs of the same system used in Figure 24 but with an organic phase consisting of a 1:1 volume mixture of DCE and cyclohexane. Scan rate = 10 mV s^{-1}. The maximum currents result from the same ion transfers shown in Figure 24.

From the CVs in Figure 26, the actual free energies of transfer, $\Delta G_{tr}^{\theta',w\rightarrow o}$, of Mg^{2+} and SO_4^{2-} were calculated. These CVs, rather than the ones in Figure 25, were used because the currents are larger, making the curve fitting method of Shao et al. more reliable.[9] This method involves the fitting of working curves relating the quotient of the end-of-scan and return peak currents to the quotient of the return peak potential and half-wave potential. The half-wave potential can then be used to calculate the Gibbs energy of transfer (Equation 12). Upon moving from DCE to mixed DCE:CH, $\Delta G_{tr}^{\theta',w\rightarrow o}[Mg^{2+}]$ rose from 114 kJ mol^{-1} to 116 kJ mol^{-1} (less than the estimated error and therefore not statistically significant) while $\Delta G_{tr}^{\theta',w\rightarrow o}[SO_4^{2-}]$ rose from 98 kJ mol^{-1} to 113 kJ mol^{-1}. This implies that the solvation energy of SO_4^{2-} is affected by the solvent much more than the solvation energy of Mg^{2+}. This corresponds to a total increase of 17 kJ mol^{-1}, although the error in each value is estimated at ±2 kJ mol^{-1} due to the error in the position of the PZC. These values are in agreement with current literature values.[23]

The PZC itself is located using the interfacial capacitance data, also shown in Figure 26, as measured by impedance spectroscopy. According to Debye-Hückel theory, the PZC is at the capacitance minimum, providing a different method for finding the PZC (the other method

being the use of an ion with an established transfer potential, in this case TMA^+).[8] The capacitance minimum as determined by both methods were within 10 mV of each other. Using the PZC as determined by impedance spectroscopy, the TMA^+ transfer potential in mixed DCE:CH, $\Delta G_{tr}^{\theta',w\rightarrow o}[TMA^+]$, was calculated as 232±10 mV. The error arises from the broad capacitance minimum which does not allow precise determination of the PZC. For future experiments, this value—which, as expected, is larger than the value for pure DCE—can now be used to locate the PZC in DCE:CH without having to use impedance spectroscopy, a substantially more time consuming and complex method.

The capacitance at the PZC decreases from 3.57 μF cm^{-2} for pure DCE to 3.25 μF cm^{-2} for mixed DCE:CH. The capacitance about the PZC is also substantially lower for the mixed solvent. In accordance with double layer theory, this decrease would be expected due to the lower relative permittivity of the mixed solvent relative to pure DCE.

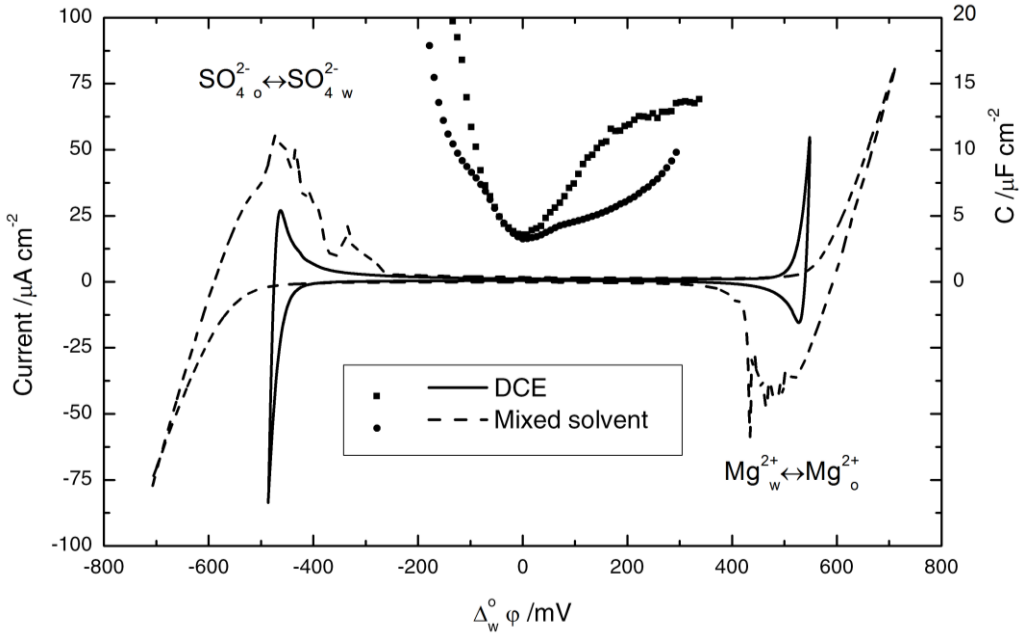

Figure 26|CVs of the same system used in Figure 24 for $MgSO_4$ in DCE and mixed DCE:CH. The scans are over a broader potential range and hence the transfer currents are larger. These large peaks are better suited to the curve fitting method of Shao et al. used to measure the Gibbs energy of transfer of the related ions. At these large currents the fine structure of the double layer current is not seen. The sharp features of the return peaks for the mixed solvent are characteristic of solvent transferring back across the interface along with the ions.[9] The capacitance of the interface about the PZC is also shown.

On the other hand, the DBH decreases the size of the window when compared with DCE, despite having a much lower relative permittivity. This is fairly surprising as a lower relative permittivity solvent is often a poorer solvent for highly charge ions.[24,25] Furthermore, from Table 1 (which shows the polarisation windows of all solvent/electrolyte combinations studied) it can be seen that with a DBH organic phase, LiF has a substantially larger polarisation window than $MgSO_4$. This is the opposite of what is seen for a DCE or mixed solvent organic phase, perhaps suggesting that there is a different mechanism of solvation in DBH compared to the other solvents.

2.1.6.4 Salting out effect

Finally, the salting out effect was investigated. This has previously been used to increase the size of the polarisation window.[7,13] However, the polarisation window needs to be limited by

the transfer of organic ions (such as when TBATPB is used) for salting out to have an effect. Therefore, salting out should not be possible for the system under study which has been shown to be limited by the transfer of aqueous ions.

At first Figure 27 confirms that the window limits are defined by the inorganic rather than the organic ions. This is because increasing the $MgSO_4$ concentration from 5 mmol dm^{-3} to 50 mmol dm^{-3} decreases the size of the polarisation window (increases the current at smaller potentials in accordance with the Butler-Volmer equation). However, the window for 2 mol dm^{-3} $MgSO_4$ is larger than for 5 mmol dm^{-3} $MgSO_4$. This is unexpected because previous results indicate that the inorganic ions are transferring into the organic phase, so increasing the aqueous phase concentration cannot 'salt out'. Therefore, the origin of this effect is currently not known.

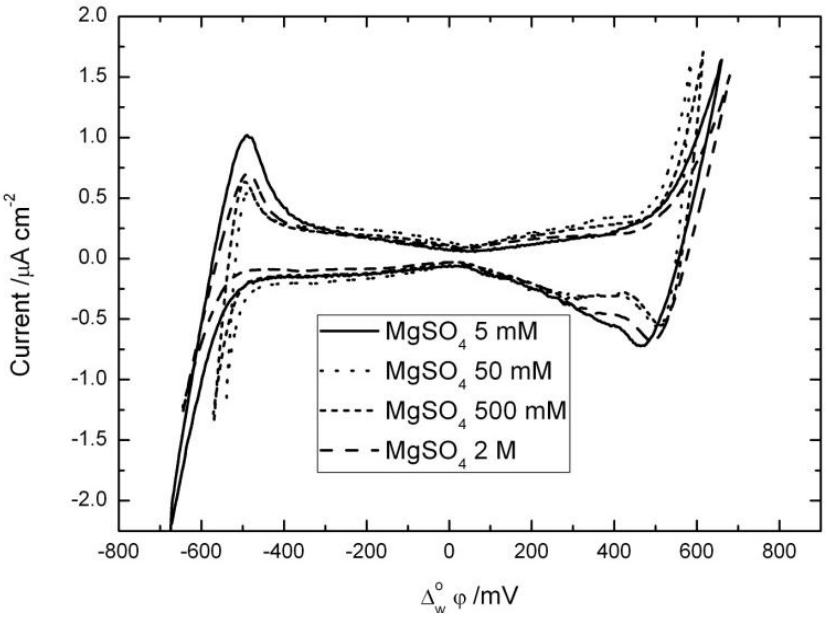

Figure 27|CVs illustrating the effect of varying the concentration of $MgSO_4$ with an organic phase of 1:1 volume mixture of DCE and cyclohexane. Scan rate = 10 mV s^{-1}.

Aqueous electrolyte	Concentration /mmol dm^{-3}	Organic solvent	Electrochemical window/mV
HCl	5	DCE	664
KCl	5	DCE	648
LiCl	5	DCE	728
LiF	5	DCE	858
$MgCl_2$	5	DCE	771
$MgSO_4$	5	DCE	911
NaCl	5	DCE	754
NaF	5	DCE	853
LiF	5	1:1 DCE:CH	1172
$MgSO_4$	5	1:1 DCE:CH	1208
$MgSO_4$	50	1:1 DCE:CH	1091
$MgSO_4$	500	1:1 DCE:CH	1134
$MgSO_4$	2000	1:1 DCE:CH	1256
NaCl	5	1:1 DCE:CH	1044
LiF	5	DBH	775
$MgSO_4$	5	DBH	684
NaCl	5	DBH	561

Table 1|Size of polarisation window for different electrolytes. In all cases the organic electrolyte was 1 mmol dm^{-3} BTPPATFPB. The limits are arbitrarily defined as the potential at which the current rises to ± 1 μA cm^{-2}.

2.1.7 Other applications

The relevance of this work to electrowetting will be further explored in Chapter 5. However, it also has application for other uses of ITIES where the size of the polarisation window is of importance such as for the reversible adsorption of nanoparticles at an ITIES. The larger the window the larger the potential that can be applied to the system creating a stronger driving force for adsorption/desorption of the nanoparticles. More details can be found in [26] and [27].

2.2 The ionic liquid|oil interface

2.2.1 Background

Interest in ionic liquids (ILs) stems from their unique combination of properties. These include very low vapour pressure, high polarity, electrochemical and thermal stability, and reasonable electrical conductivity. In particular, low melting point ionic liquids—so called room temperature ILs—are of interest for practical applications such as solvents for electroplating of base metals and as electrolytes for batteries, capacitors and electrochromic devices.[28] Furthermore, their polarity means that they are often 'greener' alternatives to organic solvents for chemical synthesis.[29]

Most ILs, being very polar, are hydrophilic and will absorb large amounts of water if exposed to the atmosphere. However, if the ionic liquids contain large ions, often with fluorinated side chains and functional groups, they become immiscible with water. By studying the transfer of the ions in such ionic liquids, Quinn et al. were able to quantify the hydrophobicity of these ions.[30] This in turn is useful for the 'task specific design' of ILs, particularly as extraction solvents for synthesis where hydrophobic ILs are particularly useful.

As discussed above, an ITIES consists of two immiscible liquids which are traditionally water and an organic solvent such as DCE or nitrobenzene.[31] Using these hydrophobic ILs, Kakiuchi has been able to make a polarisable water|IL interface, analogous to a conventional ITIES with the organic phase replaced by an IL. The largest window for such an ITIES appears to be around 300 mV for tetraoctylammonium nonafluorobutylsulfonyltrifuluromethylsulfonylimide at room temperature while at 60 °C, tetraheptylammonium tetrakis[3,5-bis(trifluoromethyl)phenyl]borate exhibits a window of 1.1 V at a micro interface.[32-34] With a window of at least 200 mV, it is possible to study the transfer of ions from the aqueous phase into the IL phase and to measure their free energies of transfer.

The size of the polarisable window can be used to quantify the hydrophobicity of the IL, where large windows indicate a high degree of hydrophobicity. The size of the window is related to the solubility of the IL in water:[35]

$$\ln K_{sp}^{w} = \frac{F}{RT}\left(\Delta_{IL}^{w}\phi_{C^+}^{\ominus} - \Delta_{IL}^{w}\phi_{A^-}^{\ominus}\right) \qquad \text{(Equation 14)}$$

$$K_{sp}^{w} = c_{C^+}^{w}\, c_{A^-}^{w} \qquad \text{(Equation 15)}$$

where K_{sp}^{w} is the solubility product in water, $\Delta_{IL}^{w}\phi^{\ominus}$ is the standard ion transfer potential, c^{w} is the aqueous concentration and subscript $C^+$and A^- are the anion and cation respectively. Therefore, this is a convenient method to accurately measure the miscibility of the two phases and assess the suitability of certain ILs as biphasic solvents.

In this section, it is shown for the first time that a hydrophilic ionic liquid can be used to replace the aqueous phase if a suitable organic solvent is used.

2.2.2 Choosing the solvent and ionic liquid

As discussed above, the aqueous phase of a polarisable ITIES contains an inorganic electrolyte, such as NaCl, which consists of small ions with a high charge density while the organic phase contains an electrolyte comprising larger ions with less localized charge such as tetrabutylammonium tetraphenylborate. Hydrophobic ILs themselves are similar in that they often consist of ions such as those in the organic phase because these large asymmetric ions pack together poorly giving them their characteristically low melting points. This means that hydrophobic ionic liquids are a good substitute for the organic phase as they are immiscible with water and their constituent ions have high free energies of transfer into water, resulting in a polarisable ITIES. Their large size also means that many of them conveniently form low melting points ILs.

On the other hand, when replacing the aqueous phase with an IL, it might seem sensible to use an IL that contains the ions used in a conventional ITIES aqueous phase. However, these ions are small and form high melting point solids. Therefore, a compromise must be made: the IL must be molten at room temperature but the ions must still be as small and highly charged as possible. Three RTILs that fit these criteria were chosen. These were ethylammonium nitrate (EAN), 1-butyl-3-H-imidazolium nitrate ($BHImNO_3$) and 1-hexyl-3-methylimidazolium chloride (HeMImCl) which melt at 12 °C, 26 °C and 5 °C respectively.[36-38] Their chemical structures are shown in Figure 28. For an IL, EAN contains very small, high charge density ions. It is known as a 'protic' IL as it is prepared by protonation of a pure Brønsted base by a pure Brønsted acid.[39] The imidazolium ions in $BHImNO_3$ and HeMImCl are somewhat larger and might not be expected to have high free energies of transfer; however, they form ILs with low melting points. This means there is more flexibility when choosing the counter ions—in this case chloride and nitrate—which should have high transfer energies. Nonetheless, as will be seen below, the careful choice of these ILs was not sufficient to make a polarised ITIES. Using DCE, currently the most common ITIES organic phase solvent, large currents were seen at all potentials and the interface could not be polarised.

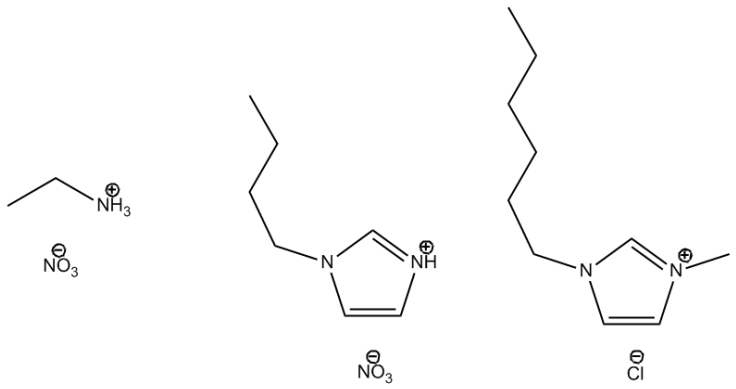

Figure 28|(Left) Ethylammonium nitrate, EAN. (Middle) 1-butyl-3-H-imidazolium nitrate. (Right) 1-hexyl-3-methylimidazolium chloride.

In Section 2.1.4, it was shown that careful selection of the organic solvent of a conventional ITIES has a significant effect on the transfer potential of aqueous phase ions.[22] This is because the Gibbs energy of transfer depends upon the solvation energies of the ions in the opposite

phase. By using this same mixed solvent, as well as the solvent DBH, the Gibbs energy of transfer of the ions in the ionic liquid could be raised, making a polarised ITIES possible.

Cyclic voltammetry of the liquid|liquid interface was again used to determine the size of the polarisation window. The PZC was also located by impedance spectroscopy.[40]

2.2.3 Experimental

Electrochemical measurements were performed with a Gamry Reference 600 potentiostat with impedance analyser. Liquid|liquid experiments were performed in a custom built glass cell with a similar design to that used by Samec et al. which had been modified to allow reference electrodes to be placed near the interface in order to reduce their impedance.[6] The surface area of the liquid|liquid interface was 28 mm^2. The complete cell was:

$$Ag|AgCl|IL|BTPPATFPB(oil)\ 10\ mmol\ dm^{-3}|AgTFPB|Ag$$

where the oil phase was either DCE, DBH or a 1:1 mixture of DCE and cyclohexane and BTPPATFPB is the organic electrolyte bis(triphenylphosphoranylidene)ammonium tetrakis[3,5-bis(trifluoromethyl)phenyl]borate. In the case of EAN and $HBImNO_3$, 10 mmol dm^{-3} ethylammonium chloride was added to provide a stable reference potential. The low chloride concentration means that its transfer is diffusion limited and so it should not affect the polarisation window.

Preparation of BTPPATFPB is reported elsewhere.[22] HeMImCl (≥97%, Sigma-Aldrich), DBH (98%, Acros Organics), DCE (≥99.0%, Sigma-Aldrich) and CH (≥99%, Sigma-Aldrich) were used as supplied. EAN and $HBImNO_3$ were prepared by equimolar addition at 0 °C of 65% nitric acid (Suprapur, Merck) to 2 mol dm^{-3} ethylamine in tetrahydrofuran (Acros Organics) and 2 mol dm^{-3} 1-butylimidazole (98%, Sigma-Aldrich) in tetrahydrofuran, respectively. All ionic liquids were dried overnight under vacuum at 110 °C to remove water and tetrahydrofuran. The AgTFPB|Ag reference electrode was prepared by anodising a silver wire in a 10 mmol dm^{-3} solution of BTPPATFPB at +1 V for 30 min. All experiments were conducted at 20±2 °C. $BHImNO_3$ was found to be liquid at this temperature despite the literature value of its melting point of 26 °C, possibly due to super cooling of the liquid or incorrect literature melting point.[37]

The impedance at 10 Hz (10 mV amplitude) was measured at 5 mV intervals in order to locate the PZC. At selected potentials, the frequency response from 0.1 Hz to 500 Hz was measured. Higher frequencies resulted in experimental artefacts as reported elsewhere.[41] In order to minimise these artefacts, the impedance of the reference electrodes must be kept as low as possible, meaning that the reference electrode on the organic side must be placed as close as possible to the interface due to the high resistivity of the organic phase.

2.2.4 Results and discussion

2.2.4.1 Cyclic voltammetry

All ITIES using $HBImNO_3$ and HeMImCl could not be polarised and instead showed purely resistive behaviour. However, using EAN with either DBH or mixed DCE:CH, a polarisable ITIES was possible. Figure 29 shows the increase in polarisation window moving from DCE (Figure 29 a) to DBH (Figure 29 b) to mixed DCE/CH (Figure 29 c).

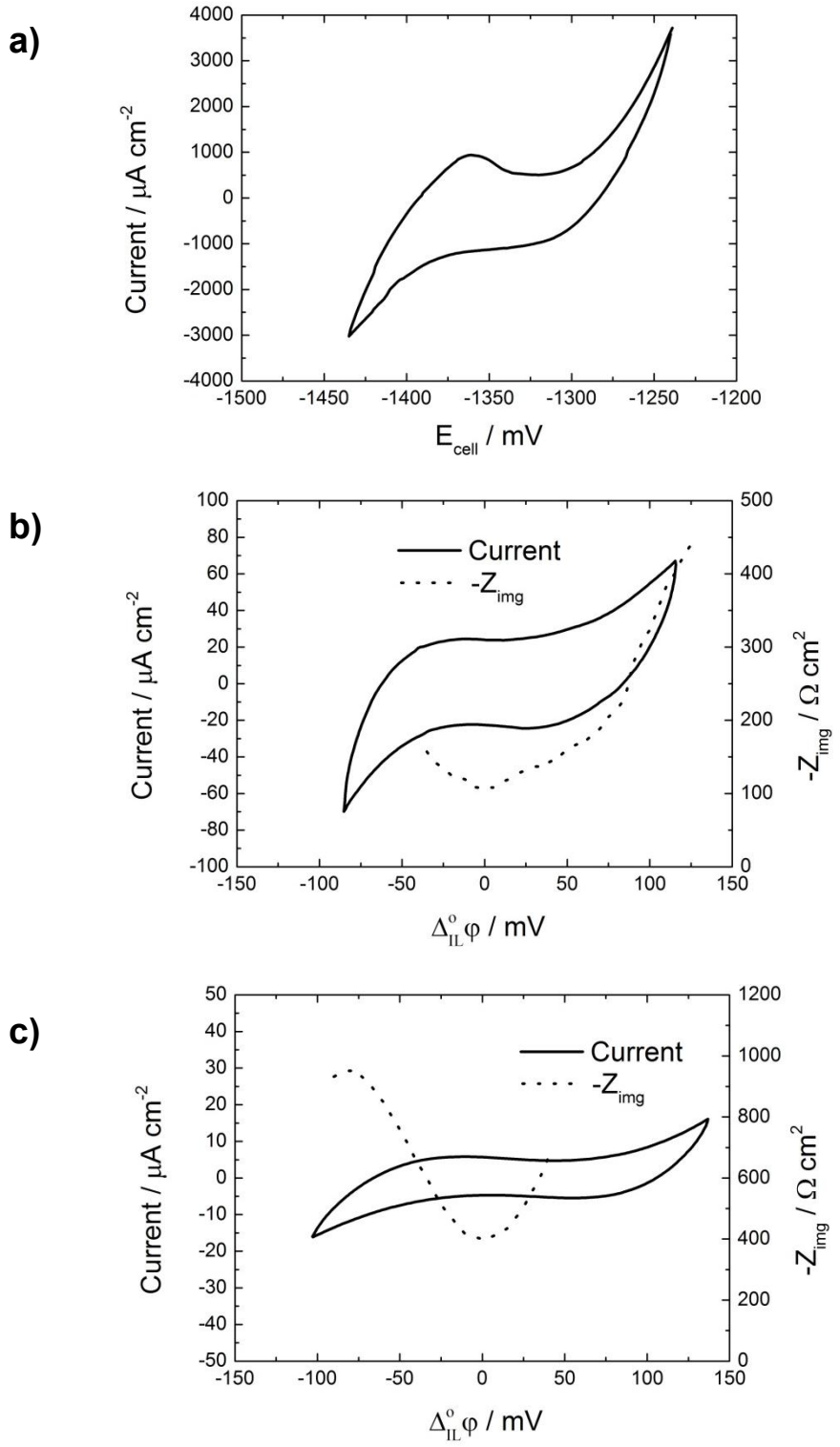

Figure 29|Cyclic voltammograms of the interface between EAN and 10 mmol dm^{-3} BTPPATFPB in various solvents: a) DCE, b) DBH and c) a mixture of DCE and CH. Scan rate 10 mV s^{-1}. Corrected for resistive losses. The imaginary component of the impedance at 10 Hz is also plotted, with the minimum assumed to be the PZC.

With DCE, while there is a small potential range within which the current levels off, the currents are still very large (>500 μA cm^{-2}) and thus cannot be attributed to double layer charging which is usually at least an order of magnitude smaller. Using DBH—which has a relative permittivity of 5.0 as opposed to 10.4 for DCE—clearly broadens the polarisation window and the currents in the middle of the window have dropped to approximately 20 μA cm^{-2}. The Gibbs energy of transfer of the ions has clearly increased. Finally, using the mixed DCE:CH solvent a polarisable window of over 150 mV can be achieved. This is very similar in size to the largest windows between IL and water at 25 °C (although much larger windows have been reported at higher temperatures with high melting point ILs).[32,33,42] It is also large enough to potentially study ion transfer of less hydrophilic ions within the window. The window extends further on the positive side suggesting that the ethylammonium ion has a larger transfer potential than the nitrate ion.

Two conclusions can be drawn from these results. Firstly, the choice of IL is crucial in achieving a polarisable window as out of the three ILs tested, only one of them (EAN) was successful. This is perhaps unsurprising as the imidazolium ion is much larger than the ethylammonium ion and therefore likely to be more soluble in the organic phase. Secondly, the organic solvent is an essential component of this new type of ITIES. It seems that a polarisable ITIES is simply not possible with conventional solvents such as DCE, which is too polar and is able to efficiently solvate the transferring ions.

2.2.4.2 Transfer of doped ions

An ITIES can be doped with extra ions which transfer within the potential limits set by the supporting electrolytes.[4] The ion of interest must have a smaller Gibbs energy of transfer than the supporting electrolyte ions and is usually not very concentrated so that peak currents are kept low. This results in a small peak within the window, even though the supporting electrolyte is higher in concentration.

Many ions were tested to see if they would transfer within the potential limits of the IL ITIES, however, none could be found. The salts tested in the IL phase were tetramethylammonium chloride, tetraoctylammonium chloride and ethylammonium tetraphenylborate at 10 mmol dm^{-3} concentration. The large organic ions in these compounds were expected to have

relatively small energies of transfer into the organic phase; however, no change in the cyclic voltammetry was seen. This is understandable as the transfer potential of tetramethylammonium (an even smaller ion) from water to DCE/CH has previously been calculated as +232 mV, well outside the available window.[22] Similarly, the addition of 0.5 mmol dm^{-3} BTPPACl, $BTPPABF_4$, BTPPATPB to the oil phase had no effect on the voltammetry within the polarisation window, suggesting that the constituent ions of these salts transfer outside of the polarisation window. On the other hand, the addition of 0.5 mmol dm^{-3} $TBAPF_6$, TBABr, BTPPACl and $BTPPABF_4$ meant that the interface could no longer be polarised, as shown in Figure 30. This suggests that the anions in these salts transfer at all potential within the ITIES polarisation window.

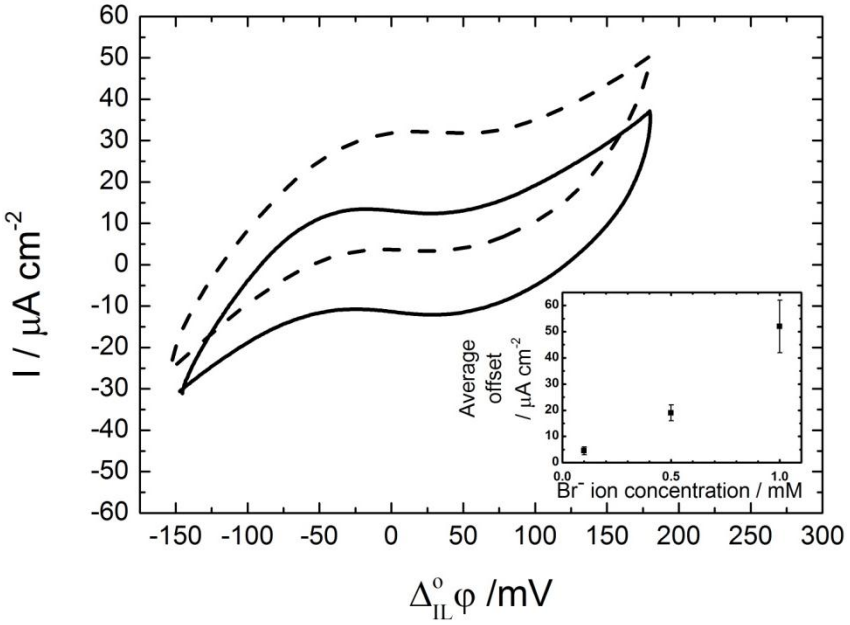

Figure 30|Cyclic voltammogram of the ITIES between EAN and 10 mmol dm^{-3} BTPPATPFB in DCE/CH (solid line). The addition of 0.5 mmol dm^{-3} tetraoctylammonium bromide shifts the cyclic voltammogram of the EAN|mixed solvent ITIES upwards (dashed line). This is the result of the addition of a mass transfer limited current (approximately 20 μA cm^{-2}) due to the transfer of Br^- across the interface. The offset of the voltammogram as a function of Br- ion concentration is also shown (inset).

2.2.4.3 Impedance measurements

Impedance measurements were used to locate the position of the PZC and study the capacitance of the interface. It was found that there was a minimum in the imaginary component of the impedance in the middle of the polarisable window (Figure 29). A minimum in the imaginary component corresponds to a maximum in the interfacial capacitance. This is unusual as for simple electrolyte solutions, a minimum in interfacial capacitance is seen (as described by Guoy-Chapman theory). This minimum in the imaginary component of the impedance, which presumably coincides with the PZC, can be explained by the ionic liquid double layer model of Bazant et al. and has also recently been reported experimentally.[43,44] Figure 31 shows Nyquist and Bode plots for the EAN|mixed solvent ITIES at PZC. The data is fit to a standard Randles circuit (inset).

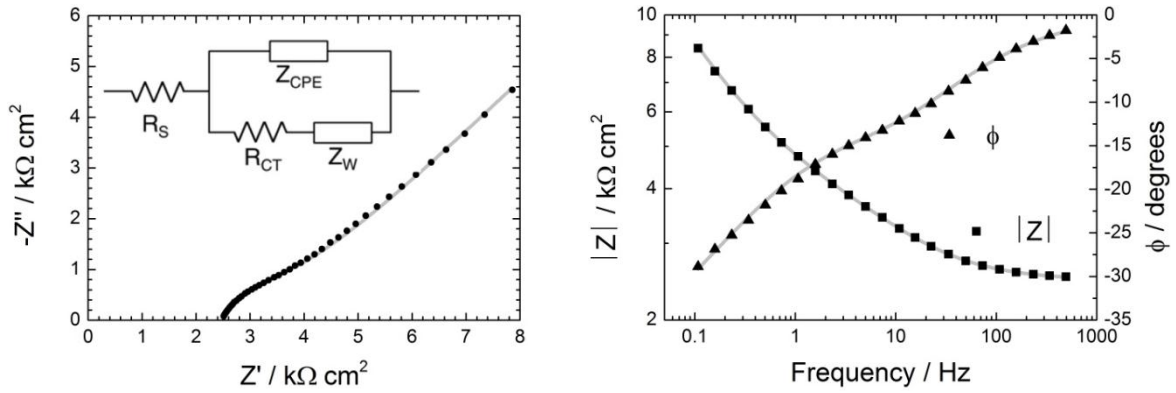

Figure 31|Impedance spectrum of $EtNH_3NO_3$|DCE/CH interface at PZC with an interfacial area of 0.28 cm^2. Scan from 500-0.1 Hz. Fit for Randles circuit shown on graph (grey line). Solution resistance R_S=8.8±0.2 kΩ, charge transfer resistance R_{CT}=5.6±1.7 kΩ, constant phase element Z_{CPE}=9.9±4.1 μS s^n, n=0.71±0.8 and Warburg impedance Z_W=54.9±3.1 μS $s^{0.5}$. This CPE corresponds to an interfacial capacitance of 137±64 μF cm^{-2}.[45]

The interfacial capacitance is calculated to be 137±64 μF cm^{-2}, while fitting a simple capacitor, as is commonly seen in the literature, yields a capacitance of 7.4±3.7 μF cm^{-2}.[40] These values are less than the value calculated using the double layer region from the cyclic voltammetry (400-500 μF cm^{-2}) which suggests that there may still be a small ion transfer current in what would be considered the double layer region. This conclusion is supported by the fairly small

charge transfer resistance of 20.0 kΩ cm^{-2} and the presence of a 45° line on the Nyquist plot indicative of a Warburg element resulting from diffusion of transferring ions.[8]

The Randles circuit with Warburg element also seem to be a good fit for the EAN|DBH ITIES. Figure 32 shows how the Warburg element becomes prominent further from the PZC where there is a large ion transfer current.

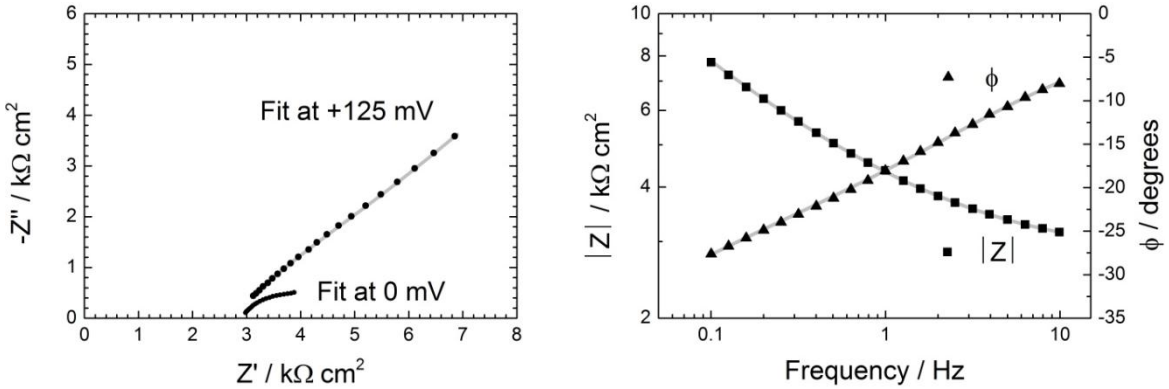

Figure 32|Impedance spectrum of $EtNH_3NO_3$|DBH interface at PZC and +125 mV with an interfacial area of 0.28 cm^2. Scan from 10-0.1 Hz.

2.3 Conclusions

In order to try to increase the polarisable potential window of an ITIES, a range of electrolytes and solvents were studied. It was shown that by using a more polar organic phase (a mixture of DCE and cyclohexane rather than pure DCE), the polarisation window could be increased by over 30%. An aqueous phase containing $MgSO_4$ combined with a mixed solvent organic phase resulted in a polarisable potential window of over 1.2 V.

It is likely that further tailoring of the organic phase, by using other solvents in or different solvent ratios, would lead to even larger potential windows. However, this will be counter balanced by a decrease in electrolyte solubility in the organic phase.

Using this mixed solvent, it was shown for the first time that a polarisable water-free ITIES is possible. A 150 mV polarisation window was achieved which is similar in size to the water|RTIL window at 25 °C of Kakiuchi.[32] This was made possible by the use of the protic ionic liquid ethylammonium nitrate, while other imidazolium based ionic liquid interfaces could not be polarised. Impedance spectroscopy results were fitted to a Randles circuit in order to successfully measure the capacitance of the interface and locate the PZC.

In the future, larger windows may well be possible using similar protic room temperature ILs, such as choline nitrate; by using ILs with higher melting points or by moving to a less polar solvent mixture.[46]

2.4 References

1 Hájková, P., Homolka, D., Mareček, V. & Samec, Z. The Double Layer at the Interface between Two Immiscible Electrolyte Solutions: Capacity of the Water|1,2-dichloroethane Interface. *Journal of electroanalytical chemistry and interfacial electrochemistry* **151**, 277-282, doi:10.1016/s0022-0728(83)80441-0 (1983).

2 Marinescu, M. *Electrovariable Liquid Interfaces for Optical Applications: Structure and Dynamics*, Imperial College London, (2012).

3 Volkov, A. & Deamer, D. *Liquid-Liquid Interfaces Theory and Methods*. (CRC, 1996).

4 Samec, Z. Electrochemistry at the Interface between Two Immiscible Electrolyte Solutions. *Pure and applied chemistry* **76**, 2147-2180 (2004).

5 Vanysek, P. & Ramirez, L. Interface between Two Immiscible Liquid Electrolytes: A Review. *Journal of the Chilean Chemical Society* **53**, 1455-1463 (2008).

6 Samec, Z., Marecek, V. & Homolka, D. Double-Layers at Liquid|Liquid Interfaces. *Faraday discussions of the Chemical Society* **77**, 197-208 (1984).

7 Geblewicz, G., Kontturi, A., Kontturi, K. & Schiffrin, D. Salting Out of Hydrophobic Ions at Immiscible Electrolyte Interfaces. *Journal of electroanalytical chemistry and interfacial electrochemistry* **217**, 261-269 (1987).

8 Bard, A. J. & Faulkner, L. *Electrochemical Methods. Fundamentals and Applications*. 2nd edn, (John Wiley and Sons, 2001).

9 Shao, Y., Stewart, A. A. & Girault, H. H. Determination of the Half-wave Potential of the Species Limiting the Potential Window. Measurement of Gibbs Transfer Energies at the Water/1,2-dichloroethane Interface. *Journal of the Chemical Society, Faraday Transactions* **87**, 2593-2597 (1991).

10 Dalvi, V. & Rossky, P. Molecular Origins of Fluorocarbon Hydrophobicity. *Proceedings of the National Academy of Sciences of the United States of America* **107**, 13603-13607 (2010).

11 Lhotsky, A., Marecek, V., Zalis, S. & Samec, Z. Specific Adsorption of Tetraalkylammonium Cations at the Water|1,2-dichloroethane Interface Revisited. *Journal of electroanalytical chemistry and interfacial electrochemistry* **585**, 269-274 (2005).

12 Berry, S., Kedzierski, J. & Abedian, B. Low Voltage Electrowetting Using Thin Fluoroploymer Films. *Journal of colloid and interface science* **303**, 517-524 (2006).

13 Kontturi, A., Kontturi, K., Murtomaki, L. & Schiffrin, D. Application of Scaled Particle Theory to the Salting Out of Single Hydrophibic Ions. *Journal of the Chemical Society. Faraday transactions* **86**, 931-936 (1990).

14 Fermin, D. J., Dung Duong, H., Ding, Z., Brevet, P.-F. & Girault, H. H. Photoinduced Electron Transfer at Liquid|Liquid Interfaces Part II. A study of the Electron Transfer and Recombination Dynamics by Intensity Modulated Photocurrent Spectroscopy (IMPS). *Physical Chemistry Chemical Physics* **1**, 1461-1467 (1999).

15 Su, B. *et al.* Reversible Voltage-Induced Assembly of Au Nanoparticles at Liquid|Liquid Interfaces. *Journal of the American Chemical Society* **126**, 915-919, doi:10.1021/ja0386187 (2003).

16 Kornyshev, A. A. *et al.* Ultra-low-voltage Electrowetting. *The Journal of Physical Chemistry C* **114**, 14885-14890, doi:10.1021/jp101051e (2010).

17 Koczorowski, Z., Paleska, I. & Geblewicz, G. Electrochemical Study of the Immiscible Electrolyte Solution Interface between Water and a Mixed Organic-Solvent. *Journal of electroanalytical chemistry and interfacial electrochemistry* **164**, 201-204 (1984).

18 Yoshida, Y. *et al.* Evaluation of Gibbs Free Energy for the Transfer of a Highly Hydrophilic Ion from an Acidic Aqueous Solution to an Organic Solution Based on Ion Pair Extraction. *Analytica Chimica Acta* **452**, 149-161 (2002).

19 *Knovel Critical Tables*. 2nd edn, (Knovel, 2008).

20 Abid, J.-P., Abid, M., Bauer, C., Girault, H. H. & Brevet, P.-F. Controlled Reversible Adsorption of Core−Shell Metallic Nanoparticles at the Polarized Water|1,2-Dichloroethane Interface Investigated by Optical Second-Harmonic Generation†. *The Journal of Physical Chemistry C* **111**, 8849-8855, doi:10.1021/jp067181x (2007).

21 *Handbook of Chemistry and Physics*. Vol. 87 (CRC Press, 2006).

22 Cousens, N. E. A. & Kucernak, A. R. Increasing the Potential Window of the Interface between Two Immiscible Electrolyte Solutions to More than 1.2V. *Electrochemistry Communications* **13**, 1539-1541, doi:10.1016/j.elecom.2011.10.015 (2011).

23 Zhou, M., Gan, S., Zhong, L., Su, B. & Niu, L. Ion Transfer Voltammetry by a Simple Two Polarized Interfaces Setup. *Analytical chemistry* **82**, 7857-7860 (2010).

24 Paruta, A. N., Sciarrone, B. J. & Lording. Correlation between Solubility Parameters and Dielectric Constants. *Journal of pharmaceutical sciences* **51**, 704-705 (1962).

25 Gorman, W. G. & Hall, G. D. Dielectric Constant Correlations with Solubility and Solubility Parameters. *Journal of pharmaceutical sciences* **53**, 1017-1020 (1964).

26 Flatté, M., Kornyshev, A. & Urbakh, M. Understanding Voltage-induced Localization of Nanoparticles at a Liquid–liquid Interface. *Journal of physics. Condensed matter* **20**, 073102 (2008).

27 Flatté, M., Kornyshev, A. & Urbakh, M. Nanoparticles at Electrified Liquid-liquid Interfaces: New Options for Electro-optics. *Faraday discussions* **143**, 109-115 (2009).

28 Buzzeo, M. C., Evans, R. G. & Compton, R. G. Non-Haloaluminate Room-Temperature Ionic Liquids in Electrochemistry—A Review. *ChemPhysChem* **5**, 1106-1120, doi:10.1002/cphc.200301017 (2004).

29 Welton, T. Room-Temperature Ionic Liquids. Solvents for Synthesis and Catalysis. *Chemical Reviews* **99**, 2071-2084, doi:10.1021/cr980032t (1999).

30 Quinn, B. M., Ding, Z., Moulton, R. & Bard, A. J. Novel Electrochemical Studies of Ionic Liquids. *Langmuir* **18**, 1734-1742 (2002).

31 Volkov, A. & Deamer, D. *Liquid-Liquid Interfaces: Theory and Methods*. (CRC Press, 1996).

32 Kakiuchi, T. & Tsujioka, N. Cyclic Voltammetry of Ion Transfer Across the Polarized Interface between the Organic Molten Salt and the Aqueous Solution. *Electrochemistry Communications* **5**, 253-256, doi:10.1016/s1388-2481(03)00039-0 (2003).

33 Ishimatsu, R., Nishi, N. & Kakiuchi, T. Wide Polarized Potential Windows at the Interface between Water and an Ionic Liquid, Tetraheptylammonium Tetrakis[3,5-bis(trifluoromethyl)phenyl]borate. *Chemistry Letters* **36**, 1166-1167 (2007).

34 Kakiuchi, T. & Nishi, N. Ionic Liquid/Water Interface: A New Electrified System for Electrochemistry. *Electrochemistry* **74**, 942-948 (2006).

35 Kakiuchi, T., Tsujioka, N., Kurita, S. & Iwami, Y. Phase-boundary Potential Across the Nonpolarized Interface between the Room-temperature Molten Salt and Water. *Electrochemistry Communications* **5**, 159-164, doi:10.1016/s1388-2481(03)00013-4 (2003).

36 Marsh, K. N., Boxall, J. A. & Lichtenthaler, R. Room Temperature Ionic Liquids and their Mixtures - A Review. *Fluid phase equilibria* **219**, 93-98 (2004).

37 Mantz, R. A. *et al. Molten Salts XIV: Proceedings of the International Symposium*. (The Electrochemical Society Inc., 2006).

38 Fendt, S., Padmanabhan, S., Blanch, H. W. & Prausnitz, J. M. Viscosities of Acetate or Chloride-Based Ionic Liquids and Some of Their Mixtures with Water or Other Common Solvents. *Journal of Chemical & Engineering Data* **56**, 31-34, doi:10.1021/je1007235 (2010).

39 Austen Angell, C., Ansari, Y. & Zhao, Z. Ionic Liquids: Past, Present and Future. *Faraday discussions* **154**, 9-27 (2012).

40 Silva, F. & Moura, C. On the Measurement of the Impedance of ITIES - The Nitrobenzene|Water and 1,2-Dichloroethane|Water Interfaces. *Journal of Electroanalytical Chemistry* **177**, 317-323 (1984).

41 Wiles, M. C., Schiffrin, D. J., VanderNoot, T. J. & Silva, A. F. Experimental Artifacts Associated with Impedance Measurements at Liquid—Liquid Interfaces. *Journal of electroanalytical chemistry and interfacial electrochemistry* **278**, 151-159, doi:10.1016/0022-0728(90)85130-w (1990).

42 Nishi, N., Imakura, S. & Kakiuchi, T. Wide Electrochemical Window at the Interface between Water and a Hydrophobic Room-temperature Ionic Liquid of Tetrakis[3,5-bis(trifluoromethyl)phenyl]borate. *Analytical chemistry* **78**, 2726-2731 (2006).

43 Bazant, M. Z., Storey, B. D. & Kornyshev, A. A. Double Layer in Ionic Liquids: Overscreening versus Crowding. *Physical Review Letters* **106**, 046102 (2011).

44 Drüschler, M. *et al.* New Insights into the Interface between a Single-crystalline Metal Electrode and an Extremely Pure Ionic Liquid: Slow Interfacial Processes and the Influence of Temperature on Interfacial Dynamics. *PCCP. Physical chemistry chemical physics* **14**, 5090-5099 (2012).

45 Hsu, C. H. & Mansfeld, F. Technical Note: Concerning the Conversion of the Constant Phase Element Parameter Y_0 into a Capacitance. *Corrosion* **57**, 747-748, doi:10.5006/1.3280607 (2001).

46 Abbott, A. P., Boothby, D., Capper, G., Davies, D. L. & Rasheed, R. K. Deep Eutectic Solvents Formed between Choline Chloride and Carboxylic Acids: Versatile Alternatives to Ionic Liquids. *Journal of the American Chemical Society* **126**, 9142-9147, doi:10.1021/ja048266j (2004).

Chapter 3: Ultra-Flat Surfaces

Previous work has shown that while low voltage electrowetting with very low contact angle hysteresis is simple to achieve on mercury, this is not the same on other electrode materials.[1-3] For example, electrodes made by sputtering gold onto quartz exhibited a large amount of hysteresis in the contact angle/voltage response.

Electrowetting on mercury is driven by a change in surface energy due to charging of the electrochemical double layer. The double layer capacitance of mercury is very similar to the double layer capacitance on other metals such as gold, so capacitance does not seem to be a plausible reason as to why electrowetting works on mercury rather than gold.[4,5] If the differences between mercury and other metals are considered, the most obvious dissimilarity is that mercury is a liquid at room temperature. As a consequence, the mercury surface is atomically smooth.[6] It is also self-healing: it cannot be scratched or damaged by physical means. Therefore, it was reasoned that if gold too could be made atomically flat, the hysteresis might be reduced and unrestricted electrowetting could be achieved on gold.

This view point has been supported by the work of Marinescu, whose work is discussed in Chapter 1.[3,7] In short, the theoretical model for an electrowetting system with pulsing suggested that reducing the frictional force on the droplet would allow the equilibrium contact angle to be achieved with fewer pulses. One of the origins of this frictional force could be surface roughness. As a result, substantial effort has been put into the preparation of such surfaces, with template stripping being the method of choice. As well as preparation of metal surfaces by conventional template stripping, the technique was extended to the preparation of ultra-flat glassy carbon surfaces.

3.1 Template stripping

3.1.1 Overview

Template stripping is a process used to transfer the smoothness of a template material to a metal surface. Today, it is commonly used to prepare atomically flat surfaces for imaging techniques such as AFM and scanning tunnelling microscopy (STM).[8] It is the principal

method chosen to produce flat surfaces for the electrowetting experiments described in Chapter 5.

In 1993, Hegner et al. were the first to use template stripping to produce large atomically flat gold surfaces intended for scanning probe microscopy.[9] The process was experimentally very simple. The first step involved epitaxial growth of a gold film on mica. The gold surface was then adhered to a silicon wafer with epoxy. Finally, the mica was either chemically or physically removed from the underside of the gold to leave an atomically flat surface, reported to have a root mean square (RMS) roughness of 3 Å over 25 μm^2. Priest et al. later suggested using gypsum to grow the gold on.[10] The benefits of this were that the gypsum was much easier to remove than the mica and larger flat domains (>2500 μm^2) could be achieved. Figure 33 shows the difference between the topside of a gold surface, and the underside of that surface once it has been stripped.

Recently, Chai and Klein have extended the original Hegner method to even larger areas by growing the gold on 3-6 μm thick single crystallographic plane facets of mica that are molecularly smooth on both sides.[11] As a result atomically flat domains (RMS roughness <3 Å) are seen over areas on the scale of 1 cm^2. This is the scale of area needed to test low voltage electrowetting as droplets are roughly 1 mm in diameter and ideally, the electrode surface should be homogeneously smooth under the entire droplet.

The stability of the surface in contact with salt solutions and organic solvents is also important to consider. The literature suggests that immersion in water has no negative effect on the roughness. However, the downside of the template stripping method is that it requires the use of an epoxy. It has been found that the epoxy, if not carefully selected, can swell as it absorbs organic solvents, damaging the metal surface.[12,13]

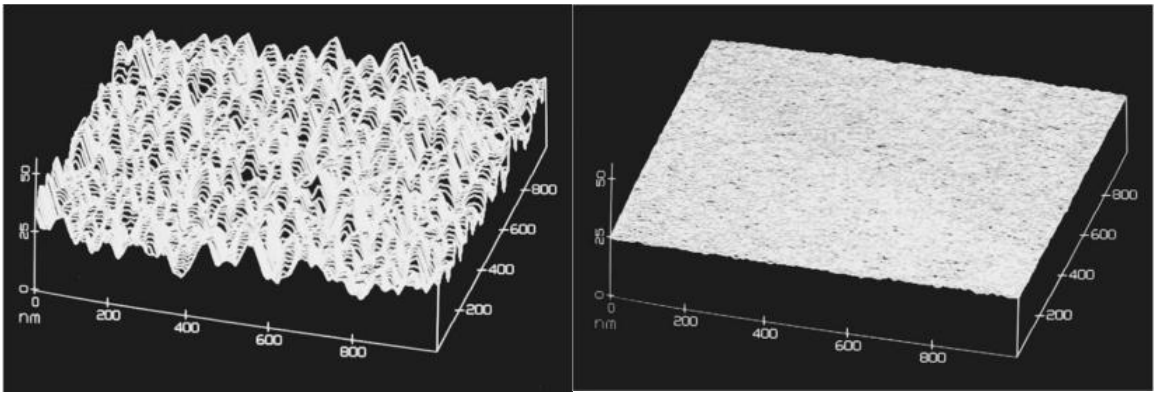

Figure 33|[Taken from Woodard[14]] The topside of a conventional evaporated gold surface (left) and its counterpart underside formed by template stripping (right).

Interestingly, it has been reported that the topside of a deposited gold surface effects the roughness of the surface below it.[10] This means that different gold deposition methods, such as sputtering and evaporation, can produce different degrees of roughness from the same template. For sputtered gold surfaces, the area which is in the plasma flame where the atoms are most energetic creates a significantly rougher surface.[15]

As noted in Chapter 1, the roughness of the surface will affect the equilibrium contact angle as increasing roughness increases the real surface area relative to the geometric area.[16] An additional effect on gold is the adsorption of organic species from the ambient atmosphere. These organics have a dramatic effect the contact angle of the surface. Upon exposure of a newly created gold surface, the contact angle of a sessile water droplet on the surface gradually changes from 20° to almost 80° (Figure 34).[11] Chai speculates that this is the result of hydrophobic organic molecules in the air adsorbing to an otherwise hydrophilic surface, although other possibilities include a moderately slow reorganisation of the gold or an interaction between the water and the gold. Chai's opinion is shared by Bewig and Zisman who state that any hydrophilic surface, when exposed to any atmosphere other than a purified gas, will develop a more hydrophobic surface as a result of organic contamination.[17]

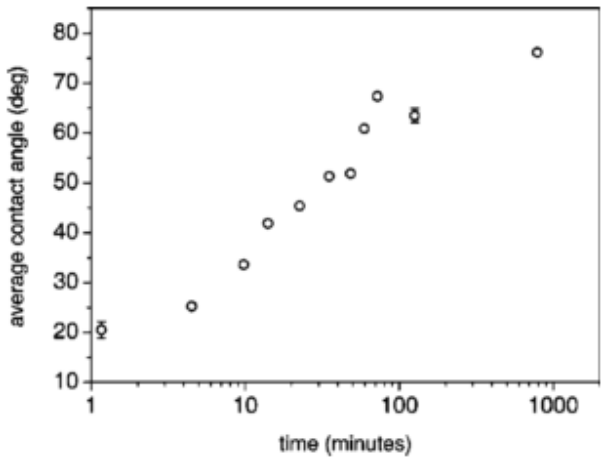

Figure 34|[Taken from Chai[11]] Variation of contact angle of a water droplet on a freshly exposed gold surface with time. The increase in the contact angle shows a change in the gold surface energy over time, supposedly as a result of adsorption of atmospheric organics.

3.1.2 Alternative methods

3.1.2.1 Annealing

Annealing—a high temperature surface treatment conducted in an inert atmosphere—is a commonly used technique for preparing smooth metal surfaces as it significantly reduces RMS roughness.[18] However, it also causes the surface to form microdomains known as clusters (Figure 35).[10] Whilst the RMS roughness may decrease (reducing frictional forces in an electrowetting experiment) the clusters may create local energy minima for the droplet to become stuck in. Therefore, annealing was not used as it was decided that regularity of the surface should be a priority.

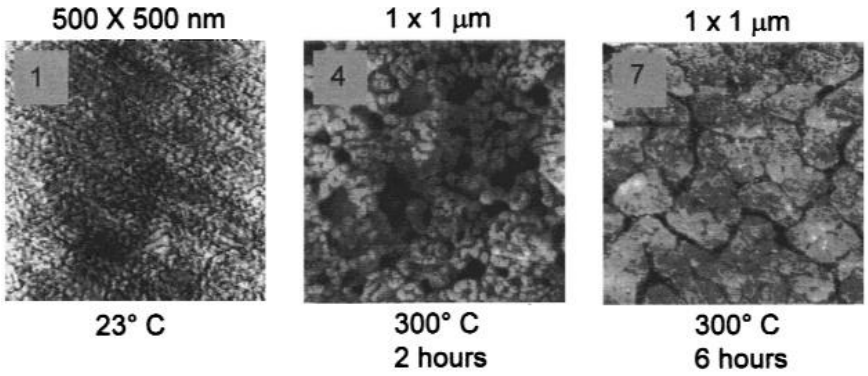

Figure 35|[Taken from Masens[18]] Scanning probe micrographs of template stripped gold films on mica. The annealing process results in the formation of large microdomains.

3.1.2.2 PDMS surface adhered gold

Gold can be adhered to polydimethylsiloxane (PDMS) functionalised with a thiol surface termination (Figure 36). The top layer is either directly deposited onto the thiol coated surface or transferred via a template to improve the surface roughness.[12,15] Simple direct deposition methods yield RMS roughnesses of 6-7 Å with a 15-20 nm grain size while more involved templating methods yield 2-4 Å RMS roughness with a 500 nm grain size. Despite the fact that this method avoids the use of an epoxy interlayer, which may not be stable in the presence of organic solvents, the relatively small grain size coupled with the additional complexity of this method meant that template stripping was preferred.

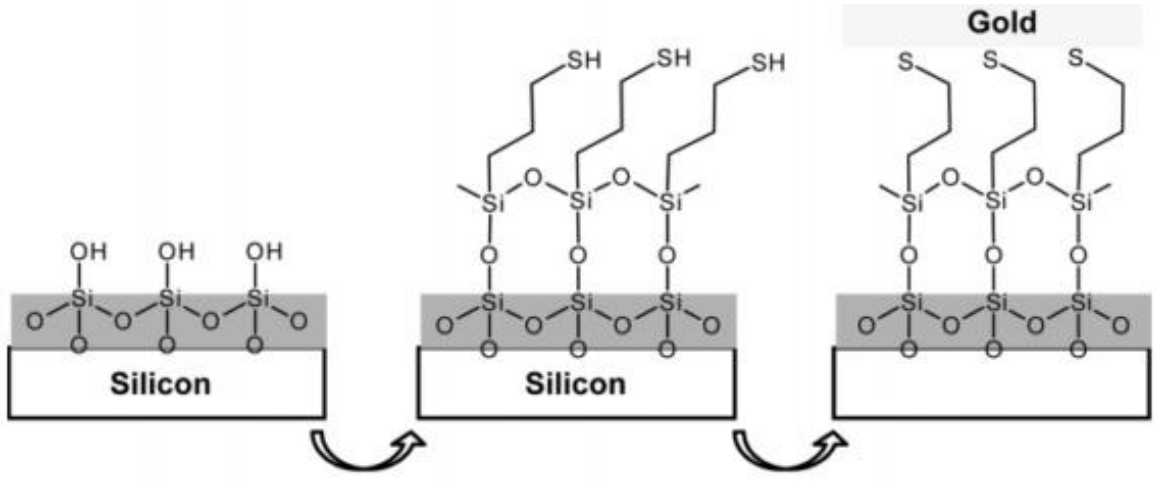

Figure 36|[Taken from Pattier[15]] Schematic route for the formation of a silicon-PDMS-thiol-gold array.

3.2 Ultra-flat metal surfaces

3.2.1 Experimental

A 100 nm layer of gold, copper or platinum was sputtered onto 2 cm × 7.5 cm VWR International Super Premium glass microscope slides. Immediately prior to sputtering, the glass was cleaned as follows:

1. Soaked in a solution of 0.1 mol dm^{-3} potassium permanganate + 0.18 mol dm^{-3} sulphuric acid for 1-2 h to oxidise any organics
2. Rinsed with acidified hydrogen peroxide solution (0.36 mol dm^{-3} H_2SO_4 + 0.18 mol dm^{-3} H_2O_2)
3. Rinsed with ultrapure water six times
4. Dried under a stream of nitrogen
5. Dried upright at 110 °C for 5 min

All sputtering was performed using an Emitech K575X sputterer; Emitech TK8859 gold targets, Emitech TK8879 titanium targets and Emitech TK8845 copper targets. Surface morphologies were characterised with an Agilent Technologies 5500 AFM using Windsor Scientific PPP-NCH probes. Image processing involved surface levelling and was performed using Agilent PicoView version 1.8 software.

Glass rectangles (approximately 1 cm × 2 cm) were then stuck to the gold coated microscope slide with one half of the glass rectangle hanging over the edge of the microscope slide. The glass was stuck down with a variety of epoxies including Buehler Epo-Thin Low Viscosity Epoxy Resin; Duralco 4525 All Purpose Room Temperature Curing Epoxy; Duralco 4703 Adhesive, Coating and Potting Epoxy; RS Quickset Epoxy; Araldite 2011 Multi Purpose Epoxy and Epo-Tek 377 High Temperature Epoxy. Following curing of the epoxies according to manufacturer guidelines, the glass rectangles were pulled off the microscope slide when needed, revealing a smooth clean metal surface.

Contact angles were measured from photographs taken with a CCD (from a Phillips SPC900NC webcam) through a video zoom microscope (Edmund Optics Infinity K2/S Long Distance Video Lens) at 20× magnification. Contact angles were subsequently measured using Fta32 2.0 contact angle software (First Ten Ångstroms). All reported contact angles are advancing contact angles averaged over five measurements.

3.2.2 Results and discussion

3.2.2.1 Roughness

Template striping was used to produce smooth electrode surfaces. The roughness of the resulting surfaces was characterised by AFM. Figure 37 shows a typical micrograph of a template stripped gold surface prepared using Buehler Epo-Thin epoxy and a glass microscope slide template. The features are on the order of only several nanometres, with an RMS roughness of 3.9 Å and peak height of 2.9 nm. The peak corresponds to roughly 12 gold atoms stacked on top of each other, and so it can be said that the roughness is on the atomic scale.[19] This surface is much smoother than the sputtered gold surfaces used for previous electrowetting experiments, which were at least an order of magnitude rougher.[14] Oddly, the roughness of the template stripped surface was less than that of the template (RMS roughness of VWR International Super Premium glass microscope slide 15.1 Å). This suggests that the gold may not exactly mate with the surface or take on its exact configuration.

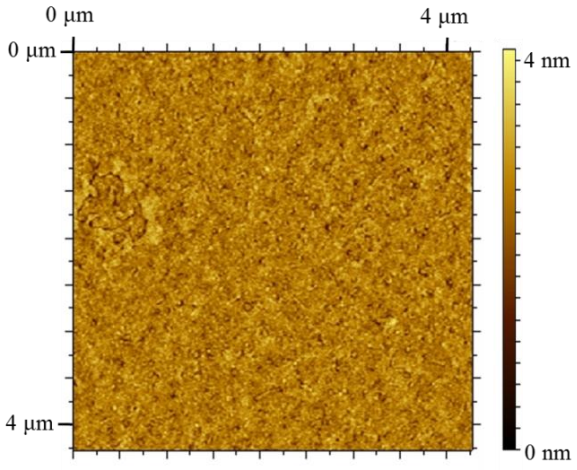

Figure 37 | AFM image (Area: 4.3 µm × 4.3 µm; RMS roughness: 3.9 Å; Peak height: 2.9 nm).

However, as electrowetting occurs over macroscopic areas, the roughness over much larger distances is perhaps more important, as the length scale effecting pinning may be important. Figure 38 shows template stripped gold and sputtered gold surfaces over 80 μm^2. As well as an order of magnitude difference in roughness, there is a much more striking difference between the surfaces: the presence of large dust particles. While the template stripped surface has only

a few large peaks over the entire area (maximum height 28.4 nm) the sputtered surface has many peaks which are substantially larger (maximum height 184 nm).

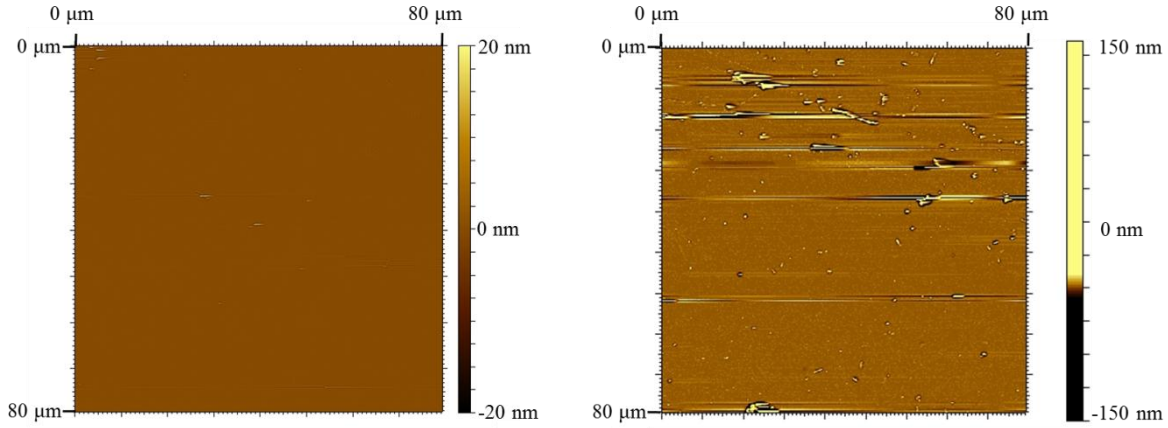

Figure 38|AFM images of template stripped gold (left) and sputtered gold (right) surfaces over a large area. template stripped gold area: 80 µm × 80 µm; RMS roughness: 4.5 Å; Peak height: 28.4 nm. Sputtered Gold Area: 80 µm × 80 µm; RMS roughness: 40.3 Å; Peak height: 184 nm. The sputtered surface is clearly contaminated with large dust particles while the template stripped gold surface only has a few small peaks.

These dust particles are not a result of prolonged exposure to the ambient atmosphere, but deposit over short time periods. Figure 39 shows a photograph of a sputtered electrode immediately after sputtering. It should be noted that while the electrode looks very dusty in the photograph, the surface appears very clean to the naked eye if not deliberately lit in such a way as to highlight the dust on the surface. The fact that the sputtered surfaces attract dust more quickly than freshly stripped surfaces suggests they may be left with a weak electrostatic charge after sputtering.

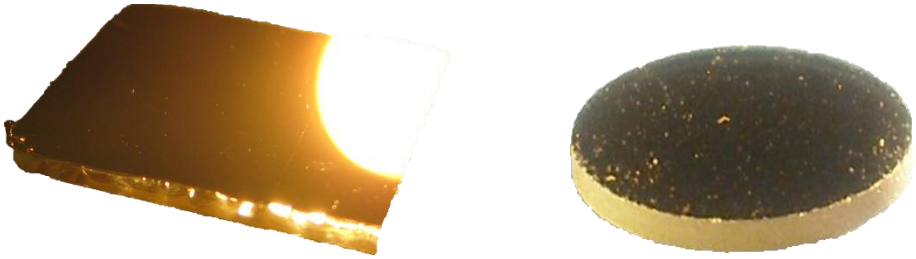

Figure 39|(Left) Photograph of template stripped gold immediately after stripping. The backlight is reflected in the right-hand corner. (Right) Photograph of sputtered gold immediately after removal from sputter machine. The images are both back lit at a shallow angle to highlight any surface contaminants. Only a few specks of dust can be seen on the freshly stripped surface while the entirety of the sputtered surface is covered with dust.

These results are an excellent illustration of one of the less obvious benefits of template stripping: the surfaces are protected from atmospheric contamination until immediately prior to use. It may also be the case that the pinning seen on template stripped surface is not so much a result of average roughness but rather because of the presence of large dust particles on the surface. This theme is discussed further in Chapter 5.

3.2.2.2 Contact angle

As mentioned in Chapter 1, surface roughness affects the contact angle of a droplet on the surface. Increasing roughness lowers the water contact angle if the surface is hydrophilic and increases it if the surface is hydrophobic. As the metal surfaces produced in this study were hydrophilic, and they were less rough than common gold surfaces, the contact angle was expected to be greater than 60-65°, the common range of contact angles for water on gold.[20]

Freshly stripped gold had a very small contact angle (measured as 25±5°). However, the contact angle slowly increased with time (as explained in Section 3.1.1) and after 24 hours the contact angle was 67° which is relatively high for gold, as expected for a smooth surface. This was presumably due to the adsorption of organics onto the surface rather than a roughening of the surface which would have the effect of reducing the contact angle.

3.2.2.3 Stability

Template stripped gold surfaces, made using the various epoxies listed in Section 3.2.1, were left in water for four hours and then dried at room temperature. AFM was then used to assess the change, if any, in surface roughness and morphology. The smoothest and most stable surfaces were made using Buehler Epo-Thin, although Epo-Tek 377 surfaces were very similar, as can be seen from Table 2.

	RMS Roughness / Å		
	Freshly stripped	**72 h in air**	**4 h in water**
Buehler Epo-Thin	3.9	6.9	8.3
Epo-Tek 377	4.6	6.7	8.9
Duralco 4525	8.7	12.7	14.6
Duralco 4703	8.2	11.0	29.1
RS Quickset	Failed	Failed	Failed
Araldite	Failed	Failed	Failed

Table 2|Variation in RMS roughness of template stripped gold with the epoxy used in the surface fabrication. Also shown is how roughness slowly increases after the gold has been exposed to the atmosphere and how the roughness increases more quickly after the gold has been submerged in water. The 'failed' surfaces were very rough immediately after being removed from their templates. They exhibited large cracks which could easily be made out by the naked eye.

As well as these microscopic changes, in many cases macroscopic blemishes and a 'rippled' texture, visible to the naked eye, also appeared on the surface following exposure to water (Figure 40). Eventually, the water would creep in between the gold and the epoxy, seriously damaging the entire surface.

Figure 40|Template stripped gold after long-term exposure to water. Clearly this surface is very different to the one shown in Figure 39.

One possible explanation for these defects is a reorganisation of the surface due to a difference in the gold|air and gold|water surface energies. Alternatively, there may have been small pinholes in the gold surface through which the water entered.

This result demonstrates that the epoxy used for template stripping has a dramatic effect on the quality and stability of the resulting gold surface, especially if the surface is exposed to water as is the case for electrowetting. Buehler Epo-Thin appears to make the most water stable surfaces. This epoxy is designed to be stable at high temperatures and also has a very low viscosity. Epo-Tek 377 is also a high temperature, low viscosity epoxy and appears to produce the second most stables surfaces, behind the Buehler Epo-Thin. This suggests that these are important properties for stability and any future work should test similar products from other manufactures for the possibility of an even better epoxy.

These results are in direct contrast to the common claim that template stripped gold is stable in water.[21] While it is possible that a difference in the method of surface preparation could be responsible, this is unlikely due to the simplicity of the process. Moreover, it seems that the surface is inherently unstable and the nature of the epoxy is critical in determining the stability.

3.3 Glassy carbon

Carbon, often in the form of glassy carbon, is a commonly used electrode material.[22] It has many desirable properties such as its excellent chemical stability, electrochemical window, mechanical strength and hydrophobicity. As will be seen in Chapter 4, it can also be effectively functionalised by diazonium compounds. For these reasons, preparation of ultra-flat glassy carbon for use as a substrate for electrowetting was attempted.

Glassy carbons are prepared by pyrolysis of an organic precursor material at 1000-3000 °C in an inert atmosphere. Many mesoporous glassy carbons have been prepared from porous templates such as zeolites and silica.[23] The precursor is polymerised inside the template, which is then etched away leaving a polymer skeleton. The skeleton will retain this structure, even after pyrolysis. The template stripping of glassy carbon described here is analogous to this process. The general method proposed was to mate a carbon polymer with a flat template and then pyrolyse the polymer. On removal of the template a flat glassy carbon surface should be left. Any previous attempts at such a process in the literature are unknown to the author

3.3.1 Properties

Glassy carbon was first made in 1962 by Yamada and Sato by the high temperature pyrolysis of a phenolic resin in an inert atmosphere.[24] Its structure was first thought to be essentially graphitic; however, recent studies using transmission electron microscopy have suggested a fullerene type structure (Figure 41).[25]

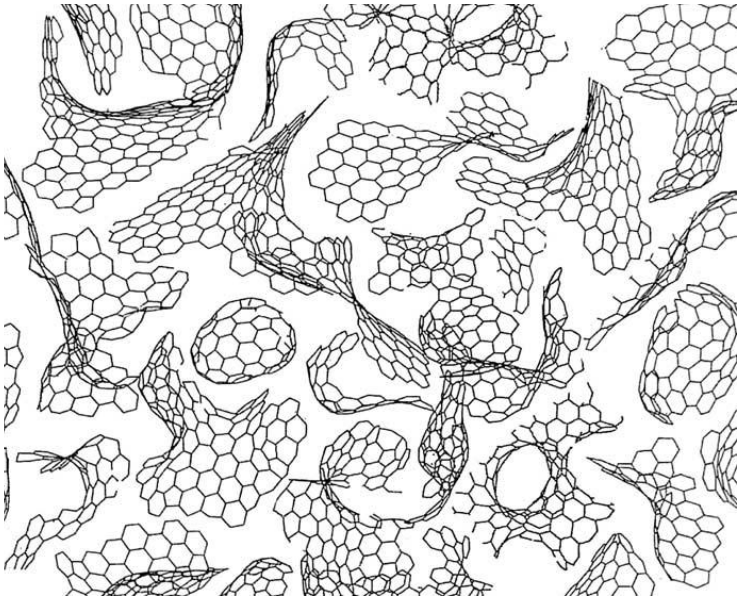

Figure 41|[Taken from Harris[25]] Illustration of the proposed structure of a non-graphitised glassy carbon based on fullerene type elements.

Owing to this unique structure, glassy carbon has a very low porosity and a very low permeability to gases, unlike graphitic carbons. This can be seen from Table 3, which contains the properties of a typical glassy carbon. Template stripped glassy carbon would have many benefits over template stripped gold (or other template stripped metals). It has a larger electrochemical window than gold, while retaining similar wetting properties, double layer capacitance and mechanical strength. Although its bulk resistivity is higher than that of gold, template stripped gold is very thin and therefore has a comparable resistance to thicker glassy carbon electrodes. Glassy carbon is also much cheaper than gold. The biggest potential advantage of template stripped glassy carbon would be its resistance to organic solvents. Due to the epoxy used, template stripped gold is not stable in certain solvents; the surface spontaneously roughens.[13] This means it may not be suitable as a substrate for electrowetting. On the other hand, template stripped glassy carbon is not expected not to have this problem as no epoxy is needed and it is itself resistant to most solvents.

	Glassy carbon	Graphitic carbon	Gold[26]
Bulk density/g cm^{-3}	1.3-1.55	1.6	19.3
Gas permeability/cm^2 s^{-1}	10^{-6}-10^{-12}	10^{-2}	N/A
Tensile strength/kg cm^{-2}	400-1000	420	1150
Thermal expansion /$^oC^{-1} \times 10^6$	2-3.5	1-3	14.3 [27]
Thermal conductivity /W cm^{-1} K^{-1}	0.24-1.43 × 10^{-2}	7.2-9.5 × 10^{-2}	2.96
Contact angle/^{o}	64±2 [28]	65	66±3 [28]
Resistivity/Ω cm	1-5 × 10^{-3}	7 × 10^{-4}	2.19 × 10^{-6}
Anodic limit, pH ~6 /V vs. SCE	1.4	1.26	0.6 [a,29]
Cathodic limit, pH ~14 /V vs. SCE	–1.6	–1.4	–1.58 [30]
Double layer capacitance, 0.9 mol dm^{-3} NaF/μF cm^{-2}	~13	16	~12 [b,5]

Table 3|Properties of high temperature glassy carbon compared with graphitic carbon. Data taken from Kinoshita unless otherwise stated.[31] Values are purely illustrative as glassy carbon properties are dependent upon precursor material and pyrolysis conditions. [a]Gold 111, defined as onset of oxide growth. [b]Measured with coumarin present in solution.

3.3.2 Precursors

Glassy carbon is produced by pyrolysis of a carbon containing precursor material at elevated temperatures. Phenolic resins (Figure 42), along with many other organic polymers such as poly(furfuryl alcohol), poly(vinyl chloride), cellulose and poly(acrylonitrile) can be used to make glassy carbon.[32,33]

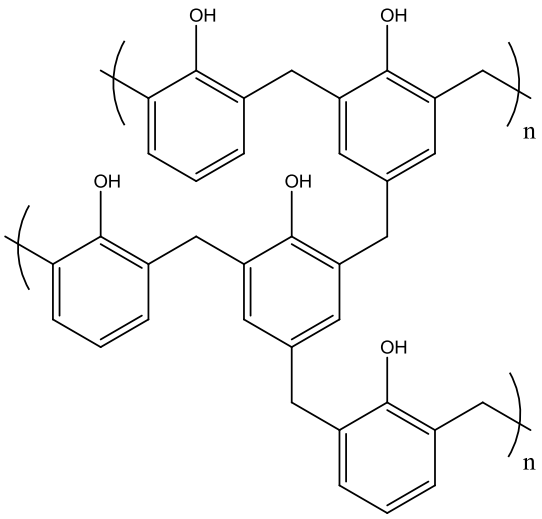

Figure 42|Phenol formaldehyde, formed by co-polymerisation of phenol and formaldehyde. The alternating phenol/methylene units form chains which are cross-linked via tri-substituted phenol units.

Pyrolysis is usually performed at temperatures between 1000-3000 °C; however, Callstrom et al. have produced high quality glassy carbons at temperatures of only 600 °C.[34] This is achieved by using precursors with a high carbon to hydrogen ratio; molecules with a high double and triple bond content. This means that less atomic rearrangement and elimination is required to form the glassy carbon structure. Therefore, glassy carbon forms at a lower than usual temperature. Template stripping uses a template to form the ultra-flat surface. At high temperatures, the glass or quartz template is liable to deform and so a low temperature pyrolysis was preferable.

In order to make template stripped glassy carbon, the precursor needs to take on the shape of the template. This means that the precursor cannot be hard but instead must flow. Yet, at the same time it must not be too liquid or else it will run off the surface of the template. In order

to achieve this, a number of precursors were tested including a low molecular weight phenol formaldehyde resin. This had a putty-like consistency which became syrup-like at 90 °C. It would then solidify as the polymer chains cross-linked or pyrolysed at higher temperatures. The molecule 9,10-bis(phenylethynyl)anthracene, which is shown in Figure 43, was also chosen because it melts at 240 °C but pyrolyses before evaporating. It also has a high double and triple bond content and may therefore form glassy carbon at a lower temperature. Other precursors tested were: phenol formaldehyde, poly(furfuryl alcohol) and poly(phenyldiacetylene), however, only phenol formaldehyde and 9,10-bis(phenylethynyl)anthracene were successfully template stripped.

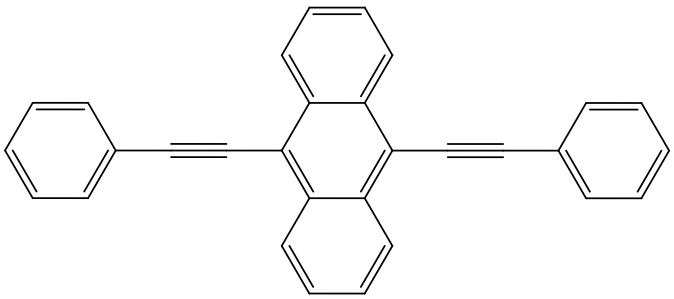

Figure 43|9,10-bis(phenylethynyl)anthracene. This molecule melts at 240 °C, allowing it to take on the shape of the template it sits on. At higher temperatures it decomposes forming a solid which can then be pyrolysed. It contains only carbon and hydrogen and has a high proportion of single and double bonds, meaning less rearrangement or mass loss is needed to form glassy carbon.

3.3.3 Sample preparation

As explained above, the precursor materials were melted onto the flat templates and then pyrolysed to form a flat glassy carbon surface. Glass and quartz microscope slides and freshly cleaved mica were tested as templates. They all have similar roughnesses however the quartz and mica can tolerate the high temperatures required for pyrolysis. The different materials also have different wetting properties, which is an important consideration when mating precursor and template.

The pyrolysis process itself can be broken down into two distinct regions. Phenol formaldehyde will be used as an example. As can be seen from Figure 44, there is a large

decrease in sample volume between 350 °C and 650 °C. This coincides with a significant reduction in mass as molecules such as water, methane, carbon monoxide and hydrogen are eliminated.[35,36] By the time the sample has been heated to 650 °C, it already conducts electricity; with a resistivity on the order of 100 mΩ cm. Beyond this temperature mostly hydrogen is lost and the gains in conductivity begin to diminish.[22] At 1000 °C the reduction in mass becomes almost insignificant and the resistivity is around 10 mΩ cm. Upon heating to 3000 °C, small defects are annealed and the resistivity peaks at around 5 mΩ cm.[37]

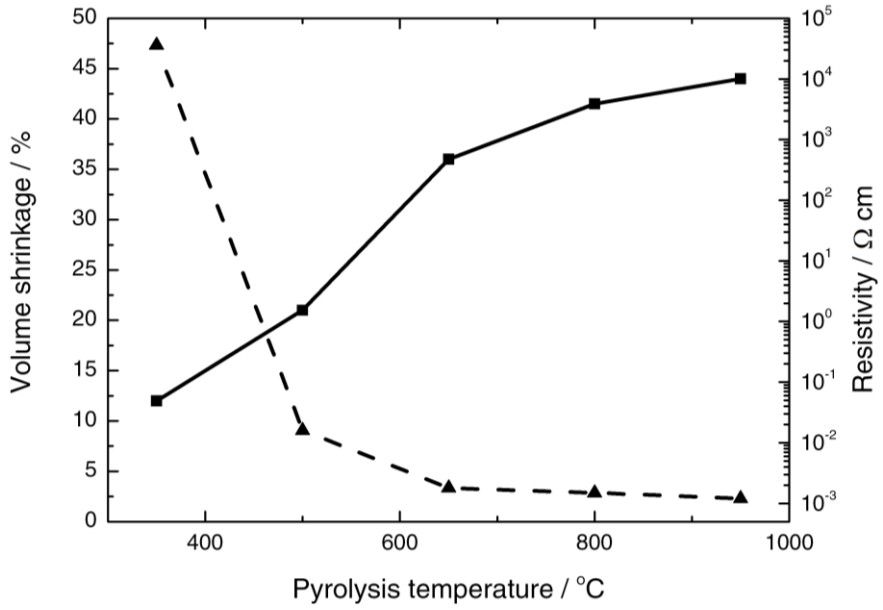

Figure 44|[Data taken from Bhatia[35]] Linear shrinkage (■) and variation of electrical resistivity (▲) of phenol formaldehyde resin with increasing pyrolysis temperature.

Due the volume reduction during pyrolysis, the sample can crack or form an inhomogeneous surface. This means that a very specific sample preparation and heating cycle are often required. Below is an example of a typical heating sequence:[38]

1. Heat to 200 °C
2. Hold for 3 hours to ensure sample is fully cured and to evaporate off any volatile species
3. Heat to 600 °C (1 °C per minute)
4. Hold for 24 hours to slowly remove hydrogen and oxygen
5. Heat to 1000 °C
6. Hold for 3 hours to improve conductivity

3.4 Ultra-flat carbon surfaces

3.4.1 Experimental

3.4.1.1 Phenol formaldehyde synthesis

All chemical were used as received from Sigma-Aldrich. 15.1 g phenol (161 mmol), 49 ml 37 % formaldehyde solution (53.4 g, 658 mmol formaldehyde) and 9 ml 28 % ammonia solution were mixed together. The solution was heated at 80 °C until opaque with a white suspension.[38] The mixture was allowed to settle and the top surface layer decanted off. The remaining solid was then dried under vacuum. Once dry, a pale yellow/green solid was left, which was very soft and could easily be easily shaped. This was placed onto circular quartz coverslips (Agar Scientific, 10 mm diameter, 1 mm thickness) and heated to 90 °C under vacuum for 1 h, forming semi-transparent amber domes on top of the coverslips ready for pyrolysis.

3.4.1.2 9,10-bis(phenylethynyl)anthracene preparation

Approximately 30 μg 9,10-bis(phenylethynyl)anthracene (Alfa-Aesar) was deposited onto a circular quartz coverslip (Agar Scientific, 10 mm diameter, 1 mm thickness). This was heated from 150 °C to 250 °C over 2 h. It was then held at 250 °C for 1h, before being cooled to room temperature over 2 h. This produced hard shiny black domes of polymerised 9,10-bis(phenylethynyl)anthracene on top of the quartz coverslip ready for pyrolysis.

3.4.1.3 Pyrolysis procedure

The carbon precursors were placed in an atmosphere of 5% hydrogen in nitrogen and subjected to the following heat ramp:

1. 25 °C to 600 °C
2. 600 °C for 12 h
3. 600 °C to *target temperature*
4. *Target temperature* for 12 h
5. *Target temperature* to 25 °C

The target temperature was 600, 700, 800, 900 or 1000 °C. The heating/cooling rate was 1 °C min^{-1}.

3.4.1.4 Conductivity measurements

Conductivity was measured using a homemade four point conductivity probe (2 mm probe spacing) and a Gamry Reference 600 potentiostat. In a four point probe measurement, current flows between the outer probes and the potential drop across the inner probes is measured. It assumes a semi-infinite, continuous film. (Equation 16 or (Equation 17 was used to calculate the resistivity:[39]

$$\rho = \frac{\pi}{\ln 2} t \left(\frac{U}{I}\right) \qquad \text{(Equation 16)}$$

$$\rho = \frac{\pi t}{\ln\left(\frac{\sinh\frac{t}{s}}{\sinh\frac{t}{2s}}\right)} t \left(\frac{U}{I}\right) \qquad \text{(Equation 17)}$$

where ρ is the resistivity, t is the sample thickness, s is the probe spacing, U is the potential drop across the inner probes and I the current between the outer probes. (Equation 16 applies when the sample thickness is less than half the probe spacing ($t < s/2$), otherwise (Equation 17 was used.

3.4.2 Results and discussion

3.4.2.1 Preparation and pyrolysis

The photographs in Figure 45 and Figure 46 show the three stages of glassy carbon preparation for the two precursor materials used. Template stripped surfaces could only be produced using quartz substrates. When mica substrates were used, the precursor materials would wet and spread over the entire surface and not form bulk glassy carbon. As can be seen from the images below, the surface in contact with the template formed islands roughly 1 mm^2 in area during pyrolysis. While the surfaces appears rough and distorted, the islands themselves are in fact very smooth as will be seen below.

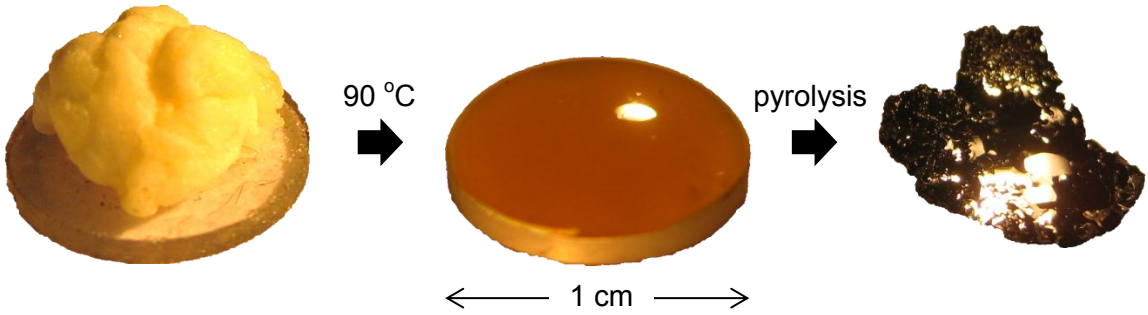

Figure 45 | (Left) Phenol formaldehyde precursor on quartz disk. (Middle) After heating to 90 °C, the precursor melts and mates with the surface of the flat template. It then begins to cross link forming a hard solid. (Right) After pyrolysis glassy carbon forms.

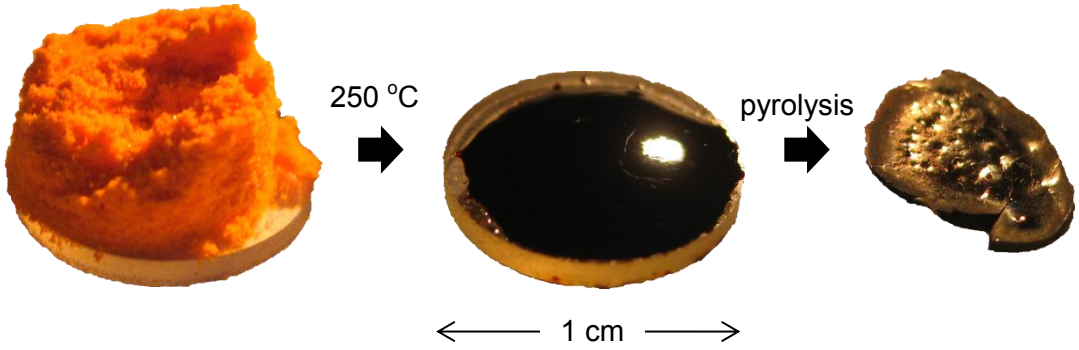

Figure 46|(Left) 9,10-bis(phenylethynyl)anthracene precursor material on quartz disk. (Middle) Upon heating to 250 °C the precursor melts and appears to polymerise, forming a hard, black and shiny solid. (Right) After pyrolysis glassy carbon forms.

3.4.2.2 Surface roughness

AFM images of the pyrolysed phenol formaldehyde and 9,10-bis(phenylethynyl)anthracene indicate smooth but wavy surfaces. The waviness is most probably a consequence of the shrinking of the glassy carbon during pyrolysis. However, the waviness is quite subtle: for the phenol formaldehyde carbon the peak-to-peak amplitude is <20 nm and the peak separation is 20 μm. For the 9,10-bis(phenylethynyl)anthracene carbon these values are <70 nm and 80 μm respectively. Therefore, this waviness is not considered as 'roughness' on the nanoscale.

If this waviness is removed from the image by the fitting of a third order polynomial, the nanoscale roughness can be seen. Figure 47 below shows the phenol formaldehyde glassy carbon surface. This is in fact incredibly smooth, with RMS roughness of 6.5 Å which is close to the roughness of template stripped gold (3.9 Å).

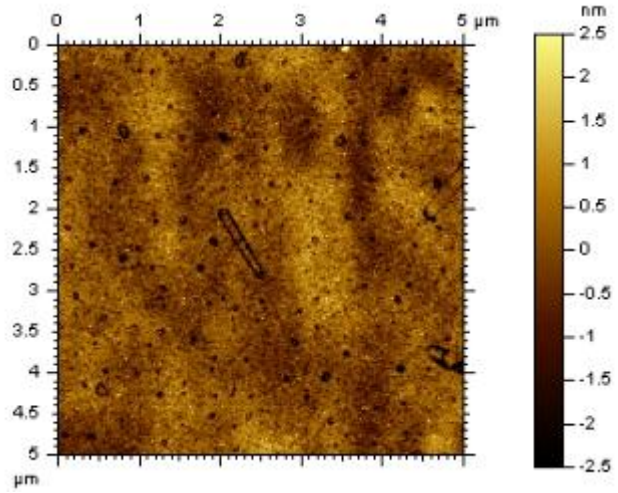

Figure 47|AFM image of template stripped phenol formaldehyde derived glassy carbon. Area 5 µm × 5 µm; RMS roughness: 6.5 Å; Peak height: 10.8 nm.

The 9,10-bis(phenylethynyl)anthracene glassy carbon surface is shown in Figure 48. Much like the phenol formaldehyde carbon surface, it too is very smooth, with an RMS roughness of 2.6 Å over 5 μm^2. The surface also appears to have fewer features than the phenol formaldehyde surface, which has regular pits on it.

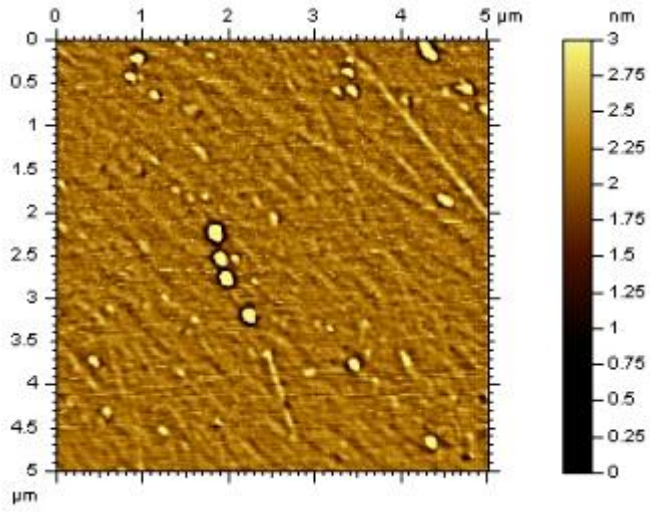

Figure 48|AFM image of template stripped 9,10-bis(phenylethynyl)anthracene derived glassy carbon. Area 5 µm × 5 µm; RMS roughness: 2.6 Å; Peak height: 8.7 nm.

Furthermore, these surfaces did not roughen over a period of several months and were also unaffected by water or acetone, which was not the case for conventional template stripped metal surfaces. This is because glassy carbon is a very stable material, as discussed above, which is clearly a huge benefit of using template stripped glassy carbon, allowing experiments on very flat surfaces to be conducted in liquids over long periods of time. The glassy carbon surfaces are also much smoother than commercially available glassy carbons. Diamond polished glassy carbon from HTW GmbH, Germany had an RMS roughness of 56.5 Å with a peak height of 54.3 nm over 10 μm^2. It should be noted that basal planes of highly oriented pyrolytic graphite (HOPG) are smoother, however, HOPG is not glassy carbon and has different chemical and physical properties as well as different electrochemistry.[40] It is also difficult to cleave over large areas and will typically have many steps. HOPG is also a very expensive material while the template stripped glassy carbon reported here can be prepared relatively cheaply.

3.4.2.3 Conductivity

Conductivity is an important property of glassy carbon, particularly if it is to be used for electrowetting. Phenol formaldehyde and 9,10-bis(phenylethynyl)anthracene glassy carbons were pyrolysed at different temperatures and their conductivities measured (Table 4). As expected, the conductivity increased with increasing pyrolysis temperature. The critical temperature at which there was a dramatic increase in conductivity was 800 °C for the phenol formaldehyde (five orders of magnitude increase) and 700 °C for 9,10-bis(phenylethynyl)anthracene (three orders of magnitude increase). Therefore, these are the temperatures at which cross linking between molecules must begin. Heating to higher temperatures results is a much smaller but nonetheless significant increase in conductivity.

The final conductivity after a 1000 °C pyrolysis temperature for phenol formaldehyde derived glassy carbon was 5.1 S cm^{-1}, while the conductivity of 9,10-bis(phenylethynyl)anthracene derived glassy carbon (1000 °C pyrolysis) was 36 S cm^{-1}. The greater fraction of double and triple bonds in the 9,10-bis(phenylethynyl)anthracene may account for this. These conductivities are slightly lower than the average glassy carbon conductivities of approximately 100 S cm^{-1} reported in the literature.[35,37] These results suggest that 9,10-

bis(phenylethynyl)anthracene is a superior template stripped glassy carbon precursor to phenol formaldehyde as it produces a more conductive sample at lower pyrolysis temperatures.

Pyrolysis temperature / °C	**Phenol formaldehyde carbon conductivity / S cm^{-1}**	**9,10-bis(phenylethynyl) anthracene carbon conductivity / S cm^{-1}**
500	Insulator	Insulator
600	1.5×10^{-5}	5.3×10^{-4}
700	9.9×10^{-5}	0.38
800	3.2	12
900	5	34
1000	5.1	36

Table 4|Conductivity of phenol formaldehyde and 9,10-bis(phenylethynyl)anthracene derived glassy carbons based on final pyrolysis temperature. There is an error of ±20% due to the difficulty in measuring the sample thickness.

3.5 Conclusions

3.5.1 Metal surfaces

Ultra-flat template stripped metal surfaces were successfully prepared as previously seen in the literature. However, it was shown that this could be achieved with much cheaper, more common-place materials such as glass microscope slides rather than freshly cleaved mica. Despite the increased roughness of such materials when compared to atomically smooth mica, the resulting surfaces have an RMS roughness of less than 4 Å, close to 'atomic roughness'. The very low RMS roughness occurred over a macroscopic area, which has only previously been reported for mica templates.[11] These provide very convenient metal surfaces which can

be prepared in advance and freshly exposed prior to use, ensuring cleanliness of the surface. As they are simple and cheap to prepare, they provide an attractive alternative to simple sputtered or evaporated metal surfaces.

The stability of template stripped surfaces in water and air was also tested. It was shown that they are not stable in water, especially over long periods of time. This is in disagreement with what is commonly stated in the literature. Similarly, albeit more slowly, the surfaces seem to degrade in air. Furthermore, it was shown that the epoxy which is used for the template stripping is critical in creating a smooth and stable template stripped surface.

Future work in this area could further explore the origin of the instability of these surfaces and search for other epoxies or adhesives which may improve the stability.

3.5.2 Carbon surfaces

Smooth glassy carbon surfaces were prepared with a modified template stripping process for the first time. This involved mating the glassy carbon precursor with a flat quartz template. The precursor was then pyrolysed while still in contact with the quartz, resulting in the formation of a very smooth glassy carbon surface.

Two different glassy carbon precursors were used: phenol formaldehyde which has been used previously and 9,10-bis(phenylethynyl)anthracene which has not. These produced surfaces with nanoscale roughnesses of 6.5 Å and 2.6 Å respectively. However, the surfaces were wavy on the microscale. Nonetheless the surfaces should still be suitable as substrates for studying nanoscale assemblies for which ultra-flat surfaces are required, and thus provides a new material (glassy carbon) for such experiments.[8] Of particular merit was the surface stability in water and organic solvents. The carbon itself had good conductivity, close to literature conductivity values (36 $S\,cm^{-1}$ after heating to 1000 ^{o}C for the 9,10-bis(phenylethynyl)anthracene).The surfaces were also cheap and simple to prepare and may provide a good alternative to HOPG.

Future research should focus on the development of other precursors which may yield higher conductivities or pyrolyse at lower temperatures. The lower pyrolysis temperature may result in a smaller degree of surface waviness.

3.6 References

1 Frumkin, A. N., Kabanow, B. & Nekrasow, M. Kapillarelektrische Erscheinungen und Benetzung von Metallen durch Elektrolytlösungen. *I. Phys. Z. Sovijetunion* **1**, 255-284 (1932).

2 Cousens, N. E. A. *Shape Changing Liquid Droplets*, Imperial College London, (2009).

3 Marinescu, M., Urbakh, M., Barnea, T., Kucernak, A. R. & Kornyshev, A. A. Electrowetting Dynamics Facilitated by Pulsing. *The Journal of Physical Chemistry C* **114**, 22558-22565, doi:10.1021/jp1052634 (2010).

4 Grahame, D. C. Capacity of the Electrical Double Layer between Mercury and Aqueous Sodium Fluoride. II. Effect of Temperature and Concentration. *Journal of the American Chemical Society* **79**, 2093-2098 (1957).

5 Bond, A. M. & Thomas, F. G. Studies of Adsorption Processes in the Absence of Added Electrolyte: Phase Changes in Coumarin Adsorbed at Conventional and Micro Mercury Electrodes. *Langmuir* **4**, 341-345, doi:10.1021/la00080a016 (1988).

6 Conroy, J. F. T., Caldwell, K., Brucknerlea, C. & Janata, J. An Examination of Surface Waving on Mercury Film Electrodes Using Scanning-Tunnelling-Microscopy. *Electrochimica Acta* **40**, 2927-2934 (1995).

7 Marinescu, M. *Electrovariable Liquid Interfaces for Optical Applications: Structure and Dynamics*, Imperial College London, (2012).

8 Vogel, N., Zieleniecki, J. & Koeper, I. As Flat as It Gets: Ultrasmooth Surfaces from Template-stripping Procedures. *Nanoscale* **4**, 3820-3832 (2012).

9 Hegner, M., Wagner, P. & Semenza, G. Ultralarge Atomically Flat Template-Stripped Au Surfaces for Scanning Probe Microscopy. *Surface science* **291**, 39-46 (1993).

10 Priest, C., Jacobs, K. & Ralston, J. Novel Approach to the Formation of Smooth Gold Surfaces. *Langmuir* **18**, 2438-2440 (2002).

11 Chai, L. & Klein, J. Large Area, Molecularly Smooth (0.2 nm RMS) Gold Films for Surface Forces and Other Studies. *Langmuir* **23**, 7777-7783 (2007).

12 Atmaja, B., Frommer, J. & Scott, J. Atomically Flat Gold on Elastomeric Substrate. *Langmuir* **22**, 4734-4740 (2006).

13 Blackstock, J. J., Li, Z. & Jung, G.-Y. Template Stripping Using Cold Welding. *Journal of Vacuum Science & Technology A: Vacuum, Surfaces, and Films* **22**, 602-605 (2004).

14 Woodard, N. & Lafyatis, G. Fabrication and Characterization of Extremely Smooth Large Area Gold Surfaces. *Journal of vacuum science & technology. A. Vacuum, surfaces, and films* **14**, 332-335 (1996).

15 Pattier, B., Bardeau, J., Edely, M., Gibaud, A. & Delorme, N. Cheap and Robust Ultraflat Gold Surfaces Suitable for High-resolution Surface Modification. *Langmuir* **24**, 821-825 (2008).

16 Adamson, A. W. *Physical Chemistry of Surfaces*. 5th edn, (John Wiley & Sons, Inc., 1990).

17 Bewig, K. W. & Zisman, W. A. The Wetting of Gold and Platinum by Water. *The Journal of Physical Chemistry* **69**, 4238-4242, doi:10.1021/j100782a029 (1965).

18 Masens, C., Schulte, J., Phillips, M. & Dligatch, S. Ultra Flat Gold Surfaces for Use in Chemical Force Microscopy: Scanning Probe Microscopy Studies of the Effect of Preparation Regime on Surface Morphology. *Microscopy and Microanalysis* **6**, 113-120 (2000).

19 Untiedt, C. *et al.* Calibration of the Length of a Chain of Single Gold Atoms. *Phys. Rev. B* **66**, doi:10.1103/PhysRevB.66.085418 (2002).

20 Erb, R. A. Wettability of Gold. *The Journal of Physical Chemistry* **72**, 2412-2417, doi:10.1021/j100853a023 (1968).

21 Wagner, P., Hegner, M., Guentherodt, H.-J. & Semenza, G. Formation and in Situ Modification of Monolayers Chemisorbed on Ultraflat Template-Stripped Gold Surfaces. *Langmuir* **11**, 3867-3875, doi:10.1021/la00010a043 (1995).

22 Van der Linden, W. E. & Dieker, J. W. Glassy Carbon as Electrode Material in Electro-analytical Chemistry. *Analytica Chimica Acta* **119**, 1-24, doi:10.1016/s0003-2670(00)00025-8 (1980).

23 Inagaki, M., Orikasa, H. & Morishita, T. Morphology and Pore Control in Carbon Materials via Templating. *RSC Advances* **1**, 1620-1640 (2011).

24 Yamada, S. & Sato, H. Some Physical Properties of Glassy Carbon. *Nature* **193**, 261-262 (1962).

25 Harris, P. J. F. New Perspectives on the Structure of Graphitic Carbons. *Critical reviews in solid state and materials sciences* **30**, 235-253 (2005).

26 *Smithsonian Physical Tables*. 9th edn, (Smithsonian Institution, 1954).

27 *Knovel Critical Tables*. 2nd edn, (Knovel, 2008).

28 Chehimi, M. M., Hallais, G. r., Matrab, T., Pinson, J. & Podvorica, F. I. Electro- and Photografting of Carbon or Metal Surfaces by Alkyl Groups. *The Journal of Physical Chemistry C* **112**, 18559-18565, doi:10.1021/jp807044j (2008).

29 Hamelin, A. Cyclic Voltammetry at Gold Single-crystal Surfaces. Part 1. Behaviour at Low-index Faces. *Journal of Electroanalytical Chemistry* **407**, 1-11, doi:10.1016/0022-0728(95)04499-x (1996).

30 Ji, C., Oskam, G. & Searson, P. in *201st ECS Meeting* (Philadelphia, PA, 2002).

31 Kinoshita, K. *Carbon: Electrochemical and Physicochemical Properties*. (John Wiley & Sons, Inc., 1987).

32 Gardziella, A., Pilato, L. A. & Knop, A. *Phenolic Resins: Chemistry, Applications, Standardization, Safety and Ecology*. 2nd edn, (Springer-Verlag Berlin Heidelberg, 2000).

33 Pocard, N. L., Alsmeyer, D. C., McCreery, R. L., Neenan, T. X. & Callstrom, M. R. Doped GlassyCarbon: A New Material for Electrocatalysis. *Journal of Materials Chemistry* **2**, 771-784 (1992).

34 Callstrom, M. R., Neenan, T. X., McCreery, R. L. & Alsmeyer, D. C. Doped Glassy Carbon Materials (DGC):Low-temperature Synthesis, Structure, and Catalytic Behavior. *Journal of the American Chemical Society* **112**, 4954-4956, doi:10.1021/ja00168a049 (1990).

35 Bhatia, G., Aggarwal, R. K., Malik, M. & Bahl, O. P. Conversion of Phenol Formaldehyde Resin to Glass-like Carbon. *Journal of materials science* **19**, 1022-1028 (1984).

36 Jiang, D., Goddard, W. & Dai, S. Simulating the Initial Stage of Phenolic Resin Carbonization via the ReaxFF Reactive Force Field. *The Journal of Physical Chemistry A* **113**, 6891-6894 (2009).

37 Soukup, L., Gregora, I., Jastrabik, L. & Koňáková, A. Raman Spectra and Electrical Conductivity of Glassy Carbon. *Materials Science and Engineering: B* **11**, 355-357, doi:10.1016/0921-5107(92)90240-a (1992).

38 Oiye, É. N., de Andrade, J. F., Balbo, V. R., dos Santos, A. L. & de Oliveira, M. F. Development of an Alternative Route for Production of Glassy Polymeric Carbon Electrodes in Laboratorial Scale. *Macromolecular symposia* **299-300**, 147-155, doi:10.1002/masy.200900127 (2011).

39 Schroder, D. K. *Semiconductor Material and Device Characterisation*. Third edn, (John Wiley & Sons, 2006).

40 Brownson, D. A. C., Kampouris, D. & Banks, C. Graphene Electrochemistry: Fundamental Concepts Through to Prominent Applications. *Chemical Society Reviews* **41**, 6944-6976 (2012).

Chapter 4: Fluorinated Electrodes

Studies on EWOD systems have shown that hydrophobic dielectric materials are important for reducing hysteresis.[1] Furthermore, organic solvent droplets on hydrophobic surfaces have low Young angles, thus lowering the minimum attainable electrowetting contact angle. For these reasons, various methods for creating fluorinated electrodes were investigated.

A common method of increasing surface hydrophobicity is the inclusion of fluorine atoms. This is because a fluorine atom bonded to an sp^3 carbon greatly disrupts the hydrogen bonding network in water increasing the surface energy.[2] However, these fluorine containing materials are usually insulating solids, such as PTFE. Any surface for electrowetting purposes must be conductive and so this chapter concerns the production of fluorine containing hydrophobic surfaces with a high degree of conductivity for use as electrowetting electrodes. Three distinct methods are used: electrochemical functionalisation, plasma fluorination and chemical fluorination of a conducting polymer.

4.1 Electrochemical functionalisation

Electrochemical functionalisation of surfaces, often known as electrografting, is a method of attaching small organic molecules to solid conducting surfaces. The reaction generally proceeds via a reactive intermediate generated by electrochemical oxidation or reduction which then attacks the surface and forms a covalent bond.[3] The strength of the bond is critical as it is important to permanently adhere the fluoro species to the surface to ensure that the surface cannot change in composition underneath the droplet (a source of hysteresis discussed in Chapter 1, as happens with chemisorbed thiols for example).[4]

4.1.1 Electrografting

4.1.1.1 Overview

Many methods for electrochemical surface functionalisation have been developed, with the generation of a radical intermediate common to all of them.[3]

The one electron oxidation of many functional groups—such as primary amines, phosphates, alcohols and carboxylates—generates a free radical and a proton. These reactions occur at moderate potentials, for example the oxidation of the amino group in 4-aminobenzylphosphonic acid is an irreversible process occurring at 0.75 V (versus the normal hydrogen electrode) while the oxidation of the phosphate group occurs at 0.90 V (Figure 49).[5] The free radical species generated then proceeds to attack the electrode, forming a covalent bond.

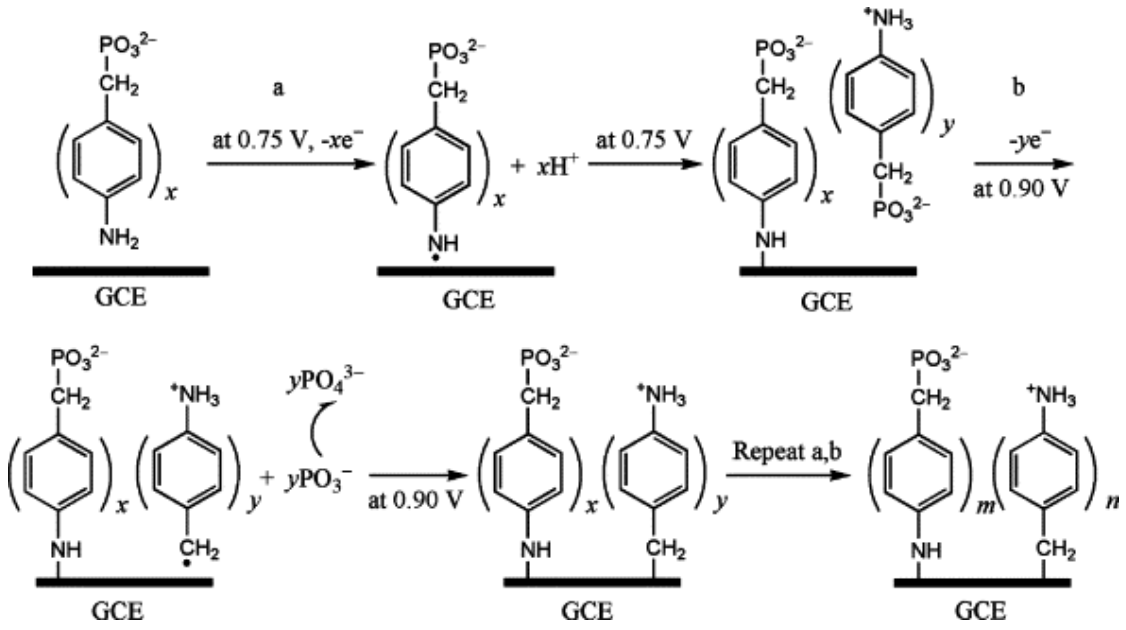

Figure 49|[Taken from Yang[5]] Illustration of the mechanism of surface functionalisation of a glassy carbon electrode (GCE) via amine or phosphate oxidation.

Similarly, other functional groups can be electrochemically reduced. These include alkyl halides, which can also be photografted with electromagnetic radiation, and vinylic compounds which subsequently undergo electropolymerisation at the double bond.[6-8]

Surfaces functionalised by the above methods have been successfully used as sensors for a plethora of molecules—such as hydrogen peroxide, nitric oxide, dopamine and alanine—and can also effectively measure pH.[9-13] However, the surfaces are of highly variable quality and examples are generally limited to solitary cases in the literature.

The precise nature of the film, including its structure and electrochemistry, is often not fully characterised. Preliminary experiments that were performed as part of this project resulted in macroscopically patchy surfaces (feature size greater than 0.1 mm). By far the most common method of electrografting is via reduction of diazonium compounds. This is covered in the next section and was the preferred method for surface functionalisation in this thesis.

4.1.1.2 Diazonium grafting

Following some preliminary experiments covering many of the above methods, diazonium chemistry was found to be the most efficient and effective surface functionalisation method. It involves the one electron reduction of an aromatic diazonium compound which creates an aryl free radical and generates molecular nitrogen in the process (Figure 50).[14]

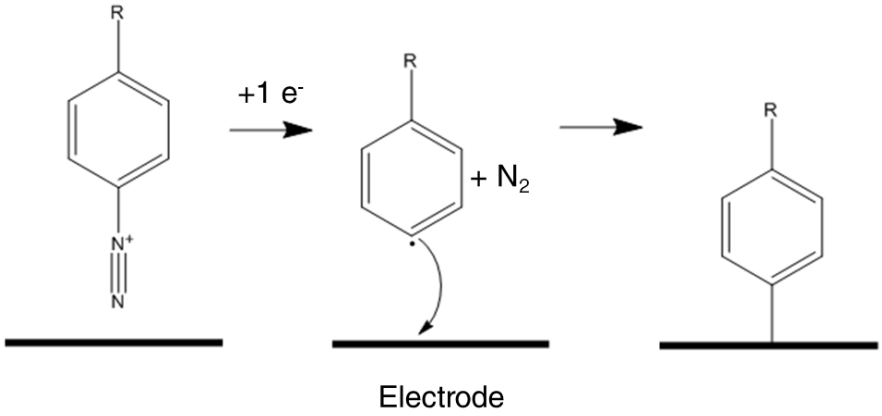

Figure 50|Mechanism of surface functionalisation by a generic diazonium compound. The one electron reduction of the diazonium species produces an aryl free radical and molecular nitrogen which diffuses away. The radical then attacks the surface forming a covalent bond.

Figure 51 shows the voltammetry of the electrochemical reduction of a typical diazonium compound, 4-nitrobenzenediazonium. It shows how after the first reductive scan, the electrochemical current disappears almost entirely. The organic layer that forms on the surface blocks the diazonium compound from diffusing to the electrode, preventing more molecules from being reduced. This layer, usually around 20 nm in thickness, cannot be removed by ultrasonication, indicating that it is securely attached. It is also commonly reported (without experimental justification) that the organic layer is a monolayer.[3] This is almost certainly not the case and, as will be seen below, special methods are required to generate a monolayer. It is clear from the thickness of the layer that it is more than one molecule thick. In fact, after the first layer has been deposited, radicals continue to be produced (the electrode surface is not blocked). However, as the electrode surface is now completely covered, the radicals proceed to attack the molecules already on the surface and a multilayer begins to grow. This process continues until the multilayer blocks the electrochemical reduction and no more radicals are formed.

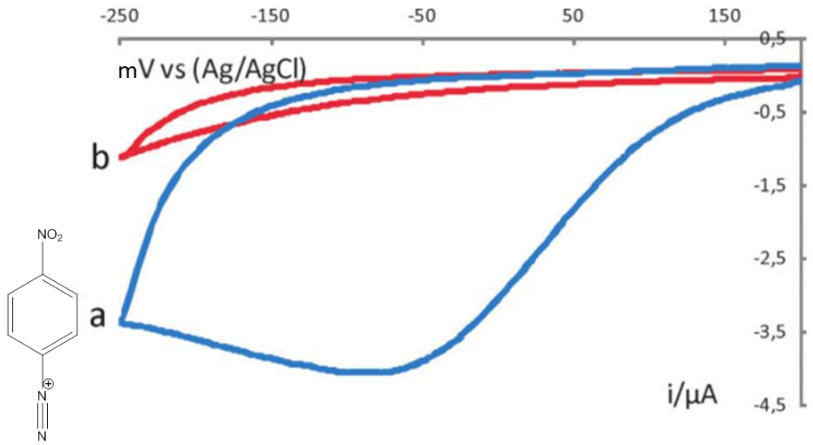

Figure 51|[Taken and modified from Belanger[3]] Voltammetry of the electrochemical reduction of 4-nitrobenzenediazonium (5 mmol dm^{-3} in 0.1 mol dm^{-3} H_2SO_4, scan rate = 100 mV s^{-1}). The first scan, scan a, shows a broad reduction peak centred on –60 mV. In the second scan, scan b, the peak has disappeared. This is explained by the formation of an organic layer which blocks access of the 4-nitrobenzenediazonium to the electrode.

The aryl group is essential to the stability of the radical and the ability of the molecule to functionalise the surface. Alkyl radicals have much shorter lifetimes, to the extent that they decompose or react with the solvent before being able to attack the electrode surface and very few aliphatic salts have been successfully grafted.[15] The functional groups attached to the aryl ring seem to have little effect on the viability of the functionalisation. As a result, almost all simple aryl diazonium species have been successfully adhered to a variety of substrates such as gold, copper, iron and the various forms of carbon.[3]

4.1.1.3 Monolayer formation

For electrowetting purposes, the formation of a surface monolayer may be important because a multilayer might be expected to be very rough while also reducing the capacitance of the metal surface. In turn, this could reduce the electrowetting response. As mentioned above, despite initial suppositions, diazonium grafting will ordinarily produce a multilayer. Therefore, several methods, which will be described below, have been developed to overcome this.

The 'formation-degradation' procedure has been reported by the group of Daasbjerg.[16,17] This method involves the grafting of aromatic diazonium compounds containing either disulphide

or hydrazone functionalities, shown in Figure 52. Following grafting of the molecules by the conventional method (resulting in multilayer formation), the first molecular layer itself is cleaved in half. This is done either electrochemically in the case disulphide or by acid hydrolysis in the case of hydrazone. The result is that the outer layers, which are attached to the outer half of the first layer, are removed entirely from the surface and a monolayer is formed.

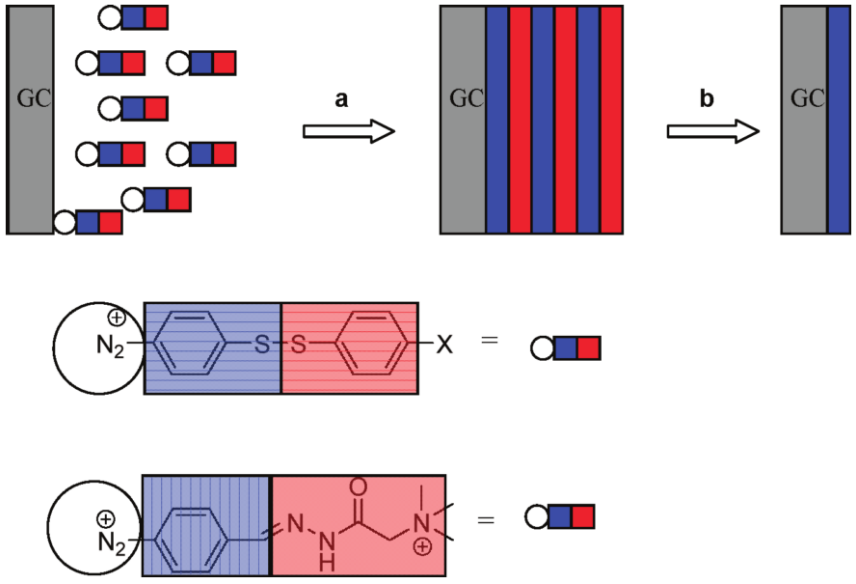

Figure 52|Illustration of the 'formation-degradation' method for surface monolayer preparation. The disulphide functionality can be oxidised to a thiol, detaching all but the first aromatic ring from the electrode surface. Similarly, the hydrazone group can be chemically cleaved, leaving behind an aldehyde.

Leroux et al. have produced monolayers by depositing diazonium compounds with triisopropylsilyl protecting groups.[18] These are very large, bulky groups and prevent radicals from attacking the aryl ring, thus preventing multilayer growth. The silyl group can then be removed chemically leaving an alkyne functionality.

The problem with the methods presented thus far, is that they don't leave molecules containing the hydrophobic functional groups needed. This means that post functionalisation is necessary. Whilst this is possible, it requires lengthy and expensive characterisation by XPS

and Raman spectroscopy to confirm the presence of the desired functional group. Furthermore, the conversion of all surface molecules is unlikely to be complete.

Two methods of monolayer formation remain which don't require any post functionalisation, allowing a single layer of hydrophobic molecules to be attached to the surface in one step. The first, oxidation of phenyl hydrazines (formed by chemical reduction of the relevant diazonium compound), has been reported by Malmos et al.[19,20] Surface physisorption of other molecules (which must later be removed by sonication) is postulated to explain the termination of growth at a monolayer. Nonetheless, it is still somewhat unclear as to why such thin layers form as the same aryl free radical intermediates seen in multilayer growth are believed to be created. The other method is similar in principle to the triisopropylsilyl protecting group method described above: it uses sterics to prevent the phenyl ring being attacked by radicals. Combellas et al. have used 3,5-di-tert-isobutylbenzenediazonium, to successfully produce monolayers, as shown in Figure 53.[21] The large tert-isobutyl groups prevent free radicals from getting near the aromatic ring which is the part of the molecule most susceptible to attack. Therefore, multilayer growth becomes very slow: after 300 seconds at a reducing potential, the thickness of the surface layer grown on gold is reported to be only 1 nm, as measured by ellipsometry. This thickness corresponds to a monolayer. Furthermore, this monolayer is reported to raise the water contact angle of copper from 49° to 74°.

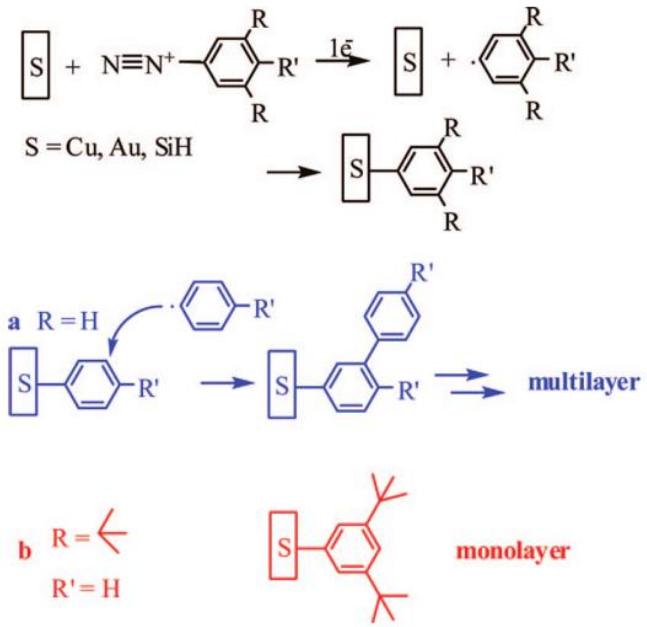

Figure 53 | [Taken from Combellas et al.[21]] Illustration of how kinetically hindering the phenyl ring of the diazo compound prevents the growth of a multilayer.

Owing to the simplicity of the steric blocking method of Combellas et al., along with the fact that no *in situ* functionalisation is needed afterwards, this was the method chosen to try to create a surface monolayer. While 3,5-di-tert-butylaniline, as used by Combellas et al., is commercially available, it is currently very expensive. Moreover, the hydrophobicity of the monolayer could be further increased by swapping the tertiary butyl groups for their fluorinated analogues. The diazonium salt 3,5-bis(2-ethoxyhexafluoroisopropyl) benzenediazonium tetrafluoroborate (Figure 54) was synthesised to achieve exactly this. Rather than having tert-butyl groups, this molecule has two trifluoromethyl groups and an ethoxy group instead. This should help to make the molecule more hydrophobic. This is based on Zisman's finding that CF_3 groups have a lower surface energy than CH_3 groups (15 J cm^{-2} rather than 30 J cm^{-2}, respectively).[22]

4.1.2 Experimental

^{1}H NMR spectra were recorded with a Bruker 400 MHz spectrometer; δ values are given in ppm relative to TMS. 1,3-Bis(2-hydroxyhexafluoroisopropyl)benzene (Fluorochem) and all

other materials (Sigma-Aldrich) were used as supplied. Contact angles were measured from photographs taken with a CCD camera (Phillips SPC900NC webcam) through a video zoom microscope (Edmund Optics Infinity K2/S Long Distance Video Lens) at 20× magnification. Contact angles were subsequently measured using Fta32 2.0 contact angle software (First Ten Ångstroms). All reported contact angles are advancing contact angles averaged over five measurements.

4.1.2.1 Synthesis of sterically hindered, fluorinated diazonium salt

10g (24.4 mmol) 1,3-Bis(2-hydroxyhexafluoroisopropyl)benzene were dissolved in 50 ml dimethylformamide. 7.9 g potassium carbonate (57 mmol) and 3 ml ethyl iodide (5.82 g, 37.3 mmol) were added. The mixture was stirred for 24 h under argon at room temperature and then quenched with saturated ammonium chloride solution and extracted three times with ethyl acetate. The combined organic extracts were washed with water and brine, dried with magnesium sulphate and concentrated. The remaining residue was filtered through silica using hexane. This gave 7.50 g of compound B, a yellow solid, yield 66 %.[23] ^{1}H NMR (400 MHz, d6-DMSO): δ=1.32 (m, CH_3, 6H), 3.59 (m, CH_2, 4H), 7.66-7.96 (m, 3H), 8.09 (s, 1H).

2 g compound B (4.28 mmol) were added to 50 ml 1:1 HNO_3:H_2SO_4 at 80 °C. The mixture was stirred for 1 h, quenched with saturated sodium bicarbonate solution and then extracted with dichloromethane three times.[24] The combined organic extracts were washed with water and brine, dried with magnesium sulphate and concentrated. This gave 1.41 g of compound C, a bright orange solid, yield 66 %. ^{1}H NMR (400 MHz, $CDCl_3$): δ=1.28 (m, CH_3, 6H), 3.75 (m, CH_2, 4H), 8.1-8.3 (m, 3H).

1 g compound C (2.00 mmol) was dissolved in 20 ml ethanol with 1 g 10% Pd/C. The mixture was stirred under a H_2 atmosphere for 6 h and then filtered under gravity.[24] The

ethanol was removed *in vacuo* to yield 0.91 g of compound D, a yellow oil, yield 97%. ^{1}H NMR (400 MHz, $CDCl_3$): δ=1.28 (m, CH_3, 6H), 3.75 (m, CH_2, 4H), 7.6-7.9 (m, 3H).

A 100 ml flask in an acetonitrile/dry ice bath was charged with nitrosonium tetrafluoroborate (0.23 g, 1.94 mmol) under argon. Dry acetonitrile (10 ml) was then added. After the solution had cooled to –30 °C, compound D (0.97 g, 1.94 mmol) in acetonitrile (10 ml) was added over 30 min. The yellow reaction mixture was stirred for 1 h at –30°C, treated with dry dichloromethane (50 ml) and filtered under vacuum. The white crystalline precipitate was washed with dry dichloromethane, and recrystallised from dry acetonitrile/dichloromethane. This gave 0.45 g of compound E, a white crystalline solid, yield 47%.[25]

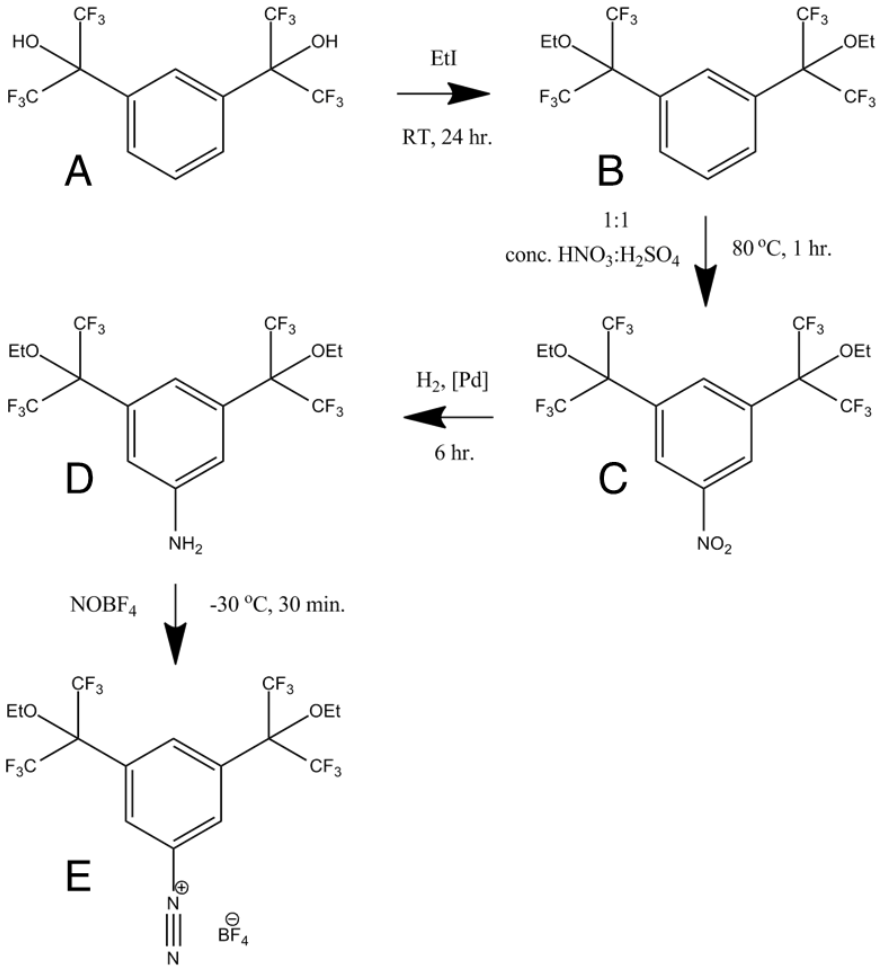

Figure 54|Reaction for the synthesis of the sterically hindered, fluorine containing diazonium salt 3,5-bis(2-ethoxyhexafluoroisopropyl)benzenediazonium tetrafluoroborate.

4.1.2.2 Electrochemical reduction of diazonium salts

Electrochemical experiments were performed with a Gamry Reference 600 potentiostat. The diazonium salts were dissolved in dry acetonitrile at 4 °C prior to electrochemical reduction. All potentials were measured against an Ag/Ag^+ reference electrode made from a silver wire in a capillary with frit filled with 0.01 mol dm^{-3} $AgClO_4$/0.1 mol dm^{-3} $TBAClO_4$ in acetonitrile. Diamond polished glassy carbon (HTW GmbH, Germany), template stripped gold and template stripped copper surfaces were utilised as surfaces for functionalisation.

4.1.3 Results

4.1.3.1 Electrochemical reduction

A broad irreversible reduction peak was seen at -800 mV versus Ag/Ag^+ on all electrode materials (copper, gold and glassy carbon). The peak disappeared after one scan, presumably due to passivation of the surface due to film growth, as is commonly seen (see Figure 51).

4.1.3.2 Contact angle

The water surface contact angle was measured before and after surface functionalisation. On glassy carbon (see Figure 55) and copper there was a substantial increase in contact angle while on gold there was no increase beyond the statistical error in the contact angle measurement. The largest contact angle increase was seen on copper, where the contact angle increased to 74° (from 49°). A comparison of changes in contact angle can be seen in Table 5. The copper contact angle is 1° larger than the contact angle reported by Combellas et al. after functionalisation of copper with the similar molecule 3,5-di-tert-butylbenzene.[21] This suggests that the surface has been successfully functionalised. It also suggests that the substitution of the tertiary methyl groups used by Combellas for trifluoromethyl groups only has a minor effect on the hydrophobicity of the surface.

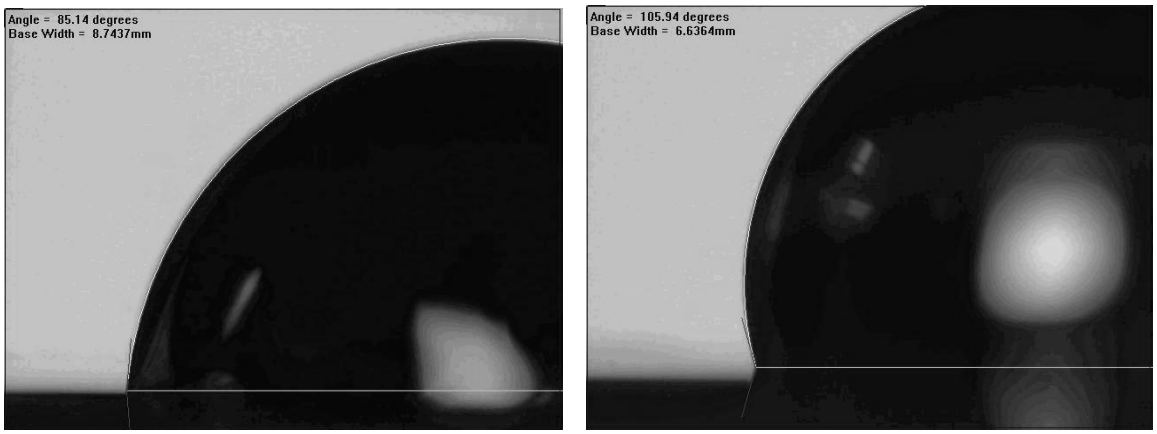

Figure 55|Contact angle of water on glassy carbon before and after 3,5-bis(2-ethoxyhexafluoroisopropyl)benzenediazonium tetrafluoroborate functionalisation.

The change in contact angle suggests that the surface has been functionalised with a hydrophobic species. Initial AFM micrographs could not detect any change in the surface structure although further characterisation with ellipsometry is still needed to confirm the presence of a monolayer.[26]

	Contact angle / degrees	
	Before functionalisation	After functionalisation
Gold	66±5	67±4
Glassy carbon	85±3	103±3
Copper	49±3	74±3

Table 5|Contact angle of water on gold, glassy carbon and copper before and after functionalisation with 3,5-bis(2-ethoxyhexafluoroisopropyl)benzene. Errors indicate ±1 standard deviation.

The small change in contact angle on gold suggests that there is a much lower surface coverage on gold, perhaps due to weaker bonding between the gold and phenyl ring. This effect may not usually be so pronounced when multilayer growth is possible. This is because the multilayer can branch out from a few molecules which have been attached to the surface, eventually covering the whole surface. There may also be some mechanical 'keying' of the film onto the surface. The contact angle on gold functionalised with 3,5-di-tert-butylbenzene is not reported by Combellas et al. and so no comparison can be made with this work in order to support this result.

4.1.3.3 Electrochemical surface area

In order to characterise the loss in electrochemical surface area after functionalisation with 3,5-bis(2-ethoxyhexafluoroisopropyl)benzene, the blocking of the one electron reduction/oxidation of potassium ferricyanide was studied. Figure 56 shows the voltammetry of a functionalised glassy carbon electrode. There is a 19% decrease in the redox peak current.

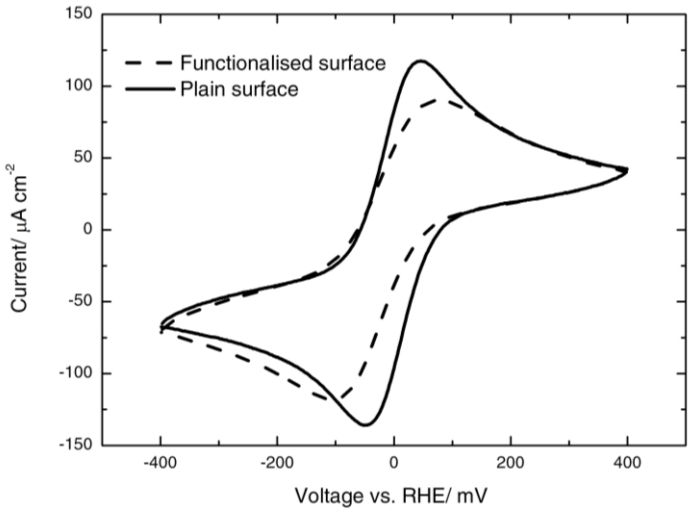

Figure 56|Reduction in redox current of $[Fe(CN)_6]^{4-}/[Fe(CN)_6]^{3-}$ couple due to blocking of surface of glassy carbon electrode functionalised by 3,5-Bis(2-ethoxyhexafluoroisopropyl)benzene. $K_3[Fe(CN)_6]$ concentration 5 mmol dm^{-3}, 0.1 mol dm^{-3} KCl, scan rate 100 mV s^{-1}.

Work by Bélanger et al. has indicated that deposition of (multilayer) 4-carboxybenzene and 4-nitrophenylbenzene blocks the $[Fe(CN)_6]^{2-}/[Fe(CN)_6]^{3-}$ redox couple.[14] Therefore, this suggests that a multilayer of 3,5-bis(2-ethoxyhexafluoroisopropyl)benzene has not been deposited.

4.2 Plasma fluorination

Many examples exist of the plasma mediated surface modification of polymer surfaces.[27] Simple gases such as O_2, N_2, Br_2 and SO_2 are fragmented in an oscillating magnetic field, creating a sea of electrons, ions and free radicals. The free radicals react with the polymer surface leaving a variety of functional groups such as –OH, $–NH_2$, –Br and $–SO_3H$ (example shown in Figure 57). These functional groups are strongly adhered to the carbon backbone of the organic polymer via covalent bonds. The surface can also be coated with a thin polymer layer via free radical polymerisation of unsaturated precursors. This method can be used to coat any material although there must be sufficient adhesion between polymer and substrate if the coating is to remain attached.

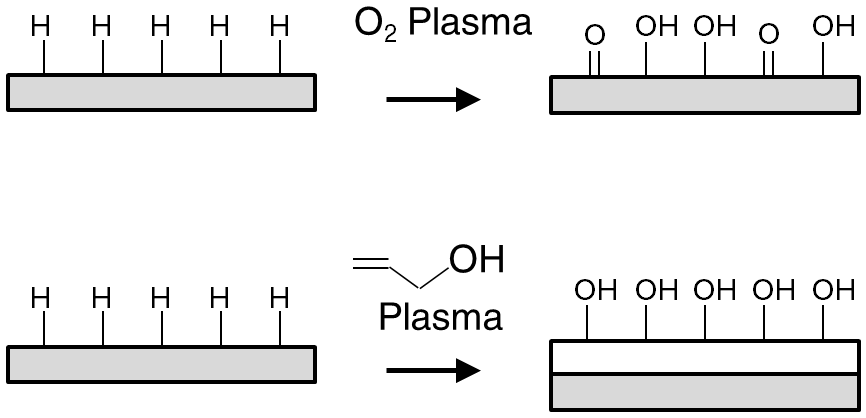

Figure 57|The exposure of common organic polymers such as polyethylene to oxygen plasma adds a variety of oxygen containing functional groups to the surface. A similar result can be achieved via the free radical (plasma) induced polymerisation of an allyl-containing monomer with the desired functionality. In this instance allyl alcohol is polymerised to produce a thin surface layer which adheres strongly to the underlying surface through Van der Waals interactions.

It was proposed that exposure of a metal surface to a plasma may functionalise the surface of the metal. Two different gases were tested: chlorodifluoromethane ($ClCF_3$, commonly known as CFC-22) and perfluoropropane (C_3F_8). CFC-22 plasma consists of fluorine, chlorine and Cl_xCF_y (x=0 or 1, y=0 to 3) free radicals. The perfluoropropane plasma consists of free radicals with a broad range of carbon to fluorine ratios. The gold-fluorine bond is generally

very unstable and very few pure gold-fluorine compounds exist. For example the enthalpy of formation of AuF_3 is –363.3 kJ mol^{-1} compared to –933.5 kJ mol^{-1} for CF_4.[28] Furthermore, the calculated enthalpy of reaction of AuF_3 with water (to hydrogen fluoride and Au_2O_3) is –887.4 kJ mol^{-1}.[29] Therefore, a fluorine terminated gold surface would almost certainly be unstable under ambient conditions. This is consistent with X-ray photoelectron spectroscopy studies on gold surfaces exposed to CF_4 plasma.[30] On the other hand, gold-carbon bonds are more common, and—as can be seen from the stability of diazonium functionalised surfaces described in Section 4.1.1—they are more stable. It was envisaged that these plasmas may therefore create Au-CF_3 or similar terminated surfaces.

4.2.1 Experimental

4.2.1.1 Fluorination

A Diener Electronic PICO Plasma System was used to generate plasmas. Template stripped gold surfaces (see 3.2.1 for preparation details) were stripped immediately prior to being placed in the plasma system. The chamber was pumped down to a pressure of approximately 0.1 mbar and then flushed with argon to ensure there was no oxygen, nitrogen or water vapour in the chamber, all to which would make hydrophilising plasmas. The power was set to 30 W which was found to be the minimum power at which a plasma could be sustained. A lower power was desirable as it allowed a slower deposition rate resulting in more control over the deposition. The optimum flow rate for a stable plasma for both gases was found to be 15 cm^3 min^{-1}. This resulted in a bright mauve plasma for CFC-22 and a slighter whiter plasma for perfluoropropane. The freshly exposed gold was then exposed to plasma for 6, 12, 18, 30, 60 or 300 seconds (with only tenths of a minute possible).

4.2.1.2 Contact angle measurements

Photographs of water on the fluorinated surfaces were taken with a CCD camera (Phillips SPC900NC webcam) through a video zoom microscope (Edmund Optics Infinity K2/S Long Distance Video Lens) at 20× magnification. Contact angles were subsequently measured using Fta32 2.0 contact angle software (First Ten Ångstroms). All reported contact angle are advancing contact angles. Four droplets were measured on each of three separate electrodes.

4.2.1.3 Electrochemical characterisation

Electrochemical measurements were performed with a Gamry Reference 600 potentiostat.

Cyclic voltammetry and impedance measurements were performed in 0.1 mol dm^{-3} NaF solution (NaF from Sigma-Aldrich, 99.5%) which is a non-specifically adsorbing electrolyte. Impedance measurements were made at 400 mV versus SCE (where no Faradaic processes occur). The frequency was scanned from 10 to 1000 Hz and the results fitted to a Randles circuit in order to extract the interfacial capacitance.

Underpotential deposition of Pb was performed in 0.1 mol dm^{-3} HNO_3 + 12 mmol dm^{-3} $PbNO_3$ + 10 mmol dm^{-3} NaCl.[31,32]

The ferricyanide/ferrocyanide redox couple (0.1 mol dm^{-3} H_2SO_4 + 1 mmol dm^{-3} $K_3Fe(CN)_6$) was used to study the blocking effect of the fluoro coating on electron transfer.

4.2.2 Contact angle

Contact angle measurements clearly show that that there is a large increase in hydrophobicity of the gold surface following exposure to the fluoro compound plasma. In the case of perfluoropropane, the contact angle increases from 66° on plain template stripped gold to 107° after 300 seconds of exposure to the plasma. Furthermore, there is a strong trend of increasing hydrophobicity with plasma exposure time as seen in Figure 58. Of the two gases used, at long exposure times the perfluoropropane produces the most hydrophobic surfaces, which is perhaps unsurprising as it has a higher fluorine content than CFC-22.

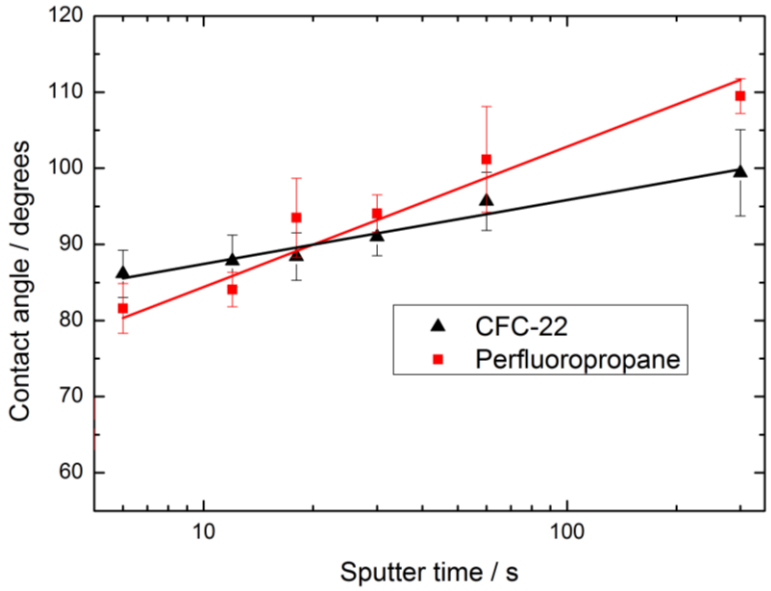

Figure 58|Contact angle of water on template stripped gold after exposure to CFC-22 and perfluoropropane plasmas. Exposure times varied from 6 s to 300 s. Contact angle measured 10 times on each of three separate gold surfaces. Error bars are ±1 standard deviation.

Rinsing the surfaces with water had no effect on the contact angles. Sonication in acetone for 60 seconds changed the contact angle of the 300 second perfluoropropane plasma surface from 108° to 103°, suggesting that the surfaces are fairly robust and well bound to the surface.

4.2.3 AFM

AFM was used to study the gold surface after fluorination in order to discern if the surface structure had changed, whether there was polymerisation of the plasma on the surface and whether there was a substantial increase in the roughness of the surface. Figure 59 shows CFC-22 coated surfaces after different plasma exposure times. Given the nanometre feature size, it is clear that there was bulk growth of a polymer on the surface rather than monolayer formation. There is a clear correlation between the thickness of the layer and the exposure time.

The surfaces are actually very smooth, and the RMS roughness of the roughest surface is 1.7 nm over 500 nm^2. This should be compared with the RMS roughness of a typical polymer surface, which is in excess of 20 nm.[33]

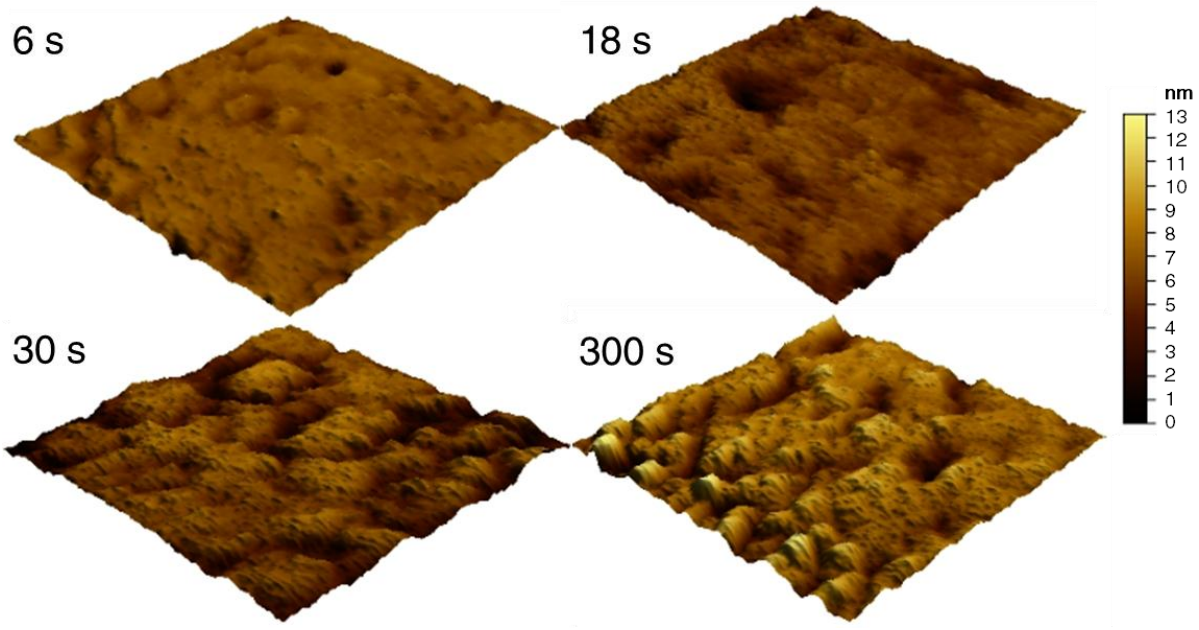

Figure 59|AFM images of template stripped gold after various CFC-22 plasma exposure times. Surface area 500×500 nm^2.

4.2.4 Electrochemistry

Cyclic voltammetry, electrochemical impedance spectroscopy and underpotential deposition were used to characterise the resulting surfaces in order to find out whether the electrochemical properties of gold were retained by the modified surfaces. These measurements also help to indicate whether the surface film is chemically bonded to the gold or if the film is simply coating the surface.

4.2.4.1 Cyclic voltammetry

The cyclic voltammetry of plasma fluorinated surfaces in 0.1 mol dm^{-3} NaF solution (Figure 60) showed no additional redox peaks when compared with plain template stripped gold surfaces. Instead there was a slight reduction in the observed current at all potentials. Nonetheless, below -0.9 V and above 1.4 V versus RHE, large currents resulting from the reduction and oxidation of water were still seen on the fluorinated surfaces. This suggests that the film does not completely block the gold surface and that the film itself shows no redox activity between -0.9 V and 1.4 V versus RHE. The unfunctionalised gold voltammograms are similar to those found in the literature.[34,35]

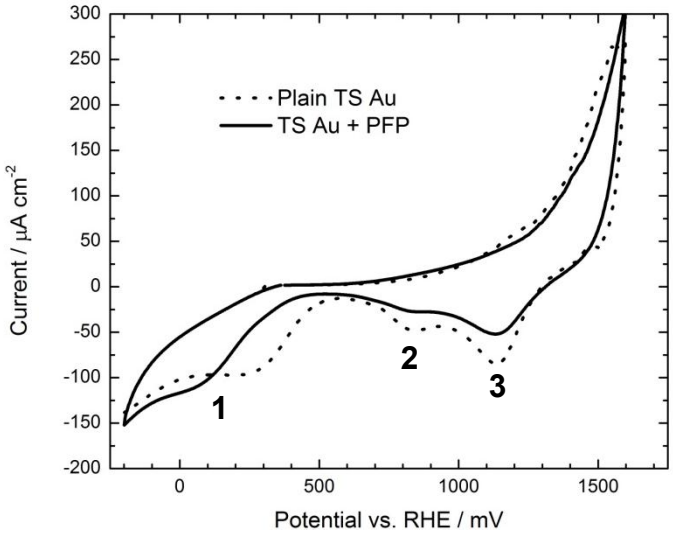

Figure 60|Cyclic voltammograms of plain template stripped gold (...) and template stripped gold after 6 s exposure to PFP plasma (_) in 0.1 mol dm^{-3} NaF solution. Scan rate 100 mV s^{-1}. Peak 1 is the result of reduction of oxygen in the solution and disappears as the solution is

degasssed. It should be noted that peak 2 increases while peak 3 decreases with subsequent scans. This is possibly due to a rearrangement of the template stripped surface.

However, if the electrode was polarised to either –0.9 V or 1.4 V, it began to lose its hydrophobicity and its water contact angle eventually returned to that of plain gold. This suggests that the hydrophobic layer had been removed by the physical agitation of the surface polymer caused by the evolution of gas bubbles.

4.2.4.2 Capacitance

Interfacial capacitance is the fundamental driving force for shape change in electrowetting. Therefore, it is crucial that any modified electrode used for electrowetting should have a large interfacial capacitance. Except in the case of perfluoropropane after a 300 second plasma exposure time, it was found that the capacitance of the gold surface was unaffected by the presence of the fluoro-film, as shown below in Table 6.

	Capacitance / μF cm^{-2}	
Fluorination time / s	**CFC-22**	**Perfluoropropane**
0	10.7	10.7
6	10.6	11.5
12	10.7	11.7
18	11.5	12.5
30	10.8	11.4
60	11.0	10.8
300	11.2	4.8

Table 6|Electrochemical capacitance as a function of gold exposure time to CFC-22 and perfluoropropane plasmas. The error in the measurements is approximately ±10% due to estimation of the surface area of the electrodes.

As the variation in the capacitance is less than the experimental error (except in one case), and these is no trend in increase or decrease of capacitance for either plasma, this suggests that there is no change in the surface capacitance. The only significant change is for 300 seconds of exposure to perfluoropropane plasma, for which the capacitance is more than halved. It is possible, therefore, that at very long plasma exposure times, a thick enough layer builds up blocking the surface. As discussed above, this layer can be removed by polarising the surface at large potentials, after which the capacitance returns to that of plain template stripped gold.

4.2.4.3 Underpotential deposition

Underpotential deposition is a common method for determination of the real surface area of a metal. The underpotential deposition of lead on polycrystalline gold is well established for this purpose.[31,36] Therefore, this method was attempted in order to quantify the loss—if any—of gold surface area as a result of the plasma fluorination process. However, as can be seen from Figure 61, it was found that the first and third deposition peaks were very poorly defined, even for freshly stripped gold surfaces (without any surface treatment). As the peaks were so small in comparison to the double layer charging current, attempts to correlate peak area with gold surface area produced radically variable results and it was not possible to use this technique to reliably measure gold surface areas.

This result is surprising as freshly stripped gold surfaces should be very clean and hence be excellent surfaces for under potential deposition. It is unclear as to why this is not the case. The electrochemistry of template stripped surfaces have not been studied in detail. Unrelated work conducted by other members of our group has indicated that the cyclic voltammetry of template stripped platinum in sulphuric acid also has poorly defined peaks, which gradually become sharper over subsequent cycles. These observations suggest that more work needs to be done on the electrochemistry of template stripped surfaces.

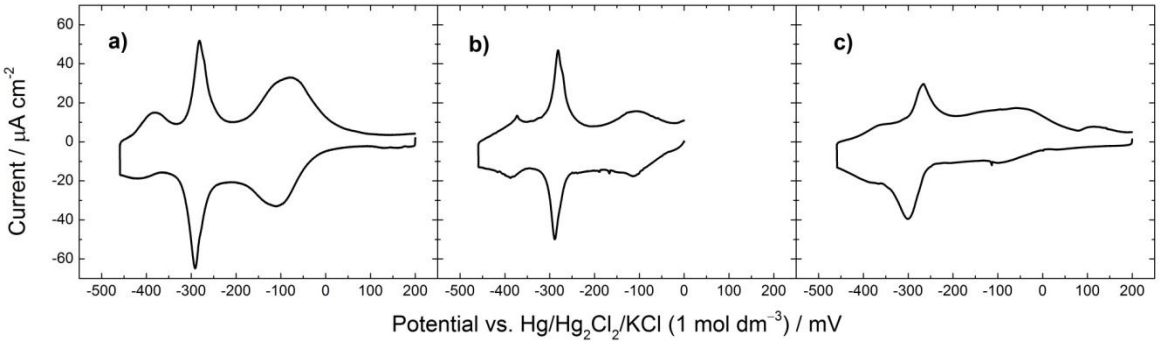

Figure 61|Underpotential deposition of 12 mmol dm^{-3} $Pb(NO_3)_2$ in 10 mmol dm^{-3} NaCl and 100 mmol dm^{-3} HNO_3 on **a)** etched gold wire, **b)** template stripped gold and **c)** template stripped gold after exposure to PFP plasma for 60 s. Scan rate 20 mV s^{-1}. When comparing **a)** with **b)** and **c)**, there is a change in ratio of the peak areas. One possible explanation for this is a change in the ratios of different crystal facets on the different polycrystalline gold surfaces.

4.2.4.4 Electron transfer

The surfaces were also not blocking to the ferricyanide/ferrocyanide redox couple. The only case for when there was a loss is redox current was for the 300 second exposure perfluoropropane, where there was a 42±5% loss. This result is in agreement with the capacitance data.

4.2.5 CFC-22 versus perfluoropropane

It should be noted that while neither compound is damaging to human health, both compounds are strong greenhouse gases and CFC-22 is also an ozone depleter. As a result, CFC-22 has been recently been banned in Europe and is slowly being phased out internationally. This means that perfluoropropane is definitely the preferred gas for surface fluorination because of its superior surface modification properties and lower environmental impact.

4.2.6 Discussion

These results clearly show that the exposure of gold to CFC-22 and perfluoropropane plasmas increases the surface hydrophobicity. AFM micrographs indicate that this is as a result of the build-up of a polymer layer, several nanometres thick, on the surface. Presumably this polymer layer is rich in fluorine atoms making it hydrophobic.

Nonetheless, this layer does not substantially alter the electrochemical properties of the underlying gold surface. The electrode maintains its electrochemical capacitance and does not block the one electron reduction of the ferricyanide ion.

However, the layer is eventually removed when hydrogen is evolved at –0.9 V or an oxide layer is grown on the surface at 1.4 V. This suggests that the polymer may be removed by physical agitation. The surface cannot be rinsed off with water but sonication in acetone does begin to reduce the hydrophobicity.

All of these observations seem to indicate that the polymer is not strongly adhered to the surface suggesting that there are no chemical bonds between the surface and the polymer. AFM images also suggest poor coverage of the surface by the polymer. Nonetheless, there is no loss at all in the capacitance of the gold. Therefore, it might be that electrolyte solution can wet underneath the polymer surface. It is only at very long plasma exposure times (300 seconds PFP plasma) that enough polymer forms and parts of the gold surface are no longer in contact with the solution.

The question remains as to why the polymer has not bonded to the gold surface when phenyl free radicals formed by the reduction of diazonium ions do bond to gold. One explanation is that the aryl carbon-gold bond is between gold and an sp^2 hybridised carbon rather than an sp^3 hybridised carbon as would be the case for a trifluoromethyl group. The latter may be a less stable bond. Another possible reason is the presence of fluorine radicals; these are incredibly reactive and mobile making them liable to bond with any carbon atoms nearby, even if this means breaking a gold-carbon bond first. Returning to the diazonium derived aryl free radical, this species, when generated, will readily displace a hydrogen atom on a nearby phenyl ring. This is the mechanism by which multilayer formation occurs during diazonium grafting (Figure 53). Therefore, it is plausible that fluorine free radicals will ‘undo’ any carbon-gold bonds which form.

4.3 Derivatised conducting polymer coatings

Conductive polymers are organic materials able to conduct electricity. Being carbon-based materials, they can be designed to exhibit specific properties by the considered selection of polymer backbone and side groups. Of particular interest to electrowetting substrates is control of the surface wettability. It has been shown by Schwendeman et al. that the addition of a perfluorinated carbon chain to the monomer precursor of poly(3,4-ethylenedioxythiophene), or PEDOT, created a polymer with a water contact angle of 110°.[37] This fluorinated version of PEDOT, shown in Figure 62 and referred to as PEDOT-F from here on, had a conductivity of 65 S cm^{-1}, which is similar to the conductivity of glassy carbon.

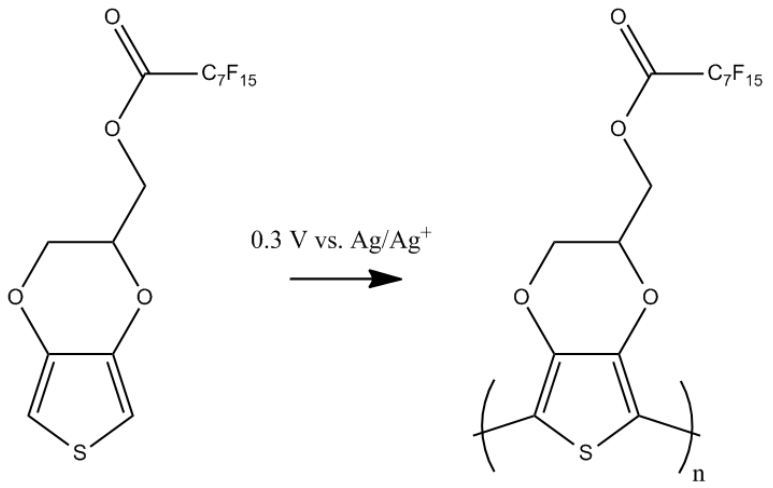

Figure 62| Pentadecafluoro-octanoic acid 2,3-dihydro-thieno(3,4-*b*)(1,4)dioxin-2-ylmethylester, or EDOT-F can be electropolymerised to form the conductive hydrophobic polymer PEDOT-F.[37]

4.3.1 Experimental

4.3.1.1 EDOT-F synthesis

The preparation of pentadecafluoro-octanoic acid 2,3-dihydro-thieno(3,4-*b*)(1,4)dioxin-2-ylmethylester (EDOT-F) is described elsewhere.[37] The yield was 67 %. ^{1}H NMR (400 MHz,

$CDCl_3$): δ=4.09 (dd, 1H), 4.25 (dd, 1H), 4.48 (m, 1H), 4.62 (m, 2H), 6.39 (s, 2H). NMR shifts were in accordance with the literature.

4.3.1.2 Electropolymerisation

EDOT-F was coated onto both sputtered gold electrodes and template stripped gold electrodes (see Sections 5.1.3 and 3.2.1 respectively). In order to make electrical contact to the gold, a wire was attached to the electrode with conductive epoxy (Circuit Works) which was itself covered with an insulating epoxy layer. The supporting electrolyte was 0.05 mol dm^{-3} tetrabutylammonium perchlorate (TBAP) and the EDOT-F concentration was 0.01 mol dm^{-3} in dry propylene carbonate (PC). Solutions were de-gassed with 99.9992% nitrogen (BOC gases). The electropolymerisation potential was 0.7 V versus 0.01 mol dm^{-3} Ag/Ag^+. A charge of 0.1 or 1.5 C cm^{-2} was allowed to pass.

The choice of PC as a solvent was based on work by Poverenov et al. who showed that PC produces much smoother PEDOT surfaces than acetonitrile.[38]

Afterwards the electrodes were rinsed in pure PC followed by de-ionised water and dried under vacuum.

Annealing of the electrodes was performed in an inert nitrogen atmosphere at 230 °C for 1 h.

4.3.1.3 Template stripping

A detailed overview of template stripping is given in 3.1.1. This technique was used to try to create flat PEDOT-F surface. After electropolymerisation of the PEDOT-F on a template stripped gold slide followed by annealing, the deposited film was attached to glass with Buehler Epo-Thin epoxy. After the epoxy had cured, the PEDOT-F film could be removed from the gold surface. AFM was used to characterise the roughness of the resulting surface.

4.3.2 Contact angle

The water contact angle on the PEDOT-F surface varied dramatically depending on the electrodeposition and whether the surface was annealed or not, as shown in Table 7.

	Electropolymerisation charge passed		
	0.1 C cm^{-2} (not annealed)	0.1 C cm^{-2} (annealed)	1.5 C cm^{-2} (not annealed)
Contact angle/ degrees	75±5	94±2	146±9

Table 7|Contact angle of water on PEDOT-F surfaces of varying thicknesses. Films were deposited from 0.05 mol dm^{-3} $TBAClO_4$ and 0.01 mol dm^{-3} EDOT-F in PC. The electropolymerisation potential was 0.7 V versus Ag/Ag^+ reference. Errors indicate ±1 standard deviation.

The superhydrophobic surface (contact angle 146±9°) results from the high surface area due to the extreme roughness of the electrode shown by the SEM image in Figure 63. This is explained by the Cassie equation (Equation 2), page 27). The microscale feature size of the polymer domains is typical of a superhydrophobic surface.[39] Almost identical results have recently been reported by Darmanin and Guittard.[40]

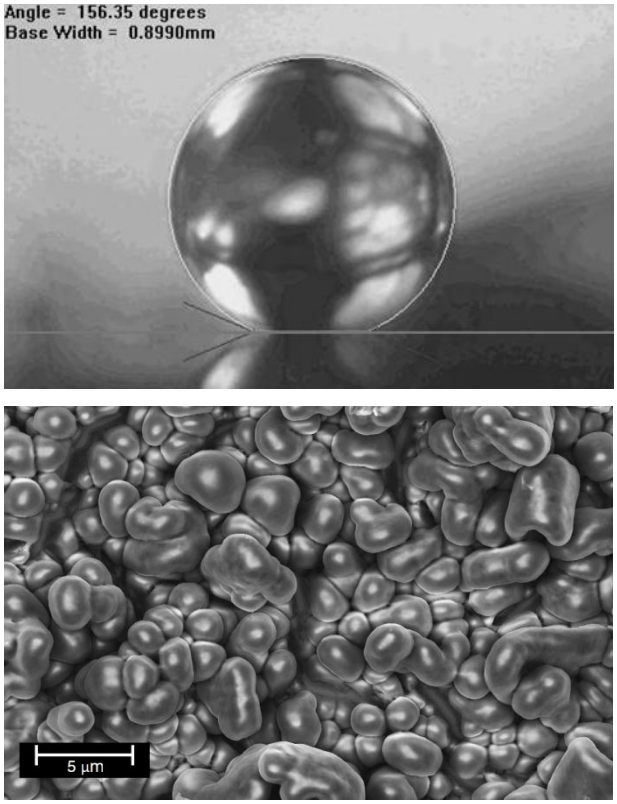

Figure 63|(Top) Photograph of a water droplet on a superhydrophobic PEDOT-F surface with a 156° contact angle. (Bottom) Scanning electron micrograph of the same surface. The high surface area and porosity of the surface dramatically increase the hydrophobicity.

4.3.3 Surface roughness

The RMS roughness of the thin (0.1 C cm^{-2}) films was 31.1 nm after annealing, as measured by AFM. Template stripping of the thicker (1.5 C cm^{-2}) films was possible. The surface is shown in Figure 64, and has an RMS roughness of 5.3 nm, suggesting that the polymer does not mate well with the underlying template. Alternatively, it may deform after being removed from the template or the surface may become damaged during the stripping, with some of the polymer remaining on the gold.

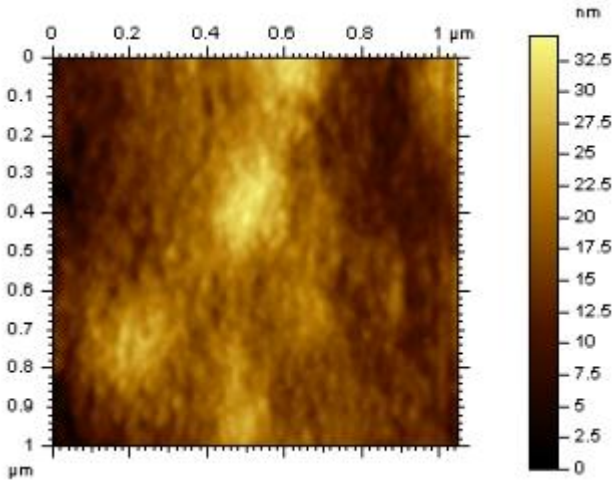

Figure 64|Template stripped PEDOT-F. 5.3 nm RMS roughness. 17.6 nm peak height.

4.3.4 Conductivity

The bulk conductivity of PEDOT-F could not be reliably measured due to the gold layer underneath the deposited film. However, the films were electrically conductive. Evidence for this includes redox activity of the film, which became sky blue when oxidised; the fact that the surface did not need to be coated with a conductive metal in order to take an SEM image and also the fact that thick polymer films could be grown.

4.4 Conclusions

A variety of methods have been used to create hydrophobic conducting surfaces. The compound 3,5-bis(2-ethoxyhexafluoroisopropyl)benzenediazonium tetrafluoroborate, which is similar to the compound 3,5-di-tert-butylbenzenediazonium tetrafluoroborate made by Combellas et al., was synthesised.[21] It was deposited on gold, glassy carbon and copper forming a hydrophobic monolayer. The properties of the functionalised surfaces were similar to the 3,5-di-tert-butylbenzenediazonium surfaces of Combellas et al. despite the fact that they

contain hydrophobic trifluoromethyl groups. The surface layer increased the water contact angle of glassy carbon by 18° and copper by 25° however the contact angle on gold was unaffected. The functionalised surfaces were only slightly blocking to the one electron reduction of the ferricyanide ion. Further measurements with AFM and ellipsometry are still required to confirm that a monolayer has indeed been produced.

The plasma polymerisation of the gases CFC-22 and perfluoropropane was performed on gold surfaces. The resulting surfaces were characterised with AFM; cyclic voltammetry; electrochemical impedance measurements of the capacitance; and underpotential deposition of lead. The plasma appears to form a thin polymer layer which is fairly weakly attracted to the underlying surface. Nonetheless the surface is stable in water and electrolyte solutions but is removed by the evolution of oxygen or hydrogen. The polymer layer substantially increases the hydrophobicity of the gold surface, with 60 seconds of exposure to perfluoropropane gas resulting in a water contact angle of 109°. Remarkably, at this exposure time the electrode retains its capacitance and does not block the reduction of ferricyanide. Underpotential deposition of lead could not accurately determine the surface coverage as the characteristic lead deposition peaks could not be resolved on template stripped gold—a potential subject for future investigation. At longer exposure times the surface becomes more hydrophobic but begins to block electrochemical processes. The thin polymer layer is very smooth when compared with typical polymer surfaces. The RMS roughness of the surfaces never exceeds 1.7 nm over 500 nm^2.

The final method of hydrophobic electrode fabrication was synthesis of PEDOT-F as originally performed by Schwendeman et al.[37] This produces a very rough hydrophobic surface. It was found that by varying the polymerisation conditions, a superhydrophobic surface could be made. Depending on the intended application, this may be desirable. In order to make a smooth surface, template stripping of the polymer was attempted. Whilst there was a substantial reduction in the roughness of the resulting surface (RMS roughness of 5.3 nm), it was not as smooth as typical template stripped surfaces.

These methods all have their respective benefits and disadvantages. Therefore, the individual requirements of a given task should be considered when deciding which type of hydrophobic conducting surface should be used.

4.5 References

1 Maillard, M., Legrand, J. & Berge, B. Two Liquids Wetting and Low Hysteresis Electrowetting on Dielectric Applications. *Langmuir* **25**, 6162-6167, doi:10.1021/la804118y (2009).

2 Dalvi, V. & Rossky, P. Molecular Origins of Fluorocarbon Hydrophobicity. *Proceedings of the National Academy of Sciences of the United States of America* **107**, 13603-13607 (2010).

3 Belanger, D. & Pinson, J. Electrografting: A Powerful Method for Surface Modification. *Chemical Society Reviews* **40**, 3995-4048 (2011).

4 Gorman, C. B., Biebuyck, H. A. & Whitesides, G. M. Control of the Shape of Liquid Lenses on a Modified Gold Surface Using an Applied Electrical Potential across a Self-Assembled Monolayer. *Langmuir* **11**, 2242-2246, doi:10.1021/la00006a063 (1995).

5 Yang, G., Liu, B. & Dong, S. Covalent Modification of Glassy Carbon Electrode during Electrochemical Oxidation Process of 4-aminobenzylphosphonic Acid in Aqueous Solution. *Journal of Electroanalytical Chemistry* **585**, 301-305, doi:10.1016/j.jelechem.2005.09.017 (2005).

6 Andrieux, C. P., Gallardo, I., Saveant, J. M. & Su, K. B. Dissociative Electron-Transfer - Homogeneous and Heterogeneous Reductive Cleavage of the Carbon Halogen Bond in Simple Aliphatic Halides. *Journal of the American Chemical Society* **108**, 638-647 (1986).

7 Chehimi, M., Hallais, G., Matrab, T., Pinson, J. & Podvorica, F. Electro- and Photografting of Carbon or Metal Surfaces by Alkyl Groups. *The journal of physical chemistry. C* **112**, 18559-18565 (2008).

8 Palacin, S., Bureau, C., Charlier, J., Deniau, G. & Mouanda, B. Molecule-to-metal Bonds: Electrografting Polymers on Conducting Surfaces. *ChemPhysChem* **5**, 1469-1481 (2004).

9 Gao, Q. A., Yang, F., Ma, Y. & Yang, X. R. The Modification of Screen-printed Carbon Electrodes with Amino Group and its Application to Construct a H_2O_2 Biosensor. *Electroanalysis* **16**, 730-735 (2004).

10 Sivanesan, A. & John, S. Highly Sensitive Electrochemical Sensor for Nitric Oxide Using the Self-Assembled Monolayer of 1,8,15,22-Tetraaminophthalocyanatocobalt(II) on Glassy Carbon Electrode. *Electroanalysis* **22**, 639-644 (2010).

11 Wang, L., Huang, P., Bai, J., Wang, H. & Zhang, L. Covalent Modification of a Glassy Carbon Electrode with Penicillamine for Simultaneous Determination of Hydroquinone and Catechol. *Mikrochimica acta* **158**, 151-157 (2007).

12 Bustos, E., Godinez, L., Rangel Reyes, G. & Juaristi, E. Chiral Recognition of Alanine Across Modified Carbon Electrodes with 3,4-dihydroxyphenylalanine. *Electrochimica Acta* **54**, 6445-6450 (2009).

13 Herlem, G., Lakard, B., Herlem, M. & Fahys, B. pH Sensing at Pt Electrode Surfaces Coated with Linear Polyethylenimine from Anodic Polymerization of Ethylenediamine. *Journal of the Electrochemical Society* **148**, E435-E438 (2001).

14 Saby, C., Ortiz, B., Champagne, G. Y. & Bélanger, D. Electrochemical Modification of Glassy Carbon Electrode Using Aromatic Diazonium Salts. 1. Blocking Effect of 4-Nitrophenyl and 4-Carboxyphenyl Groups. *Langmuir* **13**, 6805-6813, doi:10.1021/la961033o (1997).

15 Chehimi, M. M. *Aryl Diazonium Salts*. (Wiley, 2012).

16 Nielsen, L. T. *et al.* Electrochemical Approach for Constructing a Monolayer of Thiophenolates from Grafted Multilayers of Diaryl Disulfides. *Journal of the American Chemical Society* **129**, 1888-1889, doi:10.1021/ja0682430 (2007).

17 Malmos, K. *et al.* Using a Hydrazone-Protected Benzenediazonium Salt to Introduce a Near-Monolayer of Benzaldehyde on Glassy Carbon Surfaces. *Journal of the American Chemical Society* **131**, 4928-4936, doi:10.1021/ja809816x (2009).

18 Leroux, Y. R., Fei, H., Noël, J.-M., Roux, C. m. & Hapiot, P. Efficient Covalent Modification of a Carbon Surface: Use of a Silyl Protecting Group to Form an Active Monolayer. *Journal of the American Chemical Society* **132**, 14039-14041, doi:10.1021/ja106971x (2010).

19 Malmos, K., Iruthayaraj, J., Pedersen, S. U. & Daasbjerg, K. General Approach for Monolayer Formation of Covalently Attached Aryl Groups Through Electrografting of Arylhydrazines. *Journal of the American Chemical Society* **131**, 13926-13927, doi:10.1021/ja905919u (2009).

20 Malmos, K. *et al.* Grafting of Thin Organic Films by Electrooxidation of Arylhydrazines. *The Journal of Physical Chemistry C* **115**, 13343-13352, doi:10.1021/jp202911d (2011).

21 Combellas, C., Kanoufi, F., Pinson, J. & Podvorica, F. I. Sterically Hindered Diazonium Salts for the Grafting of a Monolayer on Metals. *Journal of the American Chemical Society* **130**, 8576-8577, doi:10.1021/ja8018912 (2008).

22 Jarvis, N. L., Fox, R. B. & Zisman, W. A. in *Contact Angle, Wettability, and Adhesion* Vol. 43 *Advances in Chemistry* Ch. 23, 317-331 (AMERICAN CHEMICAL SOCIETY, 1964).

23 Conte-Mayweg, A. *et al.* Indole, Indazole and Indoline Derivatives as CETP Inhibitors. United States patent (2007).

24 Clayden, J., Greeves, N., Warren, S. & Wothers, P. *Organic Chemistry*. (Oxford University Press, 2001).

25 Kosynkin, D., Michael Bockman, T. & K. Kochi, J. Fluorinated Biphenyls from Aromatic Arylations with Pentafluorobenzenediazonium and Related Cations. Competition between Arylation and Azo Coupling. *Journal of the Chemical Society, Perkin Transactions 2*, 2003-2012 (1997).

26 Lyskawa, J. & Bélanger, D. Direct Modification of a Gold Electrode with Aminophenyl Groups by Electrochemical Reduction of in Situ Generated Aminophenyl Monodiazonium Cations. *Chemistry of materials* **18**, 4755-4763, doi:10.1021/cm060752d (2006).

27 Friedrich, J. *The Plasma Chemistry of Polymer Surfaces.* (Wiley-VCH, 2012).

28 Yaws, C. L. *Yaws' Handbook of Thermodynamic Properties for Hydrocarbons and Chemicals*. (Knovel, 2009).

29 Ashcroft, S. J. & Schwarzmann, E. Standard Enthalpy of Formation of Crystalline Gold(III) Oxide. *Journal of the Chemical Society, Faraday Transactions 1: Physical Chemistry in Condensed Phases* **68**, 1360-1361 (1972).

30 Linn, J. H. & Swartz, W. E. An XPS Study of the Effects of CF_4 Plasmas on Gold Surfaces. *Appl. Spectrosc.* **39**, 755-760 (1985).

31 Kirowa-Eisner, E., Bonfil, Y., Tzur, D. & Gileadi, E. Thermodynamics and Kinetics of UPD of Lead on Polycrystalline Silver and Gold. *Journal of Electroanalytical Chemistry* **552**, 171-183, doi:10.1016/s0022-0728(03)00181-5 (2003).

32 Herrero, E., Abruna, H. D., Buller, L. J. & AbruÃ±a, H. D. Underpotential deposition at single crystal surfaces of Au, Pt, Ag and other materials. *Chemical Reviews* **101**, 1897-1930 (2001).

33 Seo, E. D. Surface Modification Studies by Atomic Force Microscopy for Ar-plasma Treated Polyethylene. *Macromolecular Research* **10**, 291-295 (2002).

34 Ikezawa, Y., Koda, Y., Shibuya, M. & Terashima, H. In Situ FTIR Study of Pyrazine Adsorbed on Au(111), Au(100) and Au(110) Electrodes. *Electrochimica Acta* **45**, 2075-2082 (2000).

35 Lezna, R. O., De Tacconi, N. R., Centeno, S. A. & Arvia, A. J. Adsorption of Phenol on Gold as Studied by Capacitance and Reflectance Measurements. *Langmuir* **7**, 1241-1246, doi:10.1021/la00054a037 (1991).

36 Herrero, E., Abruna, H. D., Buller, L. J. & Abruña, H. D. Underpotential Deposition at Single Crystal Surfaces of Au, Pt, Ag and Other Materials. *Chemical Reviews* **101**, 1897-1930 (2001).

37 Schwendeman, I., Gaupp, C. L., Hancock, J. M., Groenendaal, L. & Reynolds, J. R. Perfluoroalkanoate-Substituted PEDOT for Electrochromic Device Applications. *Advanced Functional Materials* **13**, 541-547, doi:10.1002/adfm.200304372 (2003).

38 Poverenov, E., Li, M., Bitler, A. & Bendikov, M. Major Effect of Electropolymerization Solvent on Morphology and Electrochromic Properties of PEDOT Films. *Chemistry of materials* **22**, 4019-4025, doi:10.1021/cm100561d (2010).

39 Burkarter, E. *et al.* Superhydrophobic Electrosprayed PTFE. *Surface and Coatings Technology* **202**, 194-198, doi:10.1016/j.surfcoat.2007.05.012 (2007).

40 Darmanin, T. & Guittard, F. Superhydrophobic Fiber Mats by Electrodeposition of Fluorinated Poly(3,4-ethyleneoxythiathiophene). *Journal of the American Chemical Society* **133**, 15627-15634 (2011).

Chapter 5: Electrowetting

The previous chapters have covered various ideas related to the development of a specific goal: a stable and reproducible low voltage electrowetting system. This chapter now assesses these approaches for their electrowetting effectiveness. Furthermore, other variables such as the liquids and electrolytes used in the electrowetting system are studied as these have not been looked at in detail previously.

To begin with, the generic experimental setup used to study electrowetting is described in detail. Then the effect of the different electrodes described in Chapter 3 and Chapter 4 is covered, with ultra-flat electrodes proving to greatly reduce hysteresis. Next the effect of changing electrolyte and electrolyte concentration is dealt with. This includes the effect of using a bulkier electrolyte to stabilise the interface between two immiscible electrolyte solutions (ITIES) as described in Chapter 2. Finally, different liquid compositions for the droplet are explored. Somewhat unexpectedly, this was found to have a profound effect on the electrowetting response.

5.1 Experimental

5.1.1 General experimental setup

The geometry of the cell used for all electrowetting experiments is shown in Figure 65. A working electrode was mounted on a mobile PTFE stand designed to sit inside a 5 cm × 5 cm × 5 cm glass cuvette. Also mounted in the stand was an Ag/AgCl wire used as the reference electrode and a gold counter electrode. The cuvette was fitted with a PTFE lid to reduce particulate contamination from the atmosphere. The lid contained access for a glass nitrogen bubbler.

The cuvette was filled with an aqueous electrolyte solution and a droplet was placed on the working electrode using a micropipette with plasticiser free Gilson tips. The droplet was approximately 0.5 μL and 0.5-1 mm wide. As the potential of the working electrode was varied, a photograph of the droplet (640 × 480 pixels) was automatically taken with a CCD camera (from a Phillips SPC900NC webcam) through a video zoom microscope (Edmund

Optics Infinity K2/S Long Distance Video Lens) at 20× magnification. Contact angles at each potential were subsequently measured using Fta32 2.0 contact angle software (First Ten Ångstroms). At least five points were fitted at the droplet|aqueous phase interface.

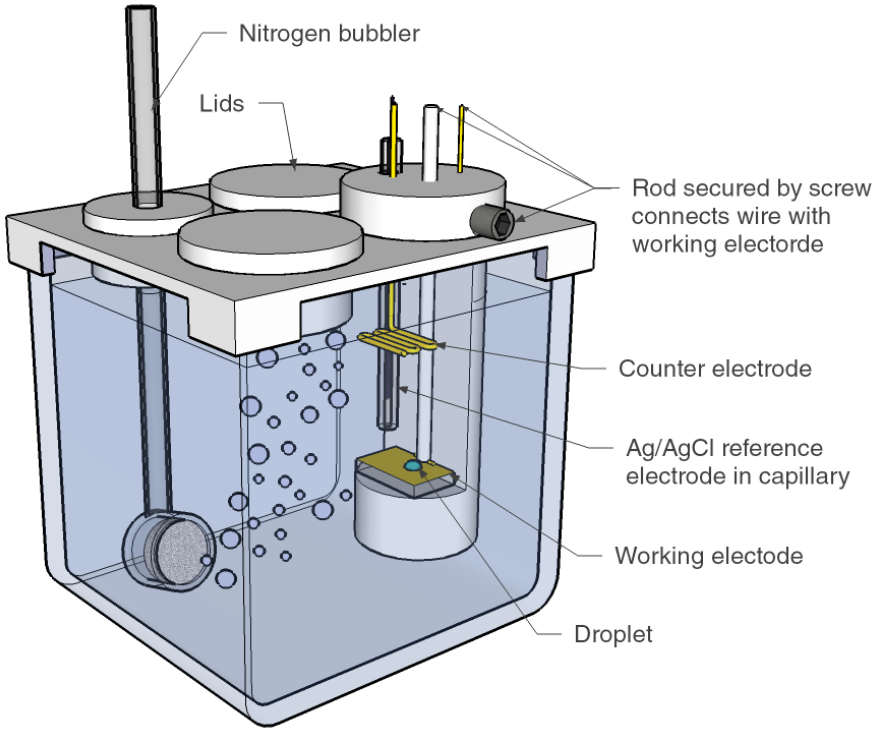

Figure 65|Experimental geometry for varying the potential across a liquid droplet. The glass cuvette is approximately 5 cm in each dimension. A CCD camera with microscope lens then records a video of the droplet through the cuvette wall and First Ten Ångstroms analysis software is used to measure the contact angle.

A Gamry Reference 600 potentiostat was used to control the applied potential. The potential was varied in 0.1 V steps with 10 s gaps between steps. The potentiostat simultaneously gave an indication of background currents, which were kept consistently low (approximately ± 20 μA cm^{-2}) to ensure that no Faradaic reactions were occurring. Experiments were completed within 15 min of submerging the electrode to minimise concerns over electrode surface stability when exposed to water (see Section 3.2.2.3).

The ambient temperature was 22±2 °C.

5.1.2 Chemicals and glassware

Ultrapure water (resistivity 18.2 MΩ cm) from a Millipore Elix 5 water purification system was used for all aqueous electrolyte solutions and soaking solutions for glassware. All solutions were only ever in contact with glass or PTFE, never other plastics, to prevent solution contamination from surfactants and plasticisers. All electrochemical cells and glassware were cleaned in the following manner:

1. Soaked in a solution of 0.1 mol dm^{-3} $KMnO_4$ + 0.18 mol dm^{-3} H_2SO_4 for 24 h to oxidise any organics
2. Rinsed with acidified hydrogen peroxide solution (0.36 mol dm^{-3} H_2SO_4 + 0.18 mol dm^{-3} H_2O_2) for 1 h
3. Rinsed 6 times with ultrapure water

All electrolytes and solvents were purchased from Sigma-Aldrich and used as received. Electrolytes were of greater than 99% purity and solvents were of greater than 98% purity.

Purging of oxygen from aqueous solutions with nitrogen had no noticeable effect on electrowetting and so this practice was considered unnecessary.

Even two 'immiscible' liquids have some mutual solubility. Therefore, all aqueous solutions and organic solutions were equilibrated with one another to prevent the small organic droplet from dissolving in the surrounding phase.

5.1.3 Sputtered electrodes

To make sputtered electrodes, a 100 nm layer of gold and a 20 nm titanium interlayer were sputtered onto 1 cm × 2 cm glass rectangles cut from VWR International Super Premium microscope slides. The titanium interlayer served to facilitate adhesion of gold to glass. The cleaning procedure for the glass was as follows:

1. Soaked in a solution of 0.1 mol dm^{-3} potassium permanganate + 0.18 mol dm^{-3} sulphuric acid for 1-2 h to oxidise any organics
2. Rinsed with acidified hydrogen peroxide solution (0.36 mol dm^{-3} H_2SO_4 + 0.18 mol dm^{-3} H_2O_2)
3. Rinsed with ultrapure water six times
4. Dried under a stream of nitrogen

5. Dried upright at 110 °C for 5 min

All sputtering was performed using an Emitech K575X sputterer; Emitech TK8859 gold targets and Emitech TK8879 titanium targets.

5.1.4 Surface tension measurements

Liquid|liquid surface tension measurements were made using the pendant drop method.[1] Fitting of the drop shapes was made with Fta32 2.0 contact angle software (First Ten Ångstroms).

5.2 Ultra-flat surfaces

5.2.1 Metal surfaces

In order to understand the effect of electrode roughness on low voltage electrowetting, a comparison was made between sputtered gold surfaces (similar to those used by Kornyshev et al.) and specially prepared template stripped gold surfaces (Section 3.2).[2] An ITIES electrowetting system, again in the style of Kornyshev et al. was used. This consisted of a droplet containing 0.1 mol dm^{-3} tetrabutylammonium tetraphenylborate (TBATPB) in 1,2-dichloroethane (DCE) surrounded by 0.01 mol dm^{-3} LiCl in water.

The potential was cycled from –1 V to 0 V versus an Ag/AgCl reference electrode and back again with 0.1 V steps, and the contact angle after each step was measured. The results can be seen in Figure 66. There are several interesting features. The Young contact angles of the two template stripped and sputtered surfaces were substantially different. This is because one surface was produced by template stripping and the other by sputtering and so they had very different roughnesses and perhaps even different surface morphologies. Also, the freshly exposed template stripped surface did not have the layer of organics on its surface which adsorbs onto gold over a period of several hours.[3,4] The consequence of this is that they had different surface energies and, as expected, the organic-coated sputtered electrode was more hydrophobic. However, the most important feature is the greatly reduced hysteresis. The

separation between corresponding contact angles on the forward and reverse scans decreased from roughly 500 mV on a sputtered surface to 200 mV on the template stripped surface. The difference in contact angle at the start of the scan compared to at the end of the return scan is also reduced on the template stripped surface. This difference in hysteresis was seen for all electrodes tested, with the scans in Figure 66 representing the lowest hysteresis scans measured for the two different surfaces. As noted above, there was a ten second pause between steps. After this time period the droplet had stopped changing shape. This ensured that the hysteresis was not affected by the 'scan rate' (although at much faster scan rates the hysteresis would be different).

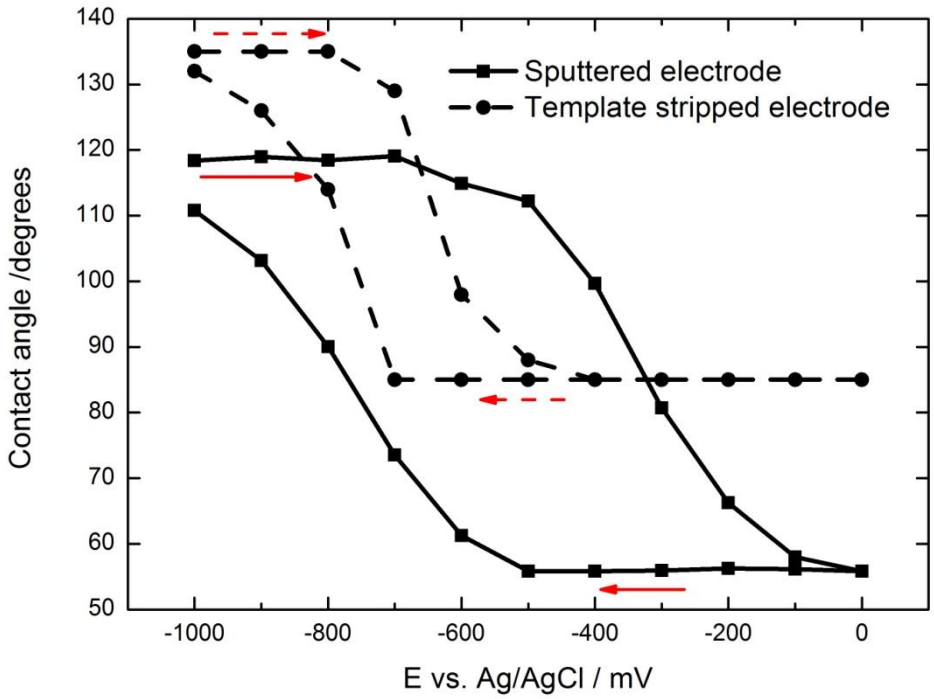

Figure 66 | Typical electrowetting responses of a 0.1 μL droplet of 0.1 mol dm^{-3} TBATPB in DCE surrounded by 0.01 mol dm^{-3} LiCl solution. Comparison between sputtered (rough surface) and template stripped (smooth surface) electrodes illustrating the effect of surface roughness on hysteresis. The droplets started at –1 V and every 10 s the potential was reduced by 0.1 V until it reached 0 V, at which point the scan was reversed. The error on each point is ±2 degrees.

These results clearly suggest that hysteresis is very strongly affected by surface roughness. What is not clear is whether this is 'nanoscale roughness' (template stripped surfaces have an

RMS roughness of 4.5 Å over 80 μm^2 compared to 40.3 Å for sputtered surfaces) or if it is in fact due to 'microscale roughness', from dust contamination. Figure 38 on page 94 clearly shows that the sputtered electrodes are covered in dust even after minimal exposure to the ambient atmosphere. Most probably the primary contribution to the hysteresis on a sputtered electrode is the dust, as this is at least two orders of magnitude larger than any inherent feature of the uncontaminated sputtered electrode. The negative effect of dust on the electrowetting response is also briefly noted by Beni and Hackwood.[5]

These results also support the idea that hysteresis is at least partly due to a physical effect and is not purely the result of some kind of chemical adsorption/desorption of ions on the electrode surface. This is important for ITIES electrowetting as a chemical effect is potentially much more difficult to address than a roughness effect, which might require a complete upheaval of the system. The results also suggest that the re-healing and atomically smooth surface of mercury is, at least in part, responsible for its low hysteresis electrowetting response.[6-8]

Despite this promising result, a perfectly flat or clean electrode is not expected to show zero hysteresis as there will always be a resistance to change in droplet shape. Examples of such a resistance include inertial effects, viscosity effects and various attractive forces between the liquid and electrode. This means that complete elimination of hysteresis is not possible.

Nonetheless, template stripped surfaces were used for all subsequent electrowetting experiments so as minimise the contribution of roughness or dust on hysteresis.

5.2.2 Carbon surfaces

As detailed in Section 3.4, ultra-flat glassy carbon surfaces were prepared. They were tested as electrowetting substrates and compared against diamond polished glassy carbon from HTW GmbH, Germany. The diamond polished glassy carbon was already very smooth, and was measured by AFM to have an RMS roughness of 56.5 Å.

However, using the ITIES electrowetting system detailed above, as well as other electrolytes and concentrations, no reversible electrowetting response was seen on either template stripped carbon or the commercially prepared carbon. No Faradaic currents were seen at the potentials

tested (0.2 V to –1.3 V vs. Ag/AgCl in 0.1 mol dm^{-3} LiCl). As the potential was made more negative, the droplet would slowly contract, however, on the reverse scan the contact angle would not change at all (as if the droplet were completely pinned).

This is the first indication that electrowetting is more complicated than initially expected. As will be seen later, electrowetting is in fact very sensitive to changes in liquid|solid surface energies. The theory behind electrowetting (see (Equation 6, page 32) suggests that any combination of surface energies and surface capacitances will produce a reversible electrowetting system. However, as was already known with gold and mercury, not all systems work in this way. This work with carbon supports this result, as conditions which work for gold surfaces do not work for a glassy carbon surface which has a similar roughness and capacitance. This is an indication that, while roughness appears to be important, a low hysteresis electrowetting response is dependent on others factors as well.

5.3 Fluorinated electrodes

Fluorinated, hydrophobic electrodes were prepared in the hope that they would reduce hysteresis in low voltage electrowetting. This was inspired by work done by Maillard, Legrand and Berge which indicated that a hydrophobic surface was conducive to a low hysteresis EWOD system.[9]

5.3.1 Plasma fluorinated surfaces

The hydrophobicity of gold electrodes was successfully increased by exposure to plasmas of CFC-22 and perfluoropropane. These surfaces retained their hydrophobicity within the potentials at which an electrowetting response is seen on plain gold and also retained their electrochemical capacitance. As can be seen from Figure 67, the contact angle of a DCE droplet on the surface is lower than for a non-functionalised surface, as expected for a more hydrophobic surface. As the potential becomes more negative, there is a very large variation in the contact angle (76°). However, on the reverse scan, there is no return to the original angle.

One possible explanation for this is that the surface is not stable underneath the DCE droplet. While this may or may not be the case, this behaviour is also seen on unfunctionalised carbon surfaces, as described previously. Furthermore, as will be seen later, at certain electrolyte concentrations similar behaviour is seen even on unfunctionalised template stripped gold surfaces. Therefore, this complete pinning may in fact be the result of a change in the balance of surface energies; an idea which will be explored in more detail later.

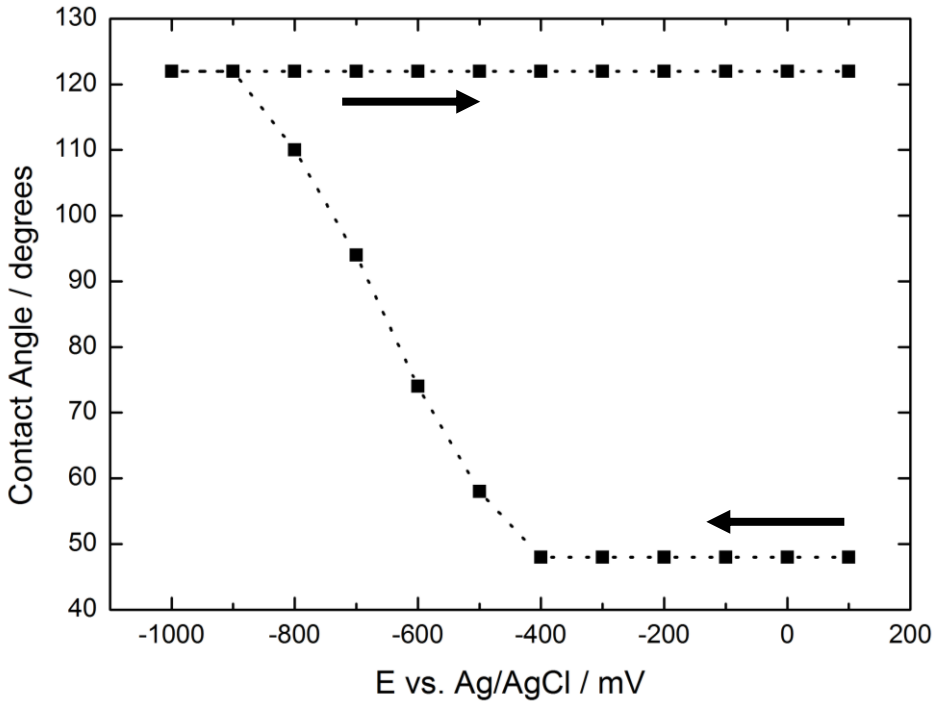

Figure 67|Typical electrowetting response for fluoroplasma functionalised gold surface. A very large change in contact angle is seen initially, with a quick response time. However, the droplet is completely pinned on the return scan. This may be caused by an unstable surface which rearranges underneath the moving droplet.

5.3.2 PEDOT-F coated surfaces

None of the PEDOT-F conducting polymer coated surfaces (reported in Section 4.3) showed any type of electrowetting behaviour. This may be because they are very rough (31.1 nm RMS

roughness). The surfaces also appeared to be permeable to DCE and other organic solvents, meaning that the droplet would only remain on the electrode surface for a short time. Therefore, these surfaces are clearly not suitable for electrowetting.

5.3.3 Diazonium functionalised surfaces

Functionalisation of gold with bulky diazonium species did not have any effect on the surface hydrophobicity. It is therefore unsurprising that these surfaces behaved similarly to normal template stripped gold surfaces.

Functionalised carbon surfaces were not effective electrowetting substrates, much like un-functionalised carbon while copper is not suitable for electrowetting as it is it not electrochemically inert.

5.3.4 Summary

While it is disappointing that these fluorinated electrodes (and ultra-flat carbon electrodes) did not reduce pinning as hoped, this in itself is an interesting result. It shows that some of the principles which apply to EWOD do not apply to this type of electrowetting system. Furthermore, as these surfaces have very similar capacitances, it suggests that there may be an important chemical contribution to the surface energies of the electrode|droplet and electrode|aqueous phase which is of fundamental importance to the electrowetting response. This is not evident from a theoretical perspective and was therefore somewhat unexpected.

5.4 Electrolyte effects

5.4.1 Organic electrolyte ions

Due to concerns regarding the stability of the ITIES during ITIES electrowetting, an ITIES with a larger polarisation potential window was used. The tetrabutylammonium tetraphenylborate (TBATPB) used by Kornyshev et al. was replaced with bis(triphenylphosphoranylidene)ammonium tetrakis[3,5-bis(trifluoromethyl)phenyl]borate (BTPPATFPB).[2] The aqueous electrolyte, LiCl, was kept unchanged. The resulting polarisation window was over 700 mV compared to approximately 200 mV for the TBATPB system, as demonstrated in Section 2.1.

It was found that there was no significant effect in moving from one electrolyte to another. Within the variation between experiments, there was no difference between the electrowetting responses of the two systems. This indicates that if the ITIES is indeed unstable when TBATPB is used, this does not affect the electrowetting response over the timescale of the electrowetting experiment. Simultaneously, it also shows that the use of BTPPATFPB does not hinder the electrowetting response. This makes it a good ITIES electrowetting electrolyte as it reduces concerns over ITIES stability.

The most important conclusion of this result is that ion transfer across the ITIES is not driving the electrowetting response, as this would be an unstable system over longer time periods.

Instead, it was found that if the organic electrolyte was removed entirely, there was less hysteresis than with electrolyte in the droplet. This means that electrowetting with an ITIES is not essential to the electrowetting response (as suggested by the electrowetting experiments of Frumkin with mercury surfaces outlined in Section 1.3.1). This was only found to be true on template stripped surfaces and not on sputtered surfaces. The effect of organic electrolyte concentration is covered in more detail in Section 5.5.1.

5.4.2 Aqueous electrolyte ions

From a theoretical viewpoint based on the common Gouy-Chapman-Stern model, changing the aqueous electrolyte is not expected to have significant impact on the electrowetting response. For example, the capacitance of gold in a NaCl solution should have almost exactly the same capacitance as an equally concentrated LiCl solution.[10] However, this simple change of electrolyte had an astonishing effect on the electrowetting response. In moving from 0.1 mol dm^{-3} LiCl with a pure DCE droplet (Figure 69) to 0.1 mol dm^{-3} NaCl with a pure DCE droplet, there was a change from a very low hysteresis system to one which is completely pinned on the return scan (qualitatively similar to that shown in Figure 67).

This was a common result and was seen with several other electrolytes including $MgCl_2$, NaF and NH_4Cl. KCl was the only exception at this concentration; it showed very large hysteresis but did return to its initial contact angle. If the concentration of these electrolytes was reduced below 0.1 mol dm^{-3}, the droplet would return to its original contact angle, albeit with a large amount of hysteresis. As will be seen next, this is consistent with how LiCl concentration affects the electrowetting response as a large LiCl concentration stops the droplet returning to its initial contact angle.

There is growing evidence that electrolyte structure at interfaces can vary dramatically even between apparently similar electrolytes (such as LiCl and NaCl).[11-13] Even if different electrolytes do not change the interfacial capacitance substantially, these varying interfacial structures may introduce hysteresis; although at the moment there is no detailed explanation as to why. An idea which is illustrated in Figure 68 and entertained further in Sections 5.5.2 and 5.6.1 is that a thin layer of water may be adsorbed onto the electrode at high potentials such that when the potential is relaxed, this film remains trapped and the droplet cannot 're-wet' the surface. It is not unreasonable to think that the electrolyte ions, which have differing hydration shells for example, could influence such a phenomenon.

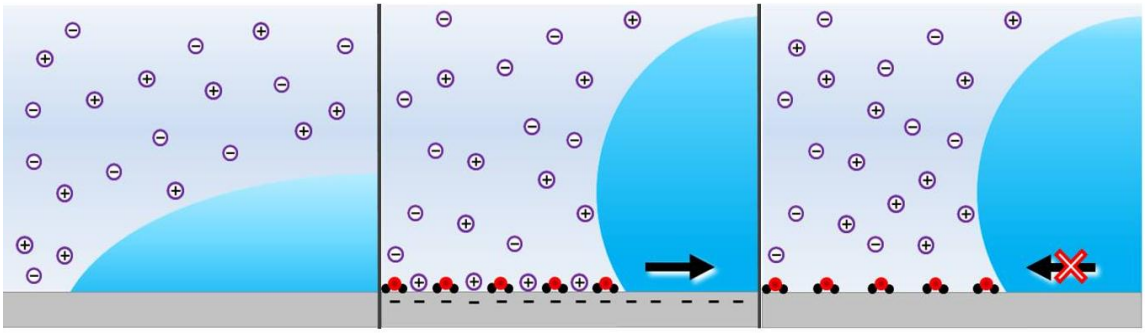

Figure 68|Cartoon illustrating a possible cause of hysteresis. When a potential is applied, the electrode is screened by an electrochemical double layer. Water molecules become aligned to the strong electric field and also screen the surface charge by adsorbing to the surface. This coincides with contraction of the droplet. Even after the potential has been relaxed, a layer of water molecules remain trapped at the surface, preventing the hydrophobic droplet from spreading back across the electrode.

Once the desired characteristics for small hysteresis electrowetting are known, the use of other electrolytes may prove beneficial; however, this thesis was predominantly limited to the use of LiCl as it was known to show a good electrowetting response.

5.5 Concentration effects

5.5.1 Organic electrolyte concentration

As has already been mentioned briefly, it was found that removing the organic electrolyte from the droplet reduced hysteresis of the electrowetting response. Four concentrations of TBATPB were tested: 0.1, 0.01, 0.001 and 0 mol dm^{-3}. When the droplet contained electrolyte, the best response was seen with 0.1 mol dm^{-3} TBATPB. As the concentration was reduced, there was a slight increase in hysteresis. However, when the electrolyte was removed entirely, the opposite was seen and there was a reduction in the hysteresis, as shown in Figure 69.

This shows that the change in surface energy at the droplet|aqueous phase interface—due to double layer charging of the ITIES—is not essential to the electrowetting response. This is an important result for two reasons: there is reduction in hysteresis and, in particular, it is the first demonstration of reversible electrowetting due to capacitive charging on a solid surface

without an ITIES (to the best of the author's knowledge). This second result, in many ways, is not surprising as electrowetting without an ITIES has been known since the time of Lippmann and Frumkin and theoretically should also occur on solids.[6,14] However, this has always required a liquid metal (namely mercury, gallium or a liquid amalgam).[5,7,15] Electrowetting systems on solids have had to employ a different mechanism such as the oxidation of surface thiols or organic polymers.[16-19] Furthermore, such methods must switch between two extreme contact angles; intermediate contact angles cannot be accessed.

Perhaps the extension of this Frumkin-type electrowetting onto solid surfaces has not been seen previously because of the sensitivity of the electrowetting response to electrode composition and morphology. Furthermore, as will be seen in the remainder of the chapter, electrowetting is even more dependent on the inorganic electrolyte and its concentration and also on the droplet composition.

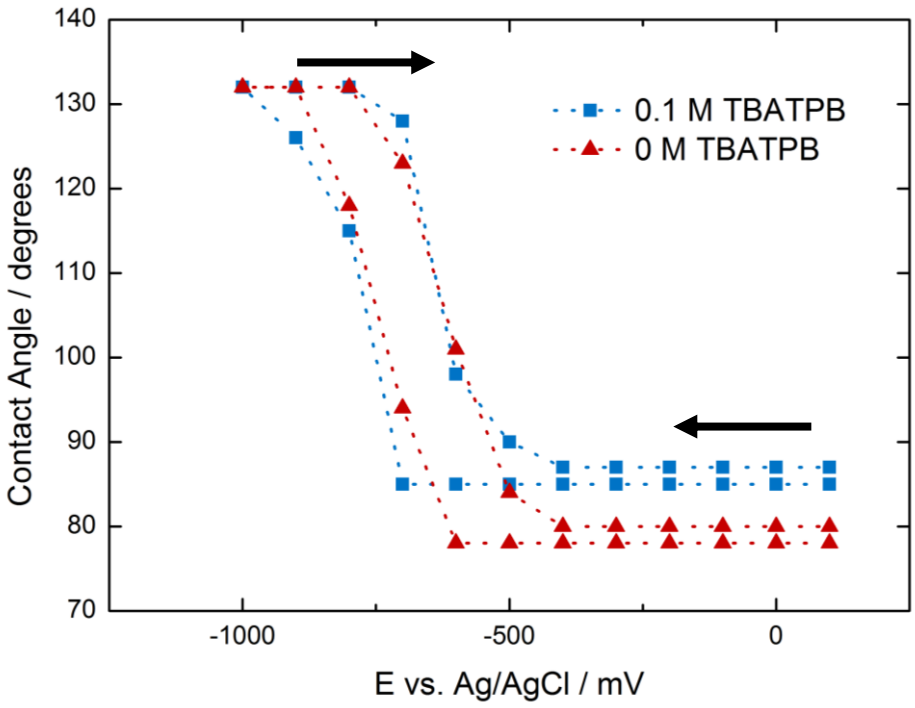

Figure 69|Electrowetting response for 0.1 mol dm^{-3} LiCl aqueous phase with DCE droplet. There is a reduction in hysteresis when TBATPB is removed from the droplet.

5.5.2 Aqueous electrolyte concentration

When compared to the organic electrolyte, the aqueous electrolyte had a much more substantial effect on the electrowetting response. It was found that the electrowetting response was noticeably affected by small variations in concentration. Figure 70 shows how as the LiCl concentration (with a pure DCE droplet) is varied in 0.01 mol dm^{-3} steps, there is a clear minimum in hysteresis at 0.10 mol dm^{-3}, with an extra 200 mV of hysteresis at 0.09 and 0.11 mol dm^{-3}. This coincides with a maximum of 42° variation between the maximum and minimum attainable contact angles. The points represent the smallest amount of hysteresis and largest change in contact angle seen for each concentration over three repeats. This representation was chosen because occasionally the system was heavily pinned, perhaps due to dust contamination, dramatically affecting the average value. Instead it was assumed that the least pinned response was a more representative measure of the system. Error bars represent the error due to the finite 100 mV step size and error associated with measuring the contact angle.

This behaviour is perhaps contrary to what would be expected. Interfacial capacitance increases with electrolyte concentration, and as energy stored in the capacitor is the driving force for electrowetting, surely increasing the capacitance should increase the electrowetting response? To a certain degree this is what was seen: the maximum angle variation increases from 10° at 0.05 mol dm^{-3} LiCl to 43° at 0.10 mol dm^{-3} LiCl. However, beyond this concentration the angle variation drops off sharply as the hysteresis increases. Again, one theory for why this happens is that the increasing electrolyte concentration may promote adhesion of a thin layer of water to the electrode surface. This hydrophilic layer remains trapped on the surface during the return scan, preventing the droplet from returning to its original shape.

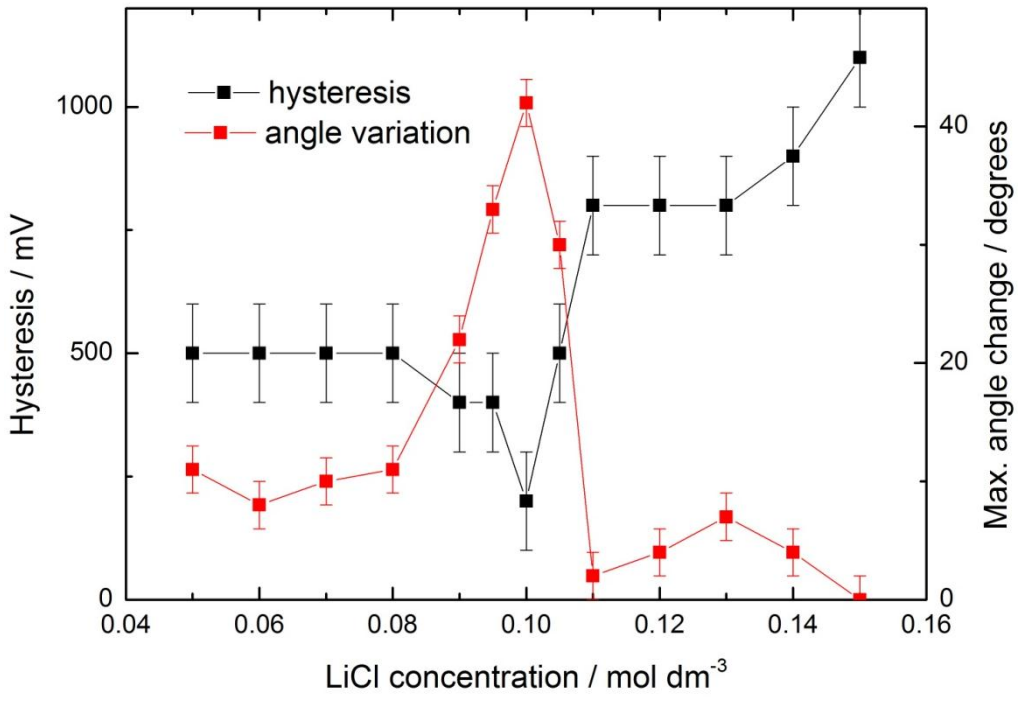

Figure 70|Change in electrowetting response of a pure DCE droplet as aqueous electrolyte concentration is varied. Template stripped gold was used as the electrode. At 0.10 mol dm^{-3} LiCl there is a minimum in the hysteresis between forward and reverse scans. This coincides with a maximum in the difference between the lowest and highest attainable contact angles.

5.5.3 Jumping droplet

Using the optimum parameters for electrowetting discussed thus far (template stripped gold, 0.10 mol dm^{-3} LiCl, 0 mol dm^{-3} TBATPB, DCE droplet) a 'jumping droplet' was studied. As shown in Figure 71, this involved stepping the potential between –0.1 V and –0.9 V versus Ag/AgCl, allowing ten seconds between steps. Upon changing the potential from –0.1 V to –0.9 V, the droplet changed shape much faster than when stepping from –0.9 V to –0.1 V. In other words, the droplet was found to contract much faster than it would 'relax' to a lower contact angle. The droplet jumped between a contact angle of 93° and 120° within the ±1° error limit associated with measuring the contact angle. This lasted for over one hundred pulses, which was the duration of the experiment.

This demonstrates that a significant change in contact angle (27°), for only a 0.8 V change in potential, is possible. It also shows the reversibility and stability of the system.

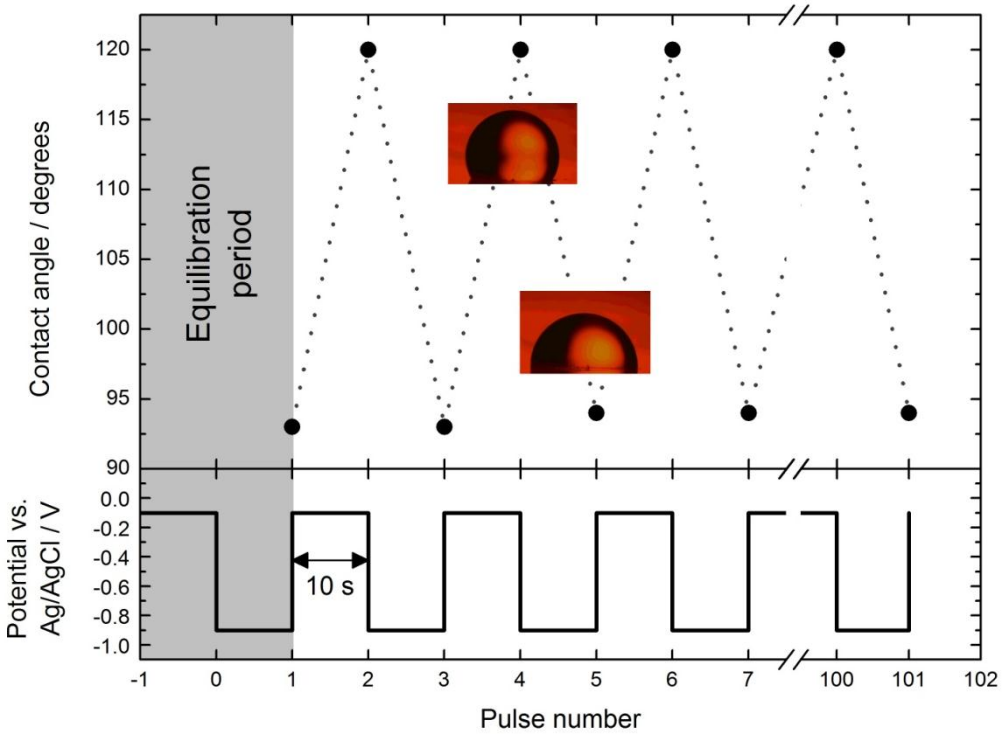

Figure 71|Electrowetting response of a DCE droplet on template stripped gold surrounded by 0.10 mol dm^{-3} LiCl solution. As the potential is switched between –0.1 V and –0.9 V, the contact angle jumps between two different values. After over 100 potential pulses the same contact angle variation is seen. The 'equilibration period' represents the first cycle before the droplet begins to reproducibly cycle between two values.

5.6 Solvent effects

5.6.1 Different solvents

Inspection of the modified Young equation for electrowetting (Equation 6) shows that there are two potential independent terms which define the equilibrium contact angle. These are the Young angle at the PZC and the droplet|aqueous phase surface energy.

$$\cos\alpha = \cos\alpha_{PZC} - \frac{C(U - U_{PZC})^2}{2\gamma_{dw}} \quad \text{((Equation 6)}$$

The Young angle at PZC defines the minimum achievable contact angle while the droplet|aqueous phase surface energy defines how dramatically the droplet will respond to a change in potential. That is to say that a low γ_{dw} means the droplet responds more to changes in potential and vice-versa for high γ_{dw}. The former case is desirable so that large changes in contact angle are achievable with small applied potentials. Nonetheless, (Equation 6 gives no hard and fast indication that certain surface energies will stop the electrowetting response altogether. Therefore, it was very surprising to find that the choice of solvent for the droplet, which affects the Young angle and droplet|aqueous phase surface energy, had a dramatic effect on the electrowetting response.

Using 0.10 mol dm^{-3} LiCl as the aqueous phase with template stripped gold—the optimised system for a pure DCE droplet—the effect of droplet composition was tested. In all cases there was no organic electrolyte in the droplet. It was found that very hydrophobic liquids, which were highly immiscible with water, were very strongly pinned. These included cyclohexane and the perfluorinated solvent FC40. Partially water miscible solvents such as butyl acetate (water solubility: 10 g dm^{-3}) and nitrobenzene (1.9 g dm^{-3}) were less pinned while n-butanol (73 g dm^{-3}) had a response close to that of DCE, which itself has a water solubility of 8.7 g dm^{-3}.[20] There is clearly a loose trend here that as solvents become more water miscible, they show less pinning. The trend is not perfect as the most water miscible solvent, n-butanol, does not exhibit the least pinning; but it must be noted that these systems were not optimised for the LiCl concentration, something which was shown to have a dramatic effect on hysteresis. Furthermore, n-butanol is less dense than water and its buoyancy may exacerbate pinning as there is an additional force pulling the droplet off the surface.

More specifically, the pinning seen with the very hydrophobic droplets was not pinning in the forward direction (from small to large contact angle) but rather pinning on the return scan, showing that the droplet was reluctant to spread back across the surface which it had just previously wetted. This, along with the electrolyte and concentration dependence on hysteresis, further supports the suggestion that the increased pinning may in fact result from a

thin hydrophilic layer of water which remains adsorbed to the electrode surface even after the potential has been relaxed.

Alternatively, it is reasonable to assume that the more water miscible solvents have lower droplet|aqueous phase surface energies owing to more favourable interactions between the component molecules and this may affect the electrowetting response. However, if we assume that the change in capacitive energy for a given potential step is independent of droplet composition, changes in droplet|aqueous phase surface energy should only serve to increase the change in contact angle between given steps (based on (Equation 6). This in itself would not reduce the hysteresis seen between forward and reverse scans. Even for the heavily pinned droplets, there was always a substantial change in contact angle on the forward scan.

These observations initiated the search for a solvent which might reduce pinning. The desired solvent characteristics were high water miscibility (although, of course, not complete miscibility), a density greater than that of water and a low viscosity. Density is important for two reasons. Firstly, although low density solvent droplets are able to adhere to the electrode surface—as surface tension forces can overcome the buoyancy—it was often found to be problematic to do this. Secondly, as has already been mentioned, the buoyancy pushes the droplet upwards which may increase hysteresis. This is because a decrease in the droplet contact angle coincides with a lowering of the droplet's centre of mass which must work against gravity. Similarly, viscosity is also believed to increase hysteresis as a result of inertial resistance to shape change.[21]

One of the first solvents tested was 3-chloro-1-propanol. It showed a remarkable electrowetting response, with no hysteresis within the error of the contact angle measurement. However, this came with one very significant problem: the response was not within the potential window imposed by the onset of Faradaic reactions. The electrowetting of 3-chloro-1-propanol is discussed in detail in the next section.

5.6.2 Electrowetting of 3-chloro-1-propanol

A search of the literature suggests that 3-chloro-1-propanol is mainly used as a reactant in organic synthesis: almost one thousand different reactions of 3-chloro-1-propanol can be found on the chemical search engine Reaxys. Conversely, there is very little reliable data on its physical properties beyond its density and boiling point. In fact, 3-chloro-1-propanol was chosen based in its predicted water solubility of 147 g L^{-1}.[22] In reality, it was found that it was completely miscible with water in all proportions. However, these mixtures exhibited fairly unusual salting-out behaviour. The addition of 0.10 mol dm^{-3} LiCl (or NaCl) would cause >20 volume per cent mixtures to separate into two phases. This behaviour is reported for some other solvents such as isopropyl alcohol, 1,4-dioxane and glycerol.[23,24] However, for these solvents this phase separation only occurs at very high salt concentrations (>1 mol dm^{-3}). Figure 72 shows the electrowetting response of a water:3-chloro-1-propanol 70:30 volume per cent system. The aqueous phase contains 0.16 mol dm^{-3} LiCl which was the optimum concentration for this system.

It is worth noting that even for this system, which shows no hysteresis with 0.16 mol dm^{-3} LiCl, the response is very sensitive to the electrolyte concentration as is the case for a DCE droplet. Remarkably, this is true to the extent that at 0.12 mol dm^{-3} LiCl and at 0.20 mol dm^{-3} LiCl there is a gap of over 700 mV between forward and reverse scans (Figure 72).

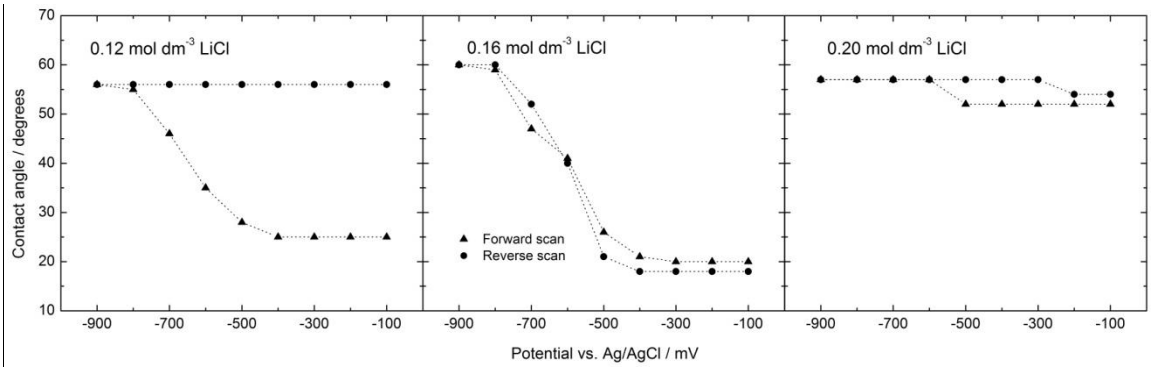

Figure 72|Electrowetting response of 3-chloro-1-propanol with an aqueous phase of LiCl of varying concentrations. At 0.12 mol dm^{-3} and 0.20 mol dm^{-3} LiCl the system is heavily pinned. Remarkably, however, at 0.16 mol dm^{-3} LiCl the pinning disappears. The contact angles at low values can only be read to an accuracy of ±2 degrees. Therefore, at 0.16 mol dm^{-3} LiCl there is almost no hysteresis within the error of the contact angle measurements.

However, as has been mentioned, there is a very significant problem with this system, which is the onset of a Faradaic reaction at -600 mV. This is the result of hydrogen evolution, which has been shifted to higher potentials. This is because the 3-chloro-1-propanol solution was mildly acidic, something which is not immediately apparent from its molecular structure. In fact, the electronegativity of the chlorine atom significantly increases the dissociation constant of the hydroxyl group in water. This is confirmed by the nuclear magnetic resonance study of various alcohols by Lee and Demchuck.[25] The pH of the solution was measured to be between 3 and 4 (pK_a of 3-chloro-1-propanol between 3.45 and 4.45). As shown in Figure 73, this reaction was stopped by the addition of 0.05 mol dm^{-3} NaOH, resulting in a shift to pH >11. This suggested that the reaction was indeed proton reduction and not reduction of the 3-chloro-1-propanol itself.

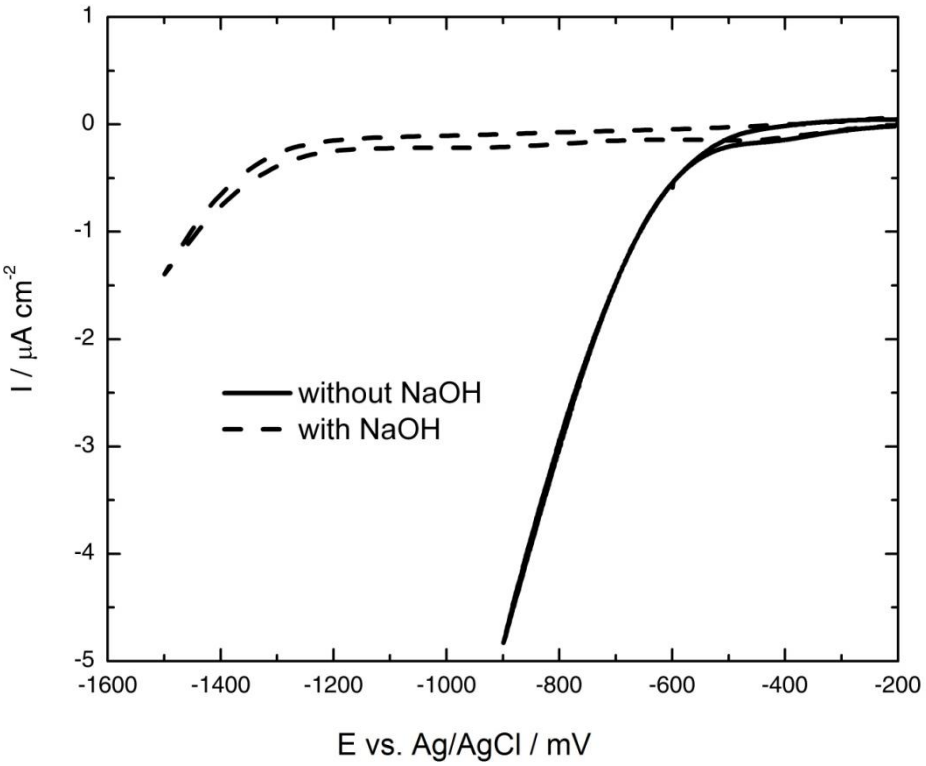

Figure 73|Cyclic voltammetry of 0.1 mol dm^{-3} LiCl saturated with 3-chloro-1-propanol. The addition of 0.05 mol dm^{-3} NaOH delays the onset of a Faradaic reaction, suggesting that the current is due to the high proton concentration in solution brought about by the Brønsted acidity of 3-chloro-1-propanol.

This provokes the obvious question of whether the low hysteresis is a result of the Faradaic processes, perhaps though agitation of the surface or through some additional pseudo-capacitance. The first attempt to try to answer this was to use LiOH or NaOH together with LiCl as the aqueous phase electrolyte. Figure 74 shows the electrowetting response for the 3-chloro-1-propanol system with an aqueous phase of 0.05 mol dm^{-3} NaOH and 0.10 mol dm^{-3} LiCl. The response is comparable with that for DCE with 0.10 mol dm^{-3} LiCl in that there is a 200 mV gap between forward and reverse scans. Similar or worse results are seen with LiOH. Of course, this is much more pinned than the system with no NaOH. While this is a disappointing result—ideally there would be no hysteresis—it still doesn't show that the low hysteresis is a result of the Faradaic reaction. This is because in adding the NaOH we have radically changed the system. The clearest indication of this is that the Young contact angle has changed from 20° to 67° and so a fair comparison between the two experiments

cannot be made. Thus, it cannot be said that the increase in hysteresis is because there is no longer a Faradaic reaction at the electrode surface.

It is also important to make the point that, as far as the author is aware, there are no reports in the literature of low voltage electrowetting systems, with no hysteresis, which do operate outside of the limits imposed by Faradaic processes (except on mercury). The electrowetting systems discussed in Chapter 1, are not designed to be methods of electrowetting *within* the potential window. Rather, they are simply methods of electrowetting on solid surfaces and are not designed in response to electrowetting systems which only work outside of a potential window.

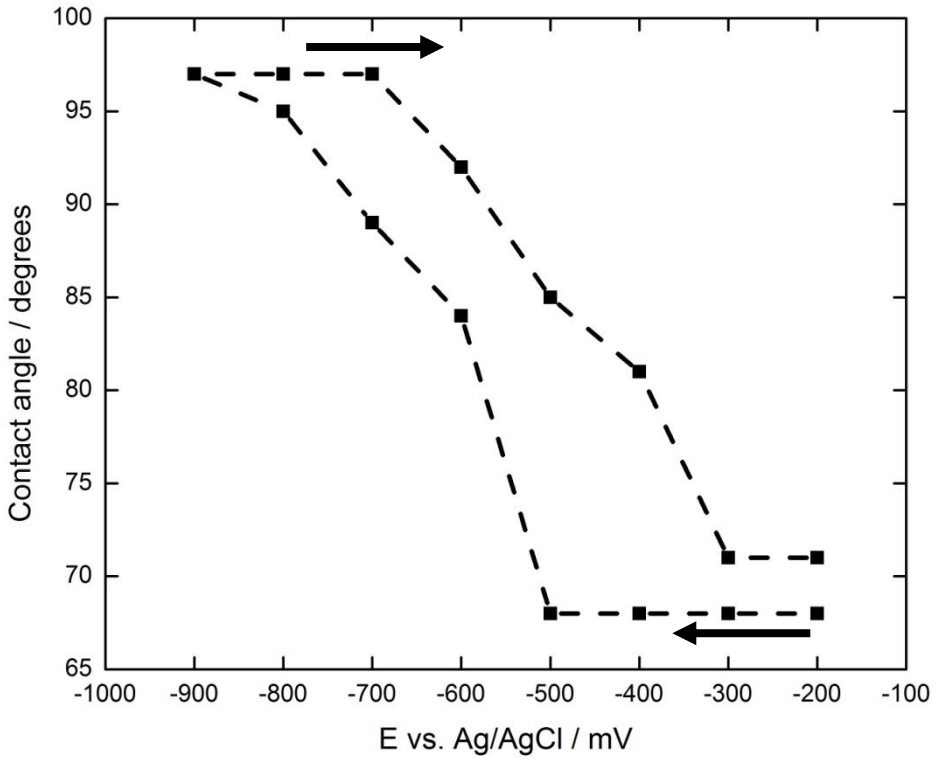

Figure 74 | Electrowetting response for the 3-chloro-1-propanol system with an aqueous phase of 0.05 mol dm^{-3} NaOH and 0.01 mol dm^{-3} LiCl on template stripped gold.

A somewhat different experiment to see whether the pH and the Faradaic reactions are responsible for the low hysteresis was done: the DCE system was acidified with HCl to see whether this reduced hysteresis. A DCE droplet with surrounding 0.10 mol dm^{-3} LiCl phase

was used. At pH 4 to 2 the droplet was completely pinned and showed no electrowetting response whatsoever, despite the presence of a background Faradaic current. This would suggest that Faradaic processes do not necessarily promote electrowetting.

Finally, another noteworthy result involving 3-chloro-1-propanol is shown in Figure 75. It shows the electrowetting response when the droplet is composed of a mixture of DCE and 3-chloro-1-propanol. It is noteworthy because it is the only example of electrowetting on a solid surface at potentials positive of the PZC. Usually there is no electrowetting seen in this region, despite the fact that the electrowetting equation suggests that there should be. This is perhaps a further indication that there is something special about the interfacial properties of 3-chloro-1-propanol. As nothing is usually seen at these potentials, the electrowetting response must therefore be weaker; however, properties of 3-chloro-1-propanol/DCE are so conducive to electrowetting that a response is still seen in this instance. This would also support the idea that the low hysteresis response of 3-chloro-1-propanol is not due to Faradaic processes, which only occur below –600 mV. Another interesting observation is that at low 3-chloro-1-propanol concentrations, with a DCE droplet, the electrowetting response is very poor even though there is a background Faradaic current, which also suggests the Faradaic current is not a driving force for electrowetting.

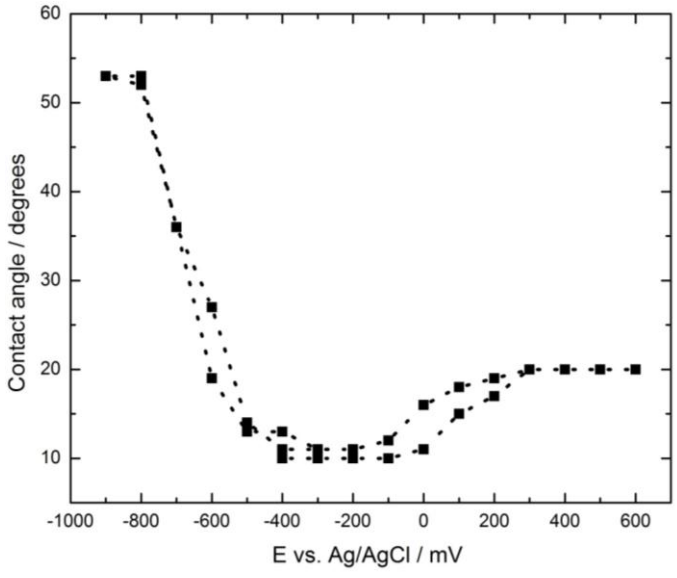

Figure 75|Electrowetting response of a mixed DCE:3-chloro-1-propanol 1:3 droplet, with 0.15 dm^{-3} LiCl in the aqueous phase. This is the only known example of low voltage electrowetting at positive potentials on a solid (rather than mercury) surface.

The next sections attempt to create a system with similar properties to the 3-chloro-1-propanol system. Namely, similar Young contact angle, water miscibility and droplet|aqueous phase surface energy but without the acidity of 3-chloro-1-propanol.

5.6.3 Salting out with other solvents

As discussed above, 3-chloro-1-propanol mixed with water requires the addition of a salt to cause phase separation. This indicates that there is a strong enthalpic interaction between the two liquids. This, in turn, may help the droplet spread across the water-coated electrode. However, it was not possible to find another solvent which salted out at similar salt concentrations. For instance, isopropyl alcohol salted out only when the aqueous phase was close to saturation with NaCl.[23,24]

An electrowetting system with isopropyl alcohol and NaCl saturated water was tested. The normal electrowetting geometry had to be inverted due to the buoyancy of the isopropyl alcohol, which constituted the surrounding phase while the droplet consisted of NaCl saturated water. It was found that upon equilibrating the system, enough NaCl dissolved in the isopropyl alcohol to enable it to conduct a small current. However, the system showed a large amount of pinning as expected for such high salt concentrations. On gold the droplet Young angle was 33° and would completely wet the surface at -1 V. On carbon the droplet angle decreased from 55° to 27°.

5.6.4 Mixed solvents

It was not possible to find another pure solvent which salted out at low salt concentrations, the way 3-chloro-1-propanol does. Density is an essential parameter for the solvent and pure hydrocarbons are all less dense than water. To be denser than water, they must contain different atoms, such as a halide or oxygen. However, the physical properties of these halide containing molecules are generally poorly classified because, excluding a select few, they are not used as solvents. This also makes them expensive to use in the quantities needed for electrowetting (10-100 ml per experiment). Therefore, mixtures of dense solvents with

hydrophilic solvents were prepared in the hope that they would mimic the properties of 3-chloro-1-propanol.

The three solvent combinations tested were 1:1 mixtures of DCE/propanol, 1-butanol/ 1,3-butanediol and 1-butanol/propylene carbonate. These were all equilibrated with an aqueous solution of 0.10 mol dm^{-3} LiCl. DCE/propanol had a very large Young contact angle of 116° and was heavily pinned. It had a very low liquid|liquid surface energy of 11±2 mJ m^{-2}. This is much lower than the liquid|liquid surface energy of pure DCE with water (28.7 mJ m^{-2}) indicating that the presence of 1-propanol did reduce the liquid|liquid surface energy as intended.[26] Although this is still not as low as the liquid|liquid surface energy of the 3-chloro-1-propanol system (measured to be 6.0±0.5 mJ m^{-2}) this suggests that low liquid|liquid surface energy is not the sole reason for the remarkable electrowetting properties of 3-chloro-1-propanol. The next solvent mixture, 1-butanol/1,3-butanediol had a very low Young contact angle. In fact, it completely wet the gold electrode surface. After the initial scan, it cycled between a contact angle of 30° and 88° with a lot of hysteresis. This seems to suggest that a low Young angle is also not the sole reason for the low hysteresis seen with 3-chloro-1-propanol. Finally, 1-butanol/propylene carbonate had a Young angle of 70° and was also heavily pinned.

These mixtures were unable to capture the electrowetting performance of 3-chloro-1-propanol despite sharing some of its properties such as its low Young contact angle or low liquid|liquid surface energy. Nonetheless, this seems to be a sensible method for trying to mimic 3-chloro-1-propanol more closely in the future, perhaps resulting in the discovery of a low hysteresis electrowetting system. It is also important to note that these systems were not necessarily optimised for LiCl concentration, which may have greatly affected the electrowetting.

5.7 Conclusions

The first part of this chapter covered the effects of using specially designed electrodes for electrowetting. These electrodes were ultra-flat template stripped gold, ultra-flat glassy carbon, fluoro-plasma treated gold, diazonium functionalised gold and PEDOT-F. Of these methods, only template stripped gold was found to reduce hysteresis in electrowetting, while the other

surfaces increased it. This suggests that a low surface energy electrode will not necessarily reduce pinning, as has been found for EWOD. Nonetheless, the unexpected finding that concentration and droplet composition have a dramatic effect on pinning means that each electrowetting system must be optimised for electrolyte concentration. When a deeper understanding of concentration and surface energy effects has been developed, these methods for tuning the hydrophobicity of a conducting surface may yet prove to be useful.

On the other hand, template stripped electrodes proved to be a valuable development. They clearly reduce the pinning of a DCE droplet when compared with sputtered gold electrodes as used previously by Kornyshev et al.[2] This is a simple and convenient method for electrode preparation which reduces concern over electrode cleanliness and roughness, allowing the effect of other variables to be studied more independently.

Of these other variables, the nature of the electrolytes used for electrowetting proved to have an unpredictable effect. The use of a more bulky electrolyte in the droplet, to stabilise the aqueous phase|droplet interface, had no effect on the electrowetting response; making it a good choice of organic electrolyte as it ensures that there is no ion transfer from the droplet to the surrounding solution. In contrast, changing the inorganic electrolyte was found to significantly increase pinning. There is currently no explanation for this, making it an interesting avenue for future investigation.

Also of significance was the concentration of the electrolytes used. This proved to be very important in reducing pinning and increasing the maximum achievable contact angle change. It was shown that the electrolyte could be made both too dilute and too concentrated, with the ideal concentration for LiCl with DCE being 0.10 mol dm^{-3}. Furthermore, it was shown that if a hydrophobic solvent was used as the droplet, the contact angle would not decrease on the return scan, while more water miscible solvents did return. These results led to speculation that one origin of hysteresis is the adsorption of a film of water at the electrode surface as the droplet contracts. As it tries to spread on the return scan, it cannot as this hydrophilic layer does not want to come off the surface even when the potential scan is reversed. This would explain why more hydrophobic droplets are reluctant to return to their original configurations. It is also feasible that with certain electrolytes, and in particular at high electrolyte concentrations, this layer of water is more strongly adhered to the surface, explaining the

concentration and electrolyte dependence. At this stage this is pure speculation and might form the basis of future investigations.

Given the hypothesis which has just been outlined, it was proposed that less hydrophobic solvents would not be so strongly repelled by this water film. As a result the highly water miscible solvent 3-chloro-1-propanol was used. This was found to be immiscible with water only in the presence of an electrolyte. It also showed no hysteresis when used in the droplet. Unfortunately, it is mildly acidic meaning that the Faradaic reduction of protons in the solution was shifted to higher potentials such that the potential of the reaction coincided with the potential of electrowetting. This means the system was unsustainable over long time periods. Other solvents or solvent mixtures were unable to recreate the electrowetting response of 3-chloro-1-propanol. This means that there is still a question as to whether the low hysteresis response of the 3-chloro-1-propanol is due to the Faradaic reactions or not, although acidification of DCE systems to a similar pH did not reduce hysteresis.

The one thing that is clear is that electrowetting is far more complicated than the relatively simple Young-Laplace equation suggests. Although some ambiguity remains, it seems that the relative surface energies of the three interfaces in an electrowetting system play a role in the hysteresis and reproducibility of an electrowetting system. On top of this there are additional factors influencing droplet relaxation which have not been previously reported or considered. Despite these complications, substantial progress has been made both in establishing which parameters are important for an electrowetting system and in finding a system with such parameters. The most effective electrowetting system, using the solvent 3-chloro-1-propanol offered fantastic performance; however, it is not a viable solution due to Faradaic processes. Whether the Faradaic processes and excellent performance are in fact related could not be determined; nevertheless, this result justifies further investigation into low voltage electrowetting, providing hope that a low voltage, hysteresis-free system is possible.

5.8 References

1 Adamson, A. W. & Gast, A. P. *Physical Chemistry of Surfaces*. 6th edn, (John Wiley & Sons, Inc., 1997).

2 Kornyshev, A. A. *et al.* Ultra-low-voltage Electrowetting. *The Journal of Physical Chemistry C* **114**, 14885-14890, doi:10.1021/jp101051e (2010).

3 Chai, L. & Klein, J. Large Area, Molecularly Smooth (0.2 nm RMS) Gold Films for Surface Forces and Other Studies. *Langmuir* **23**, 7777-7783 (2007).

4 Zisman, W. A. in *Contact Angle, Wettability, and Adhesion* Vol. 43 *Advances in Chemistry* Ch. 1, 1-51 (American Chemical Society, 1964).

5 Beni, G. & Hackwood, S. Electro-wetting Displays. *Applied physics letters* **38**, 207-209 (1980).

6 Frumkin, A. N., Kabanow, B. & Nekrasow, M. Kapillarelektrische Erscheinungen und Benetzung von Metallen durch Elektrolytlösungen. *I. Phys. Z. Sovijetunion* **1**, 255-284 (1932).

7 Ivošević, N. & Žutić, V. Spreading and Detachment of Organic Droplets at an Electrified Interface. *Langmuir* **14**, 231-234, doi:10.1021/la970986z (1998).

8 Cousens, N. E. A. *Shape Changing Liquid Droplets*, Imperial College London, (2009).

9 Maillard, M., Legrand, J. & Berge, B. Two Liquids Wetting and Low Hysteresis Electrowetting on Dielectric Applications. *Langmuir* **25**, 6162-6167, doi:10.1021/la804118y (2009).

10 Israelachvili, J. N. *Intermolecular and Surface Forces*. 2nd edn, (Academic Press).

11 Bostrom, M., Kunz, W. & Ninham, B. W. Hofmeister Effects in Surface Tension of Aqueous Electrolyte Solution. *Langmuir* **21**, 2619-2623 (2005).

12 Horinek, D., Herz, A., Vrbka, L., Sedlmeier, F. & Mamatkulov, S. Specific Ion Adsorption at the Air/water Interface: The Role of Hydrophobic Solvation. *Chemical Physics Letters* **479**, 173-183 (2009).

13 Bresme, F., Chacon, E., Tarazona, P. & Wynveen, A. The Structure of Ionic Aqueous Solutions at Interfaces: An Intrinsic Structure Analysis. *The Journal of chemical physics* **137** (2012).

14 Lippmann, G. Relation entre les Phénomènes Électriques et Capillaires. *Ann. Chim. Phys.* **5**, 494-549 (1875).

15 Beni, G., Hackwood, S. & Jackel, J. L. Continuos Electro-wetting Effect. *Applied physics letters* **40**, 912-914 (1982).

16 Sondag-Huethorst, J. A. M. & Fokkink, L. G. J. Potential-dependent Wetting of Octadecanethiol-modified Polycrystalline Gold Electrodes. *Langmuir* **8**, 2560-2566, doi:10.1021/la00046a033 (1992).

17 Sondag-Huethorst, J. A. M. & Fokkink, L. G. J. Potential-Dependent Wetting of Electroactive Ferrocene-Terminated Alkanethiolate Monolayers on Gold. *Langmuir* **10**, 4380-4387, doi:10.1021/la00023a074 (1994).

18 Gorman, C. B., Biebuyck, H. A. & Whitesides, G. M. Control of the Shape of Liquid Lenses on a Modified Gold Surface Using an Applied Electrical Potential across a Self-Assembled Monolayer. *Langmuir* **11**, 2242-2246, doi:10.1021/la00006a063 (1995).

19 Xu, L., Chen, W., Mulchandani, A. & Yan, Y. Reversible Conversion of Conducting Polymer Films from Superhydrophobic to Superhydrophilic. *Angewandte Chemie (International ed.)* **44**, 6009-6012 (2005).

20 *Knovel Critical Tables*. 2nd edn, (Knovel, 2008).

21 Marinescu, M., Urbakh, M., Barnea, T., Kucernak, A. R. & Kornyshev, A. A. Electrowetting Dynamics Facilitated by Pulsing. *The Journal of Physical Chemistry C* **114**, 22558-22565, doi:10.1021/jp1052634 (2010).

22 Estimation Programs Interface Suite™ for Microsoft Windows v. 4.10 (United States Environmental Protection Agency, Washington, DC, USA, 2011).

23 Raridon, R. J. & Kraus, K. A. Properties of Organic-Water Mixtures .4. Effect of Various Salts on Miscibility Gap of Glycerol Triacetate-Water System. *Journal of colloid science* **20**, 1000-& (1965).

24 Tabata, M., Kumamoto, M. & Nishimoto, J. Chemical-properties of Water-miscible Solvents Separated by Salting-Out and their Application to Solvent-Extraction. *Analytical Sciences* **10**, 383-388 (1994).

25 Lee, D. G. & Demchuk, K. J. A C-13 Nuclear-Magnetic-Resonance Study of the Basicities of Aliphatic-Alcohols. *Canadian journal of chemistry* **65**, 1769-1774 (1987).

26 Trojánek, A. n., Lhotský, A., Mareček, V. r. & Samec, Z. Limited Agreement between the Interfacial Tension and Differential Capacity Data for the Polarised Water|1,2-dichloroethane Interface. *Journal of Electroanalytical Chemistry* **565**, 243-250, doi:10.1016/j.jelechem.2003.10.018 (2004).

Chapter 6: Conclusions

6.1 General conclusions

This thesis has shown that one of the difficulties in studying low voltage electrowetting systems is the systematic isolation of individual variables. In trying to change just the electrode material, the capacitance, surface tensions and morphology all change at the same time. In changing the electrolyte again the capacitance and surface energies change together. In changing the composition of the droplet, three surface energies change at once while the density also changes and so on and so forth. This makes it exceedingly difficult, if not impossible, to systematically isolate individual variables—one of the tenets of good scientific practice. On top of this there is the unpredictability of studying pinned systems, which inherently introduce substantial variation between experiments. Even so, now that there is a better understanding of the important factors in low voltage electrowetting, coupled with an appreciation of its previously unexpected complexity, future work should attempt a more vigorous analysis of the effect of factors such as liquid|liquid surface energy which were only touched upon in the final stages of this thesis. This way, it will be possible to elucidate which properties of a system are responsible for both a good and not-so-good electrowetting response.

6.2 Electrowetting devices

A hysteresis-free electrowetting system using 3-chloro-1-propanol was shown. This had the performance required for a low voltage electrowetting lens. However, this did not operate within the potential limits imposed by the onset of Faradaic reactions, meaning that the system cannot be stable in the long term. Nonetheless, this suggests that a low voltage electrowetting system, suitable for an electrowetting lens, may still be possible.

However, a hysteresis free system is not essential to other devices such as certain displays and switches. These only require an on/off response corresponding to two extreme contact angles. Such a system was demonstrated in Section 5.5.3, where the contact angle was cycled between 93° and 120° continuously. Nonetheless, a similar system would need to be shown on a greater variety of electrode surfaces as template stripped gold is both impractical for a device and not

stable in water for long periods. Therefore, an improved understanding of why materials such as glassy carbon do not show an electrowetting response would be an important step in the development of a stable electrowetting device.

6.3 Future work

While almost every topic covered in this thesis has potential for expansion and more detailed investigation, one area is clearly the most interesting and important with regard to electrowetting—droplet composition. Future work would almost certainly continue the search for a solvent with similar properties to 3-chloro-1-propanol, such as density and surface energy, but which is not electrochemically active above –1 V versus Ag/AgCl. This would answer the question as to whether the effectiveness of 3-chloro-1-propanol is a result of Faradaic processes. If this is not the case, then a hysteresis free electrowetting system would have been found.

No attempt was made in this thesis to fit electrowetting results to the predictions of the electrowetting model of Monroe, Urbakh and Kornyshev. This is because this model does not accommodate for the effects of pinning and dynamics. As pinning and dynamics currently dominate, the theory is not applicable, however, if a non-pinning system were found, then the model could be applied. Alternatively, the model could be applied to a mercury system or the 3-chloro-1-propanol system although this is not at equilibrium due to Faradaic processes.

Investigation of mercury electrowetting systems may also be interesting as the absolute values of the surface energies may provide clues as to why mercury is hysteresis-free. It would also be interesting to see whether pinning could be induced on mercury with certain solvent and electrolyte combinations, thus showing that effects of concentration, electrolyte and droplet solvent are a general result not limited to gold surfaces. This in turn could help explain the origin of these effects.